MDC G1228

THE LONG-TERM MOTION OF ARTIFICIAL PLANETARY SATELLITES

Contract Number: NAS5-10782

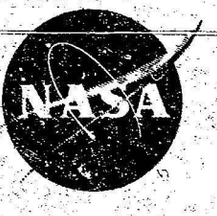

Prepared by

McDonnell Douglas Astronautics Company
Western Division
Santa Monica, California

for
Goddard Space Flight Center
Greenbelt, Maryland

NATIONAL AERONAUTICS AND SPACE ADMINISTRATION

THE LONG-TERM MOTION OF ARTIFICIAL PLANETARY SATELLITES

Contract Number: NAS5-10782

Goddard Space Flight Center
Contracting Officer
Mrs. Dorothy Burel

Technical Monitor
Mr. Robert Coady

Prepared by

McDonnell Douglas Astronautics Company
Western Division
Study Manager
C. Uphoff

for
Goddard Space Flight Center
Greenbelt, Maryland

ACKNOWLEDGMENTS

This work was performed under contract NAS5-10782 for the National Aeronautics and Space Administration. Several of the numerical integrations presented in this report were available from a previous study under NASA contract NAS7-623. The cooperation and support of the NASA agencies is gratefully acknowledged.

ABSTRACT

The described work concerns the orbit evolution problem for strongly perturbed artificial satellites of Mercury, Venus, Earth and Mars. The unifying feature is that the principal effects on the orbit elements come from the gravitational fields(s) of the Sun (and Earth's Moon) and the coupling of those effects with pericenter, node, and inclination variations caused by the non-sphericity of the central planet. Semianalytic techniques are presented that describe the long-term motion of artificial satellites disturbed by a third body, oblateness of the central planet, and atmospheric drag. The techniques are applied to the orbit evolution problem for satellites of each of the four inner planets, and a four-planet survey outlines the effects of the major perturbations for satellites of each planet.

The primary analytic results of this report are modifications to an existing method to include the effects of the disturbing body's eccentric orbit. The principal numerical results are comparisons of pericenter histories given by the method with histories obtained by numerical integration of the actual equations of motion. The major influences on dynamic lifetime are isolated and pointed out for satellites of each inner planet and the method is applied to some real planetary orbit mission opportunities in the 1970's.

It is discovered that simulation of Mercury and Venus orbiters is relatively simple since the only significant perturbations come from the solar gravitational field. For Earth and (especially) for Mars, the coupling between third body and oblateness perturbations makes orbit prediction difficult through a considerable range of possible orbits. Also, the possibility of significant atmospheric effects at very high altitudes for Martian satellites suggests that it may be difficult to get very close to that planet without appreciable risk of early orbit decay. The difficulties are isolated and discussed. Recommendations are made as to efficient resolution of these problems.

TABLE OF CONTENTS

Page intentionally left blank

LIST OF ILLUSTRATIONS

LIST OF TABLES

Section 1
INTRODUCTION AND SUMMARY

In the design of a mission to another planet, the amount of useful payload that can be placed in orbit about the planet may be so valuable scientifically that it becomes expedient (even necessary) to select an orbit having a very low pericenter and a very high apocenter. Such orbits are also of great interest for Earth satellites when it is desired to study large volumes of space with a maximum scientific payload.

The dynamic lifetime of such a satellite is very sensitive to perturbations since, by definition, the pericenter is just above the atmosphere (or surface) of the planet. Not only is the orbit affected by the oblateness of the planet, it is disturbed by the sun's gravity field and possibly the atmosphere of the central planet. In designing such a mission it is important to evaluate not only the coupling between the effects of oblateness and the long-term motion caused by third-body effects but also the effect of the periodic perturbations. Either of these can cause the pericenter distance to decrease by an amount that will end the satellite's journey.

From a scientific point of view the time history of the shape and orientation of the orbit is important since the type and amount of scientific information to be obtained depends markedly on the orbit geometry. Apart from the lifetime problem, it is advisable to have a reasonably accurate time history of the pericenter radius as well as the histories of the other orbit parameters. For preliminary mission design, orbit evolution information should be available for a wide variety of initial (planetary orbit injection) conditions. The pericenter radius history--of prime importance from the lifetime and scientific information standpoints--can be accurately predicted from the time history of the orbit's eccentricity and semi-major axis. This report suggests some approximate techniques that give insight

into the orbit prediction problem and places an emphasis on how the techniques can be used to isolate and study the principal perturbations acting on artificial planetary satellites.

The report is divided into three parts: a theoretical discussion (Section 2), some practical considerations (Section 3), and recommendations for further study (Section 4). The report is intended to be understandable without Section 2 so that the reader can, if he wishes, go on to Section 3 after these introductory remarks without serious loss of necessary information.

In Section 2, the concept of the approximate techniques is outlined and modifications to include the effects of the disturbing planet's eccentricity and the effects of atmospheric drag are presented. The idea is to combine all the slowly varying perturbations together and numerically integrate these average rates of the orbital elements. The medium-periodic third-body variations in eccentricity are then analytically superimposed onto the long-term variations. This technique has been proven very accurate for a wide range of possible orbits and permits the use of very large (several hundred days in many cases) computing intervals in the numerical integrations.

Section 3 is the substance of the report and includes a four-planet survey of the dynamic behaviour of artificial satellites of the four inner planets. The techniques of Section 2 are applied to the problem of long-term orbit prediction. The areas where the methods are, and are not, applicable are shown in terms of pericenter and apocenter altitudes for satellites of each planet. The survey is primarily concerned with dynamic lifetime and the effects of the major disturbing forces on the pericenter history of planetary orbiters. Also, the survey is concentrated on the planets Venus and Mars as these are of the most immediate interest. The Earth is included in an approximate way with the assumption that the orbits of the Earth and the Moon are coplanar. Earth is included for reference so that those familiar with the major perturbations for Earth satellites will have à reference point, in the notation of this report, for evaluation of the perturbations acting on satellites of the other planets.

The major disturbing forces for Venus orbiters are the solar gravitational field and (below about 300-km altitude) the Venusian atmosphere. The sharp drop in density of the most recent models of Venus' atmosphere and the very low estimates of the Venusian oblateness make orbit prediction relatively easy.

For Mars, the story is quite different. Even though the surface density of the Martian atmosphere is much lower than that of Venus or Earth, the maximum density models for Mar in still have a significant effect on satellite lifetime at very high altitudes. It is found that the atmospheric effects of a maximum density model, acting on a satellite in a circular orbit 1,000 km above the Martian surface, could cause the lifetime to be only a few Earth years for a normal spacecraft [$C_D A/M = 0.03(m^2/kg)$].

The possibly very dense upper Martian atmosphere is not the only difficulty. The oblateness coefficient, J_2, for Mars is nearly twice that of the Earth. The great strength of the oblateness perturbations, it is found, not only dominates the motion of Martian satellites but also causes such rapid motion of the orbit that the assumptions of the techniques of Section 2 can be violated for a considerable range of possible orbits. The very complex coupling between oblateness and third-body perturbations makes it reasonable to expect strong resonance effects between oblateness and medium-periodic third-body effects. Such resonance could result in very short lifetimes. The kinds of orbits for which these complexities exist are discussed in the survey.

In spite of these difficulties, the approximate techniques work well for a large range of orbit parameters for Mars and for nearly any orbit about Venus or Mercury. The techniques are applied to the problem of aiming point selection for three possible missions in the 1970's and the advantages of the high speed of the approximate methods are demonstrated. Also, the time histories of some scientifically important parameters are presented to show how the techniques can be used to design the orbit for maximum scientific value.

Finally in Section 3, a discussion of neglected factors indicates the need for further work in this area. The neglected items of most significance are the high-order oblateness effects (that will almost certainly be significant for Mars), high-order terms in the expansion of the disturbing function for third-body perturbations, solar radiation pressure (for abnormally large spacecraft) and short-periodic coupling between atmospheric and oblateness perturbations.

In Section 4 a system of computer subprograms is recommended as a solution that will permit mission analysts to study the orbit prediction problem in an efficient way.

At the lowest level of sophistication, the methods of Section 2 are recommended because they work so well for Venus and can provide almost instantaneous orbit prediction. The second suggested level of computer software should be designed along the same lines, but should integrate numerically the singly averaged third-body equations. This integration should be done in the planet's equatorial frame so that the analytically averaged effects of high-order oblateness terms can be easily included. This level should also include the capability to simulate the average effects of solar radiation pressure.

It is felt that the third level of the recommended system will solve nearly all the problems. It is recommended that the variational equations for the orbit elements be written in Gauss's form where the accelerations enter the equations directly. This form of the equations will permit the simulation of any perturbing effect whatever but will still retain the advantages of the variation of parameters formulation. The equations should then be averaged numerically by mechanical quadrature formulas and these averaged rates integrated with a sophisticated numerical integration scheme. The fourth and highest level is obtained by eliminating the preintegration averaging and by integrating the variational equations directly. This level, then, would provide the capability to test the approximate techniques of the three lower levels

and would provide the further advantage that the complete numerical integration would be available as a part of the same computer program. Indeed, the difference between levels three and four would be nothing more than a few logical Fortran statements and a few extra memory locations for storing the weights and abscissae necessary for a good mechanical quadrature technique. This recommended system is discussed in detail in Section 4.

A final section summarizes the major conclusions of the report, a glossary defines the nomenclature, and the appendices give pertinent formulae. If the reader wishes to skip to Section 3, he may do so at this point, but a glance at the nomenclature section is recommended.

Page intentionally left blank

Section 2
THEORETICAL CONSIDERATIONS

THE BASIC IDEA

It is frequently possible to obtain an accurate and relatively simple description of the motion of a dynamical system if the Hamiltonian can be separated into terms of different frequency. This separation can be accomplished in several ways: by an averaging technique such as that of Reference 1, or the more sophisticated many-variable expansion procedure championed by Kevorkian, Shi, and Eckstein in References 2 and 3, or by the elegant method of von Zeipel in which canonical transformations that automatically effect the separation are found. No matter how the various terms are isolated, it remains to integrate the separate terms and then to determine the validity of the assumption that the actual motion can be adequately described by the approximate solutions.

The concept of doubly averaging the differential equations of satellite motion in a three-body system was developed in the early sixties independently by Lidov (Reference 1) and by Williams and Lorell (Reference 4). By averaging the variational equations for the rates of the orbit elements over one revolution of the satellite in its orbit, they obtained a set of singly-averaged equations free of the satellite's true anomaly. These singly-averaged rates of the orbit elements were then further averaged over one revolution of the disturbing body around the central primary. The resulting doubly-averaged equations were then not only free of the satellite's true anomaly but also did not contain the true anomaly of the disturbing planet. What is better is that these equations for the long-term motion are solvable in terms of elliptic functions. The time history of the long-periodic eccentricity can be written down explicitly although the expressions are rather

complicated. This discovery was a major contribution to celestial mechanics and showed, for the first time, the analytic character of the long-term motion in the main problem of the lunar theory. At about the same time Eckstein, Shi and Kevorkian (Reference 3) applied the many-variable expansion procedure to the problem of satellite motion under third-body perturbations and showed that their solution for the long-term motion was equivalent to the solution of the doubly averaged equations. Kevorkian (Reference 2) also pointed out the similarities and differences of the two-variable expansion procedure and the von Zeipel method.

Later, both Lidov (Reference 5) and Lorell (Reference 6) modified the doubly averaged equations to incorporate the secular effects of oblateness into the equations for the long-periodic motion. It was this extension that allowed Lidov to explain the apparent stability of the moons of Uranus in the light of his earlier discoveries concerning the instability of polar satellites perturbed (only) by a third body.

This work provided a firm theoretical foundation for the application of the doubly averaged equations to the problem of long-term orbit prediction and lunar orbit mission analysts began to use the equations for lifetime predictions. It was discovered that, even if the equations are integrated numerically, they provide a very useful tool since the absence of any fast variables permits the use of extremely large computing intervals. The doubly averaged equations are written in a planetocentric nonrotating coordinate frame whose xy plane lies in the orbit plane of the central body around the disturbing (third) body. The equations can be found in the papers referenced above, or they can be easily derived from the long-periodic part of the disturbing function given in the appendix of this report. The terms dependent upon the oblateness of the central body are obtained by transforming the (secular) equatorial rates of the argument of pericenter, $\bar{\omega}_L$, and longitude of the ascending node, $\bar{\Omega}_L$, into the frame in which the doubly averaged equations are written. In this frame, there is a long-term rate of

change of inclination due simply to the motion of the node on the equator. The resulting doubly averaged equations, including the first order secular effects of oblateness, are

$$\frac{da_L}{dt} = 0$$

$$\frac{de_L}{dt} = \frac{C}{2} e_L \sqrt{1 - e_L^2} \sin^2 i_L \sin 2\omega_L$$

$$\frac{di_L}{dt} = -\frac{Ce_L^2}{4\sqrt{1 - e_L^2}} \sin 2i_L \sin 2\omega_L + \frac{nJr_e^2}{p^2} \cos \bar{i}_L \sin i'' \sin (\Omega_L - \Omega'')$$

$$\frac{d\omega_L}{dt} = \frac{C}{\sqrt{1 - e_L^2}} \left[(\cos^2 i_L - 1 + e_L^2) \sin^2 \omega_L + \frac{2}{5} \left(1 - e_L^2\right) \right] \qquad (1)$$

$$+ \frac{nJr_e^2}{p^2} \left[2 - \frac{5}{2} \sin^2 \bar{i}_L - \frac{\sin i'' \cos \bar{i}_L \cos (\Omega_L - \Omega'')}{\sin i_L} \right]$$

$$\frac{d\Omega_L}{dt} = -\frac{C \cos i_L}{\sqrt{1 - e_L^2}} \left[e_L^2 \sin^2 \omega_L + \frac{(1 - e_L^2)}{5} \right]$$

$$- \frac{nJr_e^2}{p^2} \cos \bar{i}_L \left[\cos i'' - \frac{\sin i'' \cos i_L \cos (\Omega_L - \Omega'')}{\sin i_L} \right]$$

The nomenclature is standard and is given in the Glossary. It is important to note that angular elements with a bar over them are referred to the planet's equator. Otherwise, orbital elements are referred to the central planet's orbit plane. Also notice that the doubly averaged equations (with J = 0) do not contain Ω_L on the right hand side. This means that we are still free to choose the direction of the x-axis of the coordinate system in a way that

will simplify the expressions. Later we shall find it expedient to direct the x-axis along the line from the Sun to perihelion of the central body's orbit.

In 1966, as shown in Reference 7, the medium-periodic variations in eccentricity were superimposed onto the long-periodic variations described by the doubly averaged equations (1). (These terms, which vary as the sine of twice the mean anomaly of the disturbing body, were misleadingly called short-periodic in Reference 7.) In this way, it was possible to integrate the doubly averaged equations numerically and maintain the advantages of slowly changing variables. As an introduction to the modifications that will follow, we present a brief outline of the method of Reference 7.

We begin with the very useful expression of Kozai (Reference 8) for the third-body disturbing function in the form of a trigonometric series in the satellite's orbital elements.

$$R = n'^2\mu'a^2 \left\{ [1 + 3e' \cos(\phi' - \omega' - \Omega')] \left[\left(1 + \frac{3}{2}e^2\right) A + \frac{15}{8}e^2 B \right] \right.$$

$$\left. -4e' \sin(\phi' - \omega' - \Omega') \left[\left(1 + \frac{3}{2}e^2\right) A' + \frac{15}{8} e^2 B' \right] \right\} \qquad (2)$$

where A, B, A', and B' are series very conveniently separated into terms whose trigonometric arguments depend upon the mean longitude of the disturbing body (ϕ') and those terms which do not include ϕ'.

The expressions for A and B are given in the Appendix I. A' and B' are obtained by first dropping all long-periodic terms and then replacing cos by sin in all terms depending on ϕ'. Notice that the expressions do not depend upon the position of the satellite in its orbit since the short-periodic variations were dropped in the expansion of the disturbing function.

As explained in Reference 7, the variations in eccentricity are sought in order that we may describe the variations in pericenter distance since the energy and the semi-major axis remain constant on the average. In the analysis for lunar satellites, it was possible to take the plane of the central body's orbit about the perturbing body as principal plane and to ignore the eccentricity, e', of the orbits of the primaries about each other. Under these restrictions, R became

$$R = n'^2 \mu' a^2 \left\{ \left[1 + \frac{3}{2} e^2 \right] A + \frac{15}{8} e^2 B \right\} \tag{3}$$

and A and B reduced to

$$A = \left[\frac{1}{4} \left(1 - \frac{3}{2} \sin^2 i \right) \right] + \frac{3}{8} \sin^2 i \cos 2(\phi' - \Omega)$$

$$B = \left[\frac{1}{2} \sin^2 i \cos 2\omega \right] + \cos^4 \left(\frac{i}{2} \right) \cos 2(\phi' - \omega - \Omega)$$

$$+ \sin^4 \left(\frac{i}{2} \right) \cos 2(\phi' + \omega - \Omega) \tag{4}$$

Considering the bracketed long-periodic terms separately from the medium-periodic terms with ϕ' in the arguments, the time rate of change of the medium periodic eccentricity variation, $\delta e = e - e_L$, was written as

$$\frac{d\delta e}{dt} = - \frac{\sqrt{1 - e^2}}{n a^2 e} \frac{\partial}{\partial \omega} \left\{ n'^2 \mu' a^2 \left[\left(1 + \frac{3}{2} e^2 \right) A_M + \frac{15}{8} e^2 B_M \right] \right\}$$

$$= - \frac{\sqrt{1 - e^2}}{n a^2 e} \left[n'^2 \mu' a^2 \frac{15}{8} e^2 \frac{\partial B_M}{\partial \omega} \right]$$

where A_M and B_M refer to the medium-periodic parts of Equation (4). Before integrating we wrote

$$\frac{d\delta e}{e\sqrt{1-e^2}} = \frac{15}{4}\frac{n'^2}{n}\mu'\left[\sin^4\left(\frac{i_L}{2}\right)\sin 2(\phi' + \omega - \Omega)\right.$$

$$\left.-\cos^4\left(\frac{i_L}{2}\right)\sin 2(\phi' - \omega - \Omega)\right]dt$$

breaking with tradition by not holding the long-periodic eccentricity constant during the integration with respect to time. The integration yielded

$$\int\frac{de}{e\sqrt{1-e^2}} - \int\frac{de_L}{e\sqrt{1-e^2}} = f(t) + c' \tag{5}$$

with

$$F(t) = \frac{15}{8}\frac{n'^2\mu'}{n}\left[\cos^4\left(\frac{i_L}{2}\right)\frac{\cos 2(\phi' - \omega_L - \Omega_L)}{n' - \dot{\omega}_L - \dot{\Omega}_L}\right.$$

$$\left.-\sin^4\left(\frac{i_L}{2}\right)\frac{\cos 2(\phi' + \omega_L - \Omega_L)}{n' + \dot{\omega}_L - \dot{\Omega}_L}\right] \tag{6}$$

and c' a constant of integration.

Assuming that $e - e_L$ was small enough to permit writing Equation (5) as

$$\int\frac{de}{e\sqrt{1-e^2}} - \int\frac{de_L}{e_L\sqrt{1-e_L^2}} = F(t) + c' = F(t) - F(t_o)$$

we obtained the principal result of Reference 7, viz.,

$$e(t) = \operatorname{sech}\left[\operatorname{sech}^{-1}(e_L) - F(t) + F(t_o)\right] \tag{7}$$

During the integration to obtain F(t), it was assumed that variations in i_L and nonlinear changes in ω_L and Ω_L were negligible over one revolution of the disturbing body.

This method was found to be very useful and accurate when applied to the prediction of lunar satellite lifetimes and permitted very rapid pre-mission and real-time probability analyses to be performed.

THE EFFECTS OF e'

In order to describe the third-body perturbations for a satellite of Mercury (whose orbital eccentricity is over 0.2) we should include the terms in the disturbing function at least of order e' and, as it turns out, we can easily describe variations which go as e'^2. Unfortunately, this second order analysis requires that we give up the very useful disturbing function of Kozai and follow a line developed by Brown and Shook in Reference 9. (Kozai probably took this course also, but he had no need to extend his analysis to second order in e'.)

The disturbing function for the problem at hand is given in Chapter 4 of Reference 9 as

$$R = k^2 m' \left(\frac{1}{\Delta} - \frac{r \cos S}{r'^2} \right)$$

with

$$\Delta = \sqrt{r^2 + r'^2 - 2rr' \cos S}.$$

In terms of the orbit elements

$$\cos S = \cos^2 \left(\frac{i}{2} \right) \cos (f - f' + \omega + \Omega) + \sin^2 \left(\frac{i}{2} \right) \cos (f + f' + \omega - \Omega),$$

where our variables are related to those of Reference 9 by

Reference 9	this report
v'	f'
v	$f + \omega + \Omega$
θ	Ω.

The disturbing function is next expanded in powers of r/r' as explained in Chapter 12 of Reference 10. We find that it is necessary to express $\cos^2 S$ in terms of the elements.

$$\cos^2 S = \cos^4 \frac{i}{2} \cos^2 (f - f' + \omega + \Omega) + \sin^4 \frac{i}{2} \cos^2 (f + f' + \omega - \Omega)$$

$$+ 2 \cos^2 \frac{i}{2} \sin^2 \frac{i}{2} \cos (f - f' + \omega + \Omega) \cos (f + f' + \omega - \Omega). \qquad (8)$$

The disturbing function is given to second order in r/r' by

$$R = n'^2 \mu' a^2 \left\{ \frac{r^2}{a^2} \frac{a'^3}{r'^3} \left[-\frac{1}{2} + \frac{3}{2} \cos^2 S \right] + \cdots \right\}. \qquad (9)$$

Averaging the equations with respect to true anomaly or (what is the same thing) expanding as on p. 313 of Reference 10 with the formulae

$$\frac{r^2}{a^2} = 1 + \frac{3}{2} e^2 - 2e \cos \phi - \frac{e^2}{2} \cos 2\phi + \cdots$$

$$\frac{a'^3}{r'^3} = 1 + \frac{3}{2} e'^2 + 3e' \cos \phi' + \frac{9}{2} e'^2 \cos 2\phi' + \cdots$$

$$\frac{r^2}{a^2} \cos 2f = \frac{5}{2} e^2 - 3e \cos \phi + (1 - \frac{5}{2} e^2) \cos 2\phi + e \cos 3\phi + e^2 \cos 4\phi + \cdots$$

$$\frac{r^2}{a^2}\sin 2f = -3e\sin\phi + (1 - \frac{5}{2}e^2)\sin 2\phi + e\sin 3\phi + e^2\sin 4\phi + \cdots$$

$$\frac{a'^3}{r'^3}\cos 2f' = -\frac{e'}{2}\cos\phi' + (1 - \frac{5}{2}e'^2)\cos 2\phi' + \frac{7}{2}e'\cos 3\phi'$$

$$+\frac{17}{2}e'^2\cos 4\phi' + \cdots$$

$$\frac{a'^3}{r'^3}\sin 2f' = -\frac{e'}{2}\sin\phi' + (1 - \frac{5}{2}e'^2)\sin 2\phi' + \frac{7}{2}e'\sin 3\phi'$$

$$+\frac{17}{2}e'^2\sin 4\phi' + \cdots \qquad (10)$$

it becomes clear that the terms involving ϕ will average to zero over one revolution of the satellite in its orbit.

Substituting the formulae of Equation (10) into Equation (9), dropping the terms with sines or cosines of a multiple of ϕ as a factor, and noticing that

$$\cos 2\omega - 2\sin^2 f'\cos 2\Omega + 2\sin(\omega + \Omega)\sin(\omega - \Omega) + \sin 2f'\sin 2\Omega$$

$$= \cos 2(f' - \Omega)$$

we obtain

$$R = n'^2\mu'a^2\left\{\left[(1 + \frac{3}{2}e'^2) + 3e'\cos\phi' + \frac{9}{2}e'^2\cos 2\phi'\right]\cdot\right.$$

$$\left[(1 + \frac{3}{2}e^2)\frac{1}{4}(1 - \frac{3}{2}\sin^2 i) + \frac{15}{8}e^2\frac{\sin^2 i\cos 2\omega}{2}\right]$$

$$\left. + R_{M_\omega} + R_{M_\Omega}\right\} \qquad (11)$$

where

$$R_{M_\omega} = \frac{15}{8} e^2 \Big\{ \left[\cos^4\left(\frac{i}{2}\right) \cos 2(\omega + \Omega) + \sin^4\left(\frac{i}{2}\right) \cos 2(\omega - \Omega)\right]$$

$$\cdot \left[\cos 2\phi' - \frac{e'}{2}\cos\phi' + \frac{7}{2}e' \cos 3\phi' - \frac{e'^2}{2}(5\cos 2\phi' - 17\cos 4\phi')\right]$$

$$+ \left[\cos^4\left(\frac{i}{2}\right) \sin 2(\omega + \Omega) - \sin^4\left(\frac{i}{2}\right) \sin 2(\omega - \Omega)\right]$$

$$\cdot \left[\sin 2\phi' - \frac{e'}{2}\sin\phi' + \frac{7}{2}e' \sin 3\phi'\right.$$

$$\left. - \frac{e'^2}{2}(5\sin 2\phi' - 17\sin 4\phi')\right]\Big\} \qquad (11a)$$

and

$$R_{M_\Omega} = \frac{3}{8}\left(1 + \frac{3}{2}e^2\right) \sin^2 i \Big\{ \cos 2\Omega \left[\cos 2\phi' - \frac{e'}{2}\cos\phi' + \frac{7}{2}e' \cos 3\phi'\right.$$

$$\left. - \frac{e'^2}{2}(5\cos 2\phi' - 17\cos 4\phi')\right] + \sin 2\Omega \left[\sin 2\phi' - \frac{e'}{2}\sin\phi'\right.$$

$$\left. + \frac{7}{2}e' \sin 3\phi' - \frac{e'^2}{2}(5\sin 2\phi' - 17\sin 4\phi')\right]\Big\}. \qquad (11b)$$

We now come to the basic assumption of this kind of perturbation analysis. We assume that

$$\frac{d\delta e}{dt} = -\frac{\sqrt{1 - e^2}}{na^2 e} \frac{\partial R_M}{\partial \omega}$$

where R_M is taken to be the sum of all terms of Equation (11) that involve the disturbing body's mean anomaly, ϕ', and δe represents the medium periodic variations in eccentricity.

Integrating as before, we obtain the following formula for the eccentricity as a function of time

$$e(t) = \operatorname{sech}\left[\operatorname{sech}^{-1}(e_L) - \operatorname{sech}^{-1}(e_{L_o}) + \operatorname{sech}^{-1}(e_o) + F^*(t) - F^*(t_o)\right] \qquad (12)$$

with F*(t) given by

$$F^*(t) = \frac{15}{8}\frac{n'^2\mu'}{n}\left(s^4\frac{\cos 2(\phi' + \omega_L - \Omega_L)}{DP_2} - c^4\frac{\cos 2(\phi' - \omega_L - \Omega_L)}{DM_2}\right.$$

$$- e'\left[s^4\frac{\cos(\phi' + 2\omega_L - 2\Omega_L)}{DP_1} - c^4\frac{\cos(\phi' - 2\omega_L - 2\Omega_L)}{DM_1}\right]$$

$$+ 7e'\left[s^4\frac{\cos(3\phi' + 2\omega_L - 2\Omega_L)}{DP_3} - c^4\frac{\cos(3\phi' - 2\omega_L - 2\Omega_L)}{DM_3}\right]$$

$$-\frac{5}{2}e'^2\left[s^4\frac{\cos 2(\phi' + \omega_L - \Omega_L)}{DP_2} - c^4\frac{\cos 2(\phi' - \omega_L - \Omega_L)}{DM_2}\right]$$

$$+ 17e'^2\left[s^4\frac{\cos(4\phi' + 2\omega_L - 2\Omega_L)}{DP_4} - c^4\frac{\cos(4\phi' - 2\omega_L - 2\Omega_L)}{DM_4}\right]$$

$$- \sin^2 i_L\left\{\frac{3}{2}e'\left[\frac{\cos(\phi' - 2\omega_L)}{(n' - 2\dot{\omega}_L)} - \frac{\cos(\phi' + 2\omega_L)}{(n' + 2\dot{\omega}_L)}\right]\right.$$

$$\left.\left.+\frac{9}{8}e'^2\left[\frac{\cos 2(\phi' - \omega_L)}{(n' - \dot{\omega}_L)} - \frac{\cos 2(\phi' + \omega_L)}{(n' + \dot{\omega}_L)}\right]\right\}\right) \qquad (13_a)$$

where $s = \sin(i_L/2)$, $c = \cos(i_L/2)$ and

$$DP_1 = n' + 2\dot{\omega}_L - 2\dot{\Omega}_L,\quad DM_1 = n' - 2\dot{\omega}_L - 2\dot{\Omega}_L$$

$$DP_2 = n' + \dot{\omega}_L - \dot{\Omega}_L,\quad DM_2 = n' - \dot{\omega}_L - \dot{\Omega}_L$$

$$DP_3 = 3n' + 2\dot{\omega}_L - 2\dot{\Omega}_L,\quad DM_3 = 3n' - 2\dot{\omega}_L - 2\dot{\Omega}_L$$

$$DP_4 = 4n' + 2\dot{\omega}_L - 2\dot{\Omega}_L,\quad DM_4 = 4n' - 2\dot{\omega}_L - 2\dot{\Omega}_L.$$

The denominators of the terms in Equation 13a indicate the possibility of resonance phenomena in the situations where the angular elements ω_L and Ω_L change so rapidly that the frequencies of the terms in Equation 13a become small. Such a situation could occur if very strong oblateness perturbations were present. The development of formulae valid for such resonance situations would require a lengthy analysis that would probably so complicate the technique that the expressions would be of little practical value. An alternate approach that has been found useful in practice is to ignore the long-periodic changes in ω_L and Ω_L during the integration and thus obtain the following alternate function for use in Equation 12.

$$
\begin{aligned}
F^*_{(\text{alternate})} = 15/8 \, \frac{n' \mu'}{n} \Bigg\{ & Q_M \cos 2\phi' - Q_P \sin 2\phi' \\
& + Q_P e' \Big[\sin \phi' - 7/3 \sin 3\phi' + e' \, (5/2 \sin 2\phi' \\
& - 17/4 \sin 4\phi') \Big] - Q_M e' \Big[\cos \phi' \\
& - 7/3 \cos 3\phi' + e' \, (5/2 \cos 2\phi' - 17/4 \cos 4\phi') \Big] \\
& - e' \sin^2 i_L \sin 2\omega_L \Big[3 \sin \phi' + 9/4 \, e' \sin 2\phi' \Big] \Bigg\} .
\end{aligned}
\tag{13b}
$$

with

$$
Q_M = \sin^4 \left(\frac{i_L}{2}\right) \cos 2(\omega_L - \Omega_L) - \cos^4 \left(\frac{i_L}{2}\right) \cos 2(\omega_L + \Omega) \text{ and}
$$

$$
Q_P = \sin^4 \left(\frac{i_L}{2}\right) \sin 2(\omega_L - \Omega) + \cos^4 \left(\frac{i_L}{2}\right) \sin 2(\omega_L + \Omega_L).
$$

This alternate expression for F* circumvents a great many numerical difficulties but it must fail to describe a situation where terms of vanishing frequency dominate the motion. In such a situation, the double averaging theory should be abandoned in favor of more versatile techniques. The numerical integration of the singly averaged third-body equations would eliminate the difficulties.

The author feels that these resonance phenomena are worthy of further study in more than an academic sense. Resonance between medium-periodic third-body perturbations and oblateness effects could have a marked effect on the lifetimes of artificial Martian satellites.

In this analysis, we have not assumed (as in Reference 7) that e_{L_o} is the same as e_o. This modification complicates the method slightly but gives a considerably better representation of the long-periodic motion. The complication is that we must calculate a starting value for e_{L_o} by writing

$$e_{L_o} = e_o + e_o \sqrt{1 - e_o^2}\, f'(t_o) \tag{14}$$

The three terms of Equation (12) with subscript o can then be lumped into one constant of integration and the time history can be obtained as before.

The formulations above provide efficient means for one to obtain the time history of the eccentricity, including the medium-periodic variations, without having to solve the singly averaged equations. The idea is to collect the slowly varying parts of the equations (which may include oblateness and drag effects) and solve them by whatever means are most expedient. The medium-periodic variations in eccentricity can then be superimposed onto the long-periodic solution as in Equation (12). We shall show in later sections that this idea works well in practice and, in many cases, allows us to integrate numerically using an interval of several hundred days.

ATMOSPHERIC DRAG

In the following paragraphs, a method is presented that has found recent acceptance among several investigators of long-term orbit behavior. It allows study of the effects of various model atmospheres on highly eccentric orbits without the unrealistic assumption of an exponential density profile. The idea is to average the differential equations numerically by Gauss's mechanical quadrature formula and then to include these averaged rates of the orbital elements in the evaluation of the long-term motion of the orbit. We can integrate the averaged rates numerically using very large computing intervals or, if the rates are fairly linear, we can simply update the orbit

elements once per revolution of the satellite. The latter procedure (Euler's method) is not recommended for long simulations since the process is numerically unstable.

This method is capable of a great deal more than the purpose for which we use it here. For example, atmospheric rotation or asymetrical atmospheric models would present no problem for the quadrature formula since the technique requires only the values of the integrand at certain points. This is in sharp contrast to the analytic averaging of the previous section since, with Gauss's technique, we need not develop the accelerations in a convergent series.

For the purposes of this study, some standard assumptions will be made about the character of the atmospheric perturbations and use will be made of the Gaussian quadrature technique to describe the effects of a nonrotating atmosphere alone. In a later section, techniques will be recommended for further study to eliminate the need for all the assumptions except the realistic one of Newtonian flow.

For this study, we assume that the acceleration imparted to the satellite is given by

$$\vec{a} = -\frac{C_D A \rho}{2 m_s} |\vec{V}| \vec{V}$$

where

C_D = (constant) drag coefficient
A = (average) cross-sectional area of the satellite
m_s = mass of the satellite
ρ = atmospheric density
$\vec{V}$ = velocity and
$\vec{a}$ = acceleration.

The vector quantities are referred to a nonrotating coordinate system with origin at the planet's center.

Following McCuskey in Reference 11, we obtain for the rates of the Keplerian orbital elements

$$\frac{da}{dt} = -\frac{C_D A}{m_s} \frac{\rho V^2 \sqrt{1 + e^2 + 2e \cos f}}{n \sqrt{1 - e^2}}$$

$$\frac{de}{dt} = -\frac{C_D A}{m_s} \frac{\rho V^2 \sqrt{1 - e^2}\,(e + \cos f)}{na \sqrt{1 + e^2 + 2e \cos f}}$$

$$\frac{d\omega}{dt} = -\frac{C_D A}{m_s} \frac{\rho V^2 \sqrt{1 - e^2} \sin f}{nae \sqrt{1 + e^2 + 2e \cos f}} \qquad (15)$$

where n is the mean motion and f is the true anomaly. We now average these equations over one revolution of the satellite, writing the integral in terms of the true anomaly to obtain the following equations for the average rates of the orbit elements:

$$\frac{da_L}{dt} = -\frac{C_D A}{2\pi m_s}(1 - e_L^2)^{3/2} \frac{a_L^2}{k^2 m} \int_{-\pi}^{\pi} \frac{\rho(f)\, V^3(f)\, df}{(1 + e_L \cos f)^2}$$

$$\frac{de_L}{dt} = -\frac{C_D A}{2\pi m_s}(1 - e_L^2)^{3/2} \int_{-\pi}^{\pi} \frac{\rho(f)\, V(f)\, (e + \cos f)\, df}{(1 + e_L \cos f)^2}$$

$$\frac{d\omega_L}{dt} = -\frac{C_D A}{2\pi m_s} \frac{(1 - e_L^2)^{3/2}}{e_L} \int_{-\pi}^{\pi} \frac{\rho(f)\, V(f) \sin f\, df}{(1 + e_L \cos f)^2} \qquad (16)$$

where it is to be understood that the integrations are performed by Gaussian quadrature with the assumption that the orbit is Keplerian during the integration. This is exactly what happens during the analytic averaging process except that now we are not required to find analytic expressions for the integrands.

In the above equations, we have written the density as a function of true anomaly. Since the radius vector and, therefore, the altitude are defined by the true anomaly in two-body motion, we can consider the density to be a function of the true anomaly. The density function may also depend upon the orientation of the orbit in space and the geometric flattening of the planet. These complications present no theoretical difficulties since the orbit elements (assumed constant during the integration) along with the true anomaly define the position of the vehicle in space. Therefore, they define the density for any atmospheric model (no matter how complicated).

In the next sections we shall assume that the density is a function only of altitude above a spherical planet. This implies that $\rho(f)$ is an even function of cos (f) which implies that the average rate of change of the pericenter argument, $\dot{\omega}_L$ is zero and that the third of Equations (16) may be dropped. This simplification would not be valid if a non-symmetric atmosphere model (such as the Jacchia Earth model of Reference 12) were used. Similarly, the equations for the average rates of inclination and node position would no longer be zero if a rotating atmosphere were simulated. Westerman (Reference 13) states that errors of several percent in the averaged rates can be incurred if we ignore the rotation of Earth's atmosphere.

The complexities above are pointed out to show that we have barely scratched the surface of the atmosphere problem. In Section 4, we shall suggest methods that will not only resolve the difficulties above, but will also deal with the very complex problem of coupling between the short-periodic oblateness effects and those of atmospheric drag.

Section 3

PRACTICAL CONSIDERATIONS

FOUR PLANET SURVEY

It is the major intent of the author to present the important aspects of the orbit evolution problem for satellites of the four inner planets. The theoretical considerations of Section 2 are tools to aid in the attainment of the primary goal--an understanding of the complex dynamical relationships of satellite motion. It is important to note that the general solution to the real-world problem of satellite motion is unknown to our science and that we must resort to approximate techniques to predict the motion of satellites. Even the most sophisticated techniques must fail if we try to predict too far into the future. It is of interest, then, not only to determine what the major perturbations are, but also to evaluate the approximate techniques available to us for orbit prediction in the context of their accuracy and efficiency as study tools.

There are three principal disturbing effects that will cause satellites of each planet to deviate from two-body motion. Before separate discussions of each planet are begun, general descriptions of the three disturbing forces are in order. The three effects are (1) third-body perturbations, (2) central-planet nonsphericity, and (3) atmospheric drag. In the separate discussions of each planet, the three forces are evaluated in terms of their effects on orbit evolution (particularly on lifetime) and the ranges of orbit parameters in which the approximate techniques of Section 2 may and may not be used are determined. The survey is followed by a discussion of the factors which were neglected and a final section recommends the development of a system of computer subprograms that will permit efficient study of the orbit evolution problem from preliminary mission design to final orbit selection.

Third Body Perturbations

The effect of the Sun on the motion of the first Mercury and Venus orbiters will almost certainly be the major disturbing force for those satellites. Unless our best estimates of the dynamic flattening and atmospheric densities of the planets are much too small, the Sun's influence will be the primary contributor to changes in orbit shape and will effectively determine the lifetimes. Obviously, at some point during the life of a satellite whose pericenter altitude is descending to the surface of the planet, atmospheric drag will take over and dominate the motion. Presumably, the orbit will have been designed to start out above the effective atmosphere and we conclude that, initially, the solar gravitational field will be the dominant perturbing force. This is not the case for Earth and especially for Mars. The dynamic flattening of these planets is sufficient to disturb satellites more strongly than the Sun and the Moon over a significant range of possible orbits. Later we shall discuss this coupling of third-body and oblateness perturbations and isolate the regions where one or the other effect is dominant. First let us take up the effects of third-body perturbations alone.

In the early 60's, several authors (References 1, 3 and 4), independently applied averaging techniques to the differential equations of satellite motion disturbed by a third body. By averaging the equations initially over one revolution of the satellite in its orbit and then over one revolution of the disturbing body around the central primary, these authors were able to derive and solve the doubly averaged equations for the very long-term motion of the orbit. Among the significant analytic results of this fine work was the discovery that the average change in the energy of the orbit vanishes up through terms of second order in the ratio of satellite distance to disturbing body distance (r/r'). A more startling result, however, was that for high-inclination orbits, the eccentricity could increase to very large values (approaching 1 for polar orbits). Lidov (Reference 1) indicated that this phenomenon could be an explanation for the infrequency in the solar system of satellites highly inclined to the orbit planes of their parent planets. He then considered the counter example of the satellites of Uranus (whose orbits are almost perpendicular to Uranus' orbit plane) and subsequently showed that the oblateness of the seventh planet is sufficient to offset the instability caused by the solar gravitational field.

In 1966, it was found possible to superimpose the medium-periodic variations in eccentricity onto the long-term changes (Reference 7). This technique (described in Section 2) was found useful in predicting the very large pericenter deviations of strongly perturbed lunar satellites. The work brings out two basic qualitative results. First, the long-periodic eccentricity variations are most pronounced at high inclinations and the medium periodic variations are largest at low inclinations. Secondly, the medium-periodic variations depend upon the magnitude of the eccentricity. Hence, as the eccentricity increases under the influence of long-periodic perturbations, the magnitude of the medium-periodic variations will increase accordingly. This implies that, as the pericenter altitude approaches zero, the medium-periodic variations become increasingly important not only because they are larger but also because there is less room for variation before the pericenter radius becomes less than the effective planetary radius.

More specifically, Lidov showed that the maximum value of the long-periodic eccentricity is given by

$$e_{L_{max}} = \sqrt{\frac{1}{2}\left\{\left[1 - \frac{5}{3}(C_1 + C_2)\right] + \sqrt{\left[1 + \frac{5}{3}(C_1 + C_2)\right]^2 - \frac{20}{3}C_1}\right\}}$$

where

$$C_1 = (1-e_{L_o}^2)\cos^2 i_{L_o}$$

and

$$C_2 = e_{L_o}^2\left(\frac{2}{5} - \sin^2 i_{L_o} \sin^2 \omega_{L_o}\right).$$

This implies that, within the framework of the doubly averaged system, all eccentric polar orbits whose initial pericenter argument is within certain ranges (see Reference 5) will ultimately impact the central planet. The above statement, although subject to qualification in the real-world case, is certainly an indication that highly inclined orbits can have short lifetimes.

That this is the case in the real world is readily ascertained by numerical integration or reference to the ephemerides of some highly eccentric Earth orbits designed to be nearly normal to the ecliptic. To be more specific about the time scale, we consider a short lifetime to be less than a planetary year and a long lifetime to be greater than 15 Earth years. These rather arbitrary definitions come from scientific and planetary quarantine considerations respectively.

Reference to the doubly averaged Equation (1) will show that the stronger the disturbing function (or, equivalently, the larger the orbit), the higher the frequency of the long-periodic terms. In most cases (singularities excepted), the larger the orbit, the shorter the long-periodic cycle. Orbits for which $\sin^2 i_L \sin^2 \omega_L = 2/5$ are examples of asymptotic behavior of the elements. If the eccentricity is increasing initially it continues to increase to some maximum value and then will asymptotically approach zero. If, however, the maximum value is greater than the critical value, the spacecraft will impact before the eccentricity reaches its maximum. Orbits of this type, then, can be considered safe if the eccentricity is decreasing initially ($\sin 2\omega_o < 0$) and unsafe if $(de_L/dt)_o > 0$.

In a more practical sense we may ask if such considerations have much significance on a 15-year time scale. The kinds of orbits with which mission analysts will be primarily concerned are not strongly enough perturbed by third-body effects to go through more than a portion of a long periodic cycle in a 15-year period. The questions of importance from a lifetime standpoint are:

1. Will the eccentricity increase to the critical value? and, if so,
2. How long will it take?

The answer to the first question depends upon the initial eccentricity, inclination and argument of pericenter. The maximum long periodic eccentricity the orbit will attain does not depend upon the semi-major axis. The medium-periodic eccentricity variation, δe, does depend on a_L as well as the three quantities mentioned before - e_L, i_L, and ω_L - since δe_{max} depends upon the maximum value of e_L. The relative phase of the long- and medium-periodic terms is also important in the marginal cases where

$e_{L_{max}}$ is near the critical eccentricity. But the marginal cases are rare in practice and it is usually easy to determine whether or not the eccentricity will reach the critical value. We are then faced with the second question--if the satellite will impact, when will it happen?

Williams and Lorell (Reference 4) have given explicit formulae for lifetime in the sense of the doubly averaged Equations (1). No doubt, an inversion of Equation (12) of this report would put some light on the problem where the medium-periodic effects are concerned. But the reader would have little more practical information at the end of such an analysis than at the outset. Moreover, any concrete results would be immediately invalidated by the presence of strong oblateness effects. For these reasons, we present the following qualitative discussion in response to the second question posed.

One may imagine a plot of long-periodic eccentricity versus time as a sine wave extending to infinity in both directions along the time scale. The orbit's position on the sine wave at any instant depends upon the value of the argument of pericenter. The extreme values of e_L occur when sin $2\omega_L$ is zero. For a given inclination, the eccentricity will have its largest rate of change when sin $2\omega_L$ is equal to 1 (ω_L = 45° or 225°). If a satellite of Venus or Mars remains within about 50,000 km of the planet, the third-body effects on ω_L are so small that only a small segment of the e_L versus time curve is covered in a 15 year period and, <u>if no oblateness is present</u>, the long-periodic eccentricity variation is nearly linear in time. If we wish the long-term third-body perturbations to raise the pericenter, a good rule of thumb is to choose ω_L near 135° or 315°. If we want no long-periodic change in pericenter altitude, ω_L should be near 0°, 90°, 180°, or 270°; ω_L = 45° or 225° will lower the pericenter at the maximum rate. We can obtain an estimate of the lifetime by a simple calculation.

$$\text{Lifetime} = \frac{(e_{crit} - e_{Lo})}{\left(\frac{de_L}{dt}\right)_o}$$

but such an approximation should be used only when we are certain that we are operating on a linear portion of the e_L versus time curve and when no significant oblateness is present.

If the initial eccentricity is close enough to the critical value and the medium-periodic terms are large enough to make up the difference, the vehicle may impact during the first half planetary year. Reference to Equations (12) and (13) will show that the medium-periodic eccentricity variations are maximized at low inclinations (where the long-periodic variations are at a minimum). At these low inclinations the medium-periodic variation δe can be as large as

$$\delta e = \frac{15}{8} \frac{n' \mu'}{n} \left(1 + \frac{4}{3} e'\right) e \sqrt{1 - e^2}.$$

This is the maximum δe to first order in e' if the long-periodic rates of ω_L and Ω_L are negligible.

Using this value and assuming that the eccentricity starts out on the bottom of a medium-periodic cycle, we can define the regions in which the above medium-periodic variations can cause short lifetimes. This does not imply that other regions are safe from a lifetime standpoint but that the regions called out as possible short lifetime regions are probably marginal and selection of orbits in those ranges could result in very short missions.

The dot-dashed curves of the figures to be presented later were generated as if the planets were 150-km larger in radius than they actually are to account for very strong atmospheric effects. To be strictly correct, we should place these curves above the 1-year (or half-year) atmospheric effects lifetime curves (to be described later). Such information, however, would be overly conservative since we do not expect the atmosphere to be at a maximum but, rather, we wish to know what would happen if it were. To add the maximum medium-periodic effects to those of a maximum atmosphere would be unrealistic since neither of these "worst" effects is very likely.

Third-Body Oblateness Coupling

It has been known for some time that the effects of the oblateness of the central planet, when coupled with third-body perturbations, can cause the orbital eccentricity variations to change radically from those which would

occur if third-body perturbations were present alone. It is important to understand how this phenomenon comes about in order to explain the effects of oblateness on satellite lifetime.

The long-periodic variations in eccentricity, e_L, caused by third-body perturbations are dependent upon the variations in argument of pericenter, ω_L, since the doubly averaged rate of change of eccentricity is proportional to the sine of twice ω_L. That is,

$$\frac{de_L}{dt} \sim \sin 2\omega_L$$

The eccentricity will go through two long-periodic cycles as ω_L goes through one cycle. As long as $\sin 2\omega_L$ remains positive, the eccentricity will increase and may reach the critical value at which the pericenter distance becomes less than that of the effective atmosphere. Clearly, these perturbations to the orbit occur whether or not the central body is oblate. However, if oblateness dominates the motion of the argument of pericenter, the time history of the eccentricity will change accordingly. In addition, if ω_L changes rapidly because of oblateness, and does not remain in the same quadrant very long, the eccentricity will not have time to increase so much as it would have if only third-body perturbations were present. We may, therefore, expect e_L to oscillate with about twice the frequency of ω_L if oblateness perturbations are strong compared with those resulting from a third body.

If, however, the changes in ω_L caused by the two disturbing forces are of the same order of magnitude, the motion may become extremely complex. For example, the oblateness perturbations may nearly cancel the change in ω_L due to a third body in such a way as to cause ω_L to remain essentially constant. In such a situation, the eccentricity could increase to the critical value where it may not have done so if the oblateness effects were absent.

Finally, if the oblateness perturbations are no more than a few percent of the third-body effects, we may expect the eccentricity to behave nearly as it would if no oblateness were present. The main point of the above discussion is that it is through the argument of pericenter that the coupled effects

of oblateness and third body perturbations act on the shape (and lifetime) of the orbit. The understanding of this coupling mechanism leads to a natural way of classifying the orbits. To this end we define strong coupling between the two effects as the situation which exists when the maximum rate of change of argument of pericenter caused by either disturbing force is within one order of magnitude of the maximum rate due to the other disturbing force.

The maximum first order rate of change of $\bar{\omega}_L$ (the argument of pericenter with respect to the equatorial plane) resulting from oblateness alone is

$$\left|\frac{d\bar{\omega}_L}{dt}\right|_{max} = \frac{2Jr_e^2}{a_L^2(1-e_L^2)^2}$$

with $J = 3/2\ J_2$ and r_e the equatorial radius of the oblate planet. We have chosen the equatorial element, $\bar{\omega}_L$, in order to simplify the definition of strong coupling.

The maximum long-periodic rate of change of ω_L (measured with respect to the central planet's orbit plane) due to third body perturbations alone is

$$\left|\frac{d\omega_L}{dt}\right|_{max} = \frac{15}{4}\frac{n'^2\mu'}{n}\frac{(1+\frac{3}{2}e'^2)}{\sqrt{1-e_L^2}}\left|\left[(\cos^2 i_L - 1 + e_L^2)\sin^2\omega_L + \frac{2}{5}(1-e_L^2)\right]\right|_{max}$$

where i_L and ω_L are chosen in such a way as to maximize $\left|d\omega_L/dt\right|$ for a given value of e_L. A few numerical experiments will show that, if the quantity $1-e_L^2$ is less than about 0.85, the maximum value of the quantity in square brackets is $3/5\ e_L^2 + 2/5$. If $1-e_L^2$ is greater than about 0.85, the square bracket can become as negative as $-3(1-e_L^2)/5$.

We can now determine the values of a_L and e_L at which the maximum rates due to the two perturbing forces are numerically equal. This definition need not correspond to a particular physical situation--indeed, for arbitrary

inclination of the equator to the planet's orbit plane, it is not always possible to have both effects maximized for the same orbit. The point is that we can define the regions where one effect is likely to dominate the other as well as regions where the two effects will probably interact strongly. The figures, to be presented after these preliminary remarks, will show (in terms of pericenter and apocenter altitudes) the regions where strong coupling is likely to occur. The figures do not imply that strong coupling cannot occur elsewhere -- the regions on either side of the strong coupling region for Mars are susceptible to many complexities including the resonances discussed in Reference 14.

Consider an imaginary planet whose equator lies in the orbit plane of the planet around the sun. A satellite whose inclination were 63.4° to the two planes would experience no first order oblateness effects on argument of pericenter. Its orbital eccentricity then, could be expected to change almost as if no oblateness were present. Conversely, an orbit whose pericenter argument is minimally disturbed by third-body perturbations might be strongly influenced by the oblateness of the planet even though the orbit lies well above the strong coupling region. These examples serve to point out the kinds of problems we may expect to encounter in planetary satellite mission analysis and suggest a need for approximate techniques that can deal efficiently with the difficulties.

Atmospheric Effects

The effects of atmospheric drag on orbit evolution are far more complex than the perturbations discussed previously. The difficulties become almost insurmountable at high (above 300 km) altitudes because of the dynamic nature of upper atmospheres. Fortunately, some simplifying assumptions permit us to study the effects of various assumed atmospheric models. The primary assumption is that of a static density profile where the density is a function of altitude only. By studying the effects of a "worst possible" density function we can draw some conclusions about the ranges of orbit altitudes where atmospheric effects can and cannot be ignored.

In this survey, no attempt is made to describe or evaluate the coupling effects between atmospheric perturbations and the other disturbing forces.

That this is a formidable problem is readily seen from the theory developed by Brouwer and Hori (Reference 15) where an exponential atmosphere was assumed and the results are valid only for moderately eccentric orbits. We shall, however, describe the uncoupled effects of drag on lifetime in order to isolate the regions in which atmosphere alone can prevent satisfactory lifetime. Later we may argue that a region where both drag and some other perturbing effect cause low lifetimes will probably be a good region to avoid. On the other hand, it may be possible to select orbits where the other disturbing forces (by raising the pericenter) reduce the effects of drag to a negligible level. Such "balanced" orbits, however, should be studied with care and numerical integration.

The technique used to study the drag problem is described in an earlier section and consists of a numerical integration of a set of numerically averaged differential equations. Atmospheric rotation is neglected as being insignificant compared with our lack of knowledge of the upper atmosphere and the potential fields of the planets. The technique does not suffer from convergence problems at high eccentricities nor are any assumptions made about the density versus altitude function. If we keep in mind that the results obtained by this technique are not the complete solution to the atmosphere problem, we can gain a valuable "feeling" for the dynamics and the numbers.

Figures 3.1.1 through 3.1.4 show contours of constant orbit period (sublabel a) and the regions in which the major disturbing forces act on artificial satellites of the four inner planets (sublabel b). The displays are in terms of pericenter and apocenter altitudes above a fixed mean planetary radius. The figures are presented in order of ascending distance from the Sun for ease of reference but, for the purposes of discussion, let us begin with Venus (Figure 3.1.2).

Venus

Venus is only slightly smaller and slightly less massive than the Earth. The nearness of Venus to the Sun, however, makes the solar gravitational disturbing function for a Venus orbiter almost 2 1/2 times larger than that

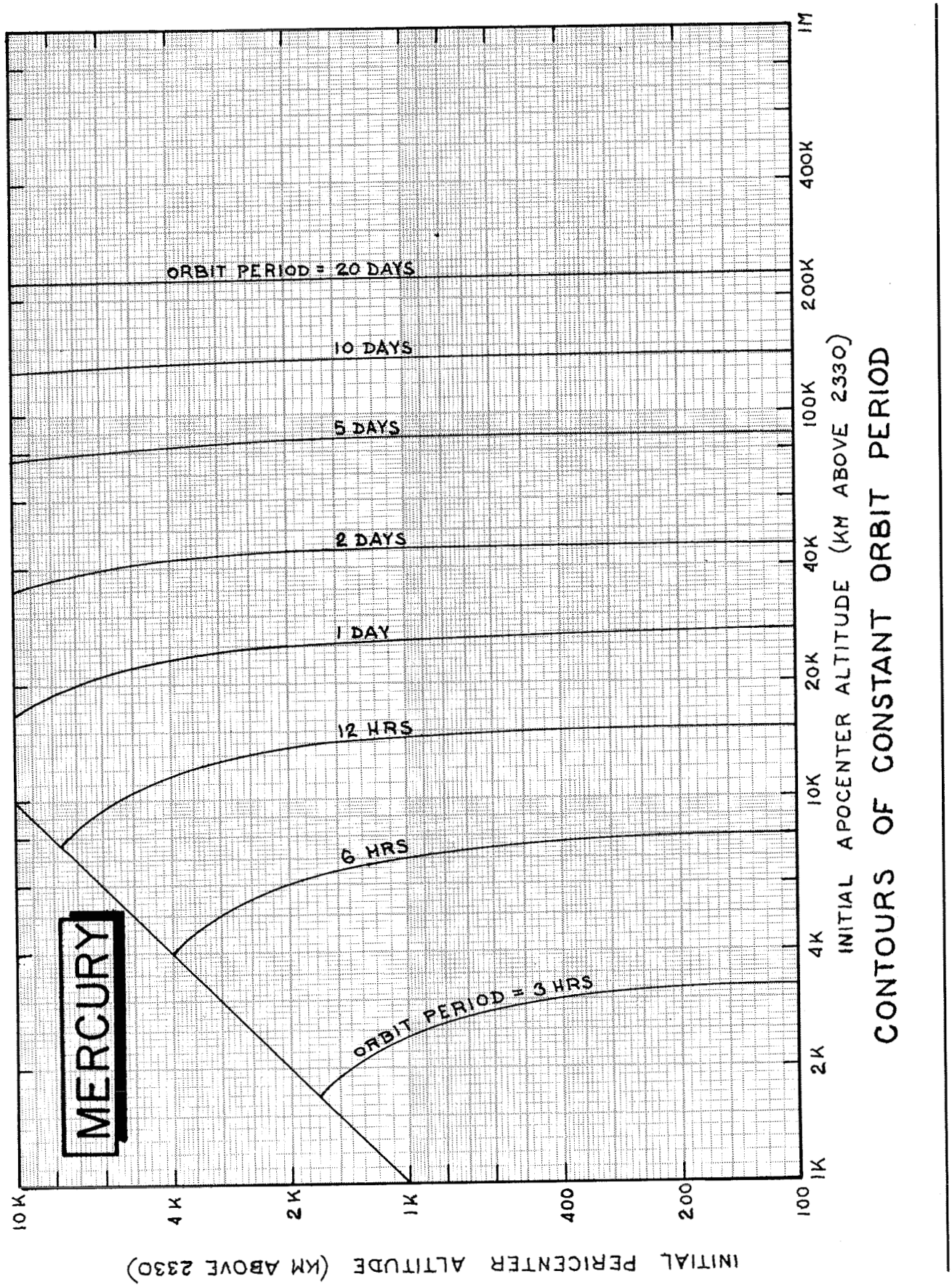
CONTOURS OF CONSTANT ORBIT PERIOD
MERCURY
ORBIT PERIOD = 20 DAYS
10 DAYS
5 DAYS
2 DAYS
1 DAY
12 HRS
6 HRS
ORBIT PERIOD = 3 HRS
INITIAL APOCENTER ALTITUDE (KM ABOVE 2330)
1K
2K
4K
10K
20K
40K
100K
200K
400K
1M
INITIAL PERICENTER ALTITUDE (KM ABOVE 2330)
100
200
400
1K
2K
4K
10K

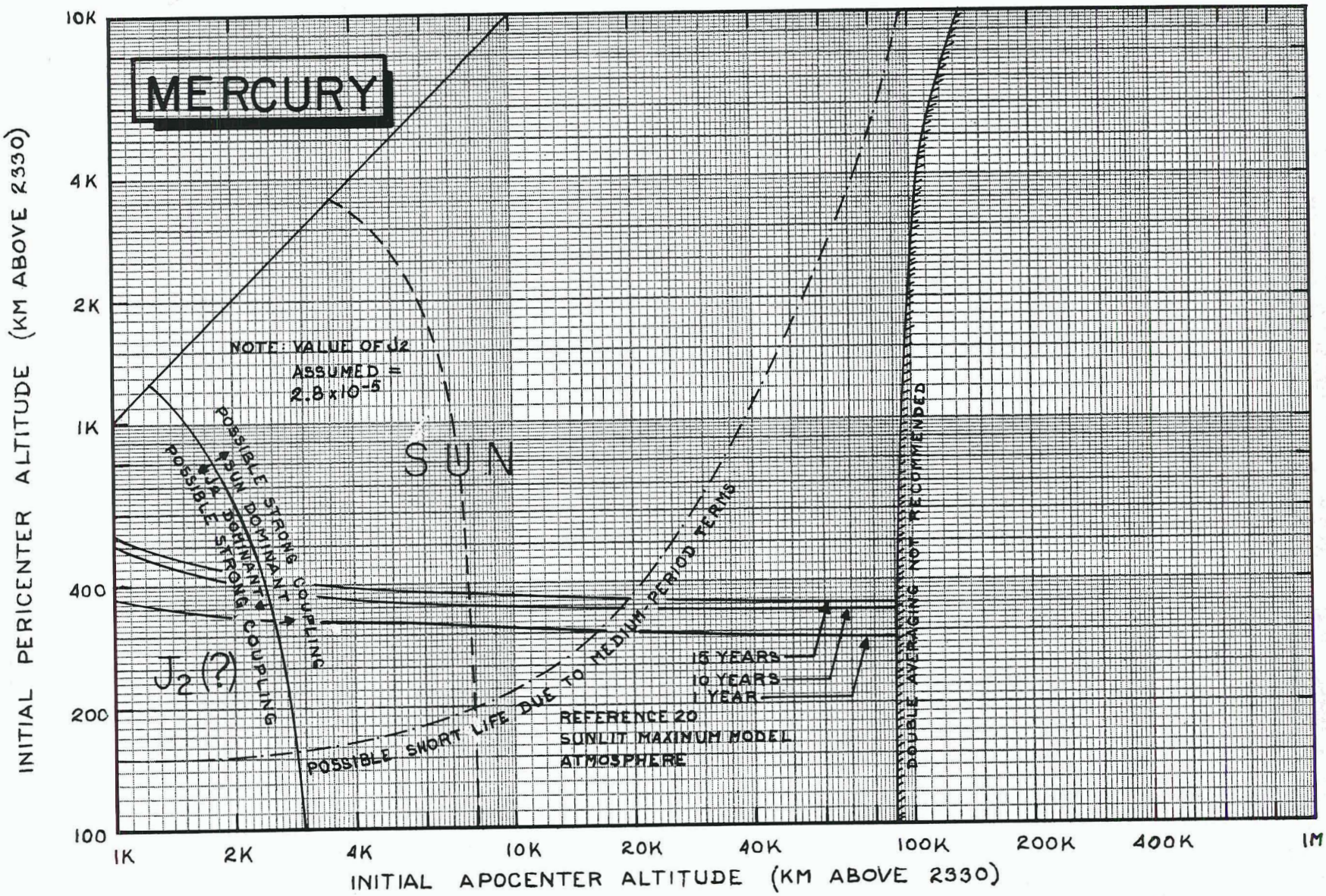

PERTURBATIONS TO THE ORBITS OF MERCURIAN SATELLITES

Figure 3.1.1b
Contract No. NAS 5-10782

Figure 3.1.2a

Contract No. NAS 5-10782

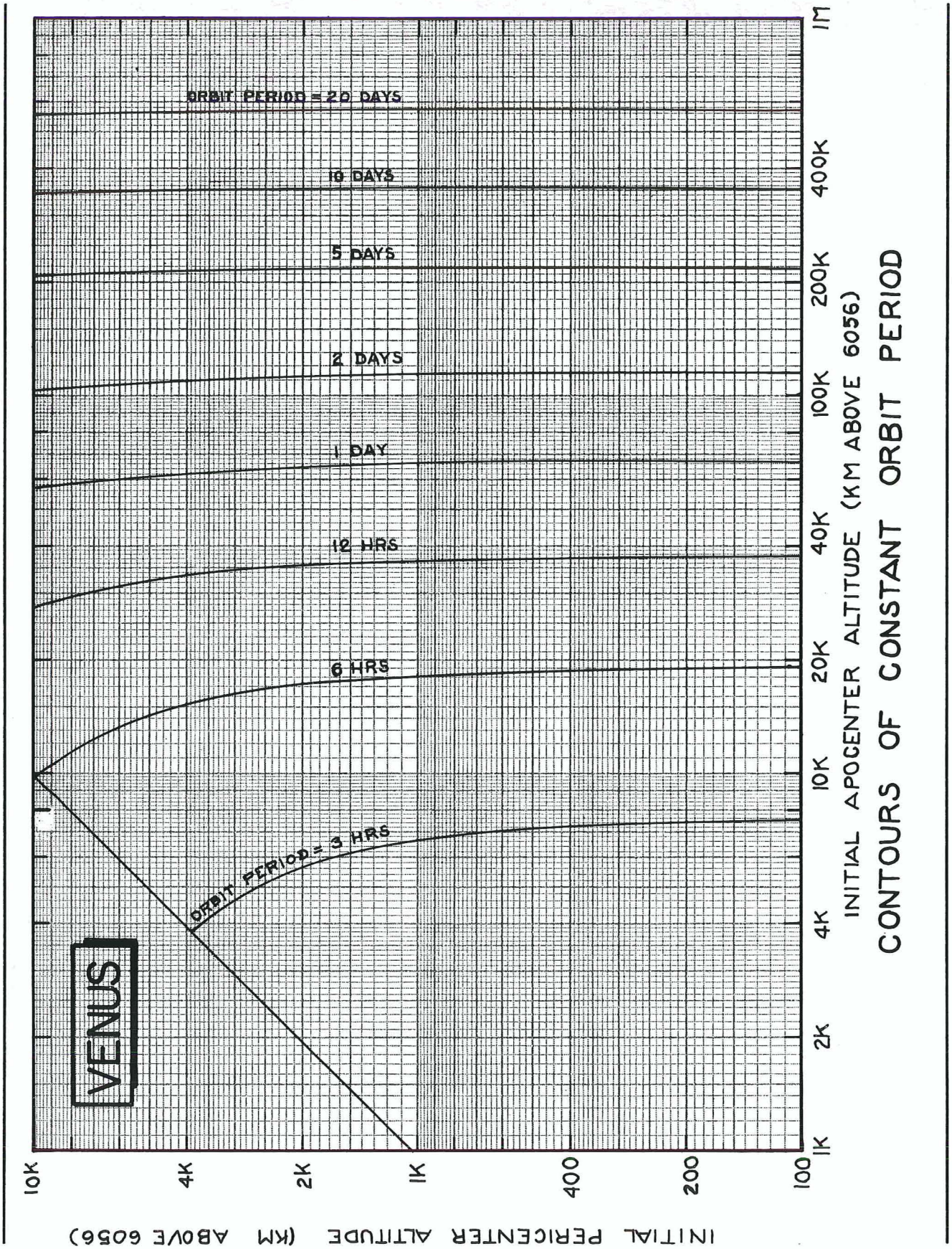

Figure 3. 1. 2b

Contract No. NAS 5-10782

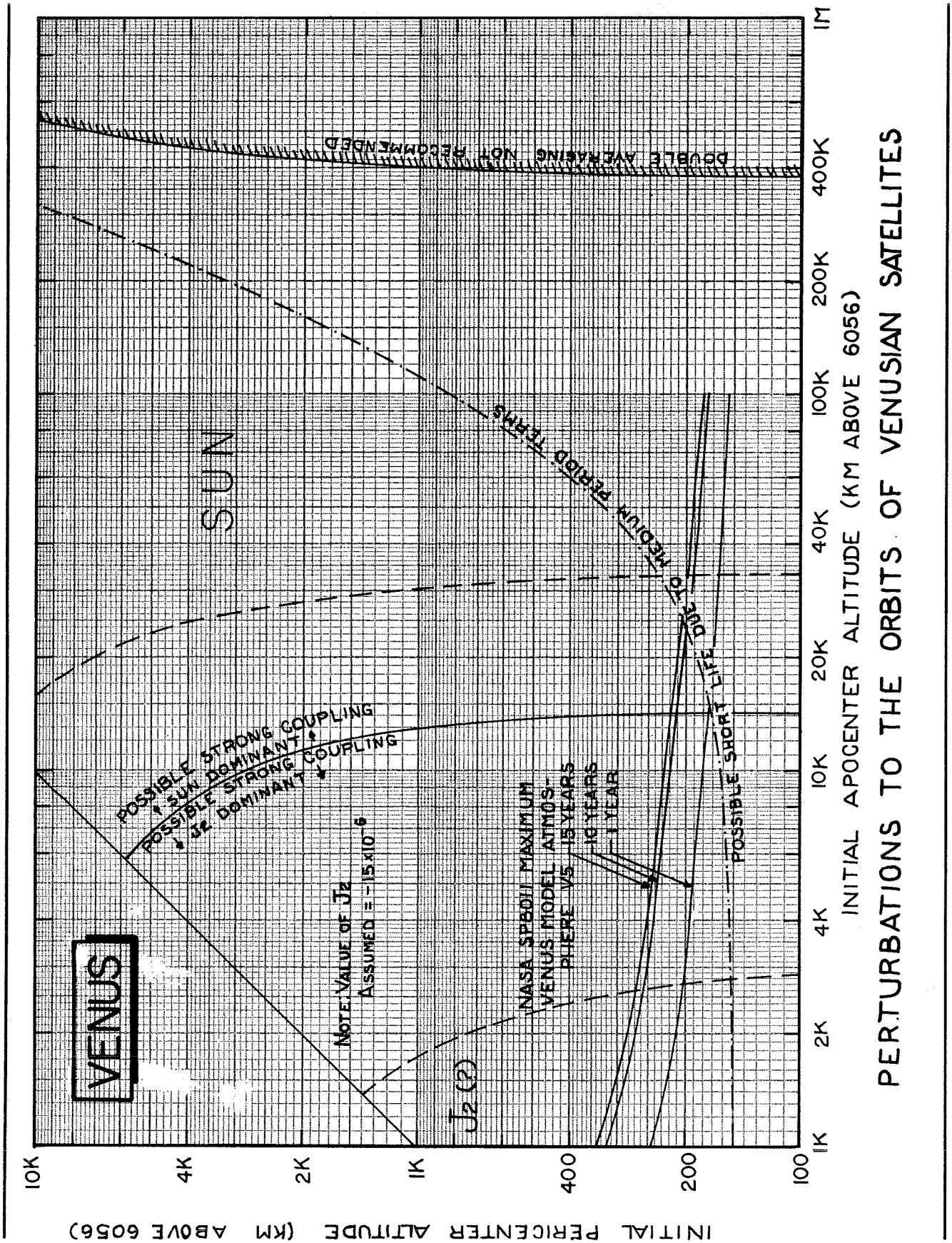

Figure 3.1.3a

Contract No. NAS 5-10782

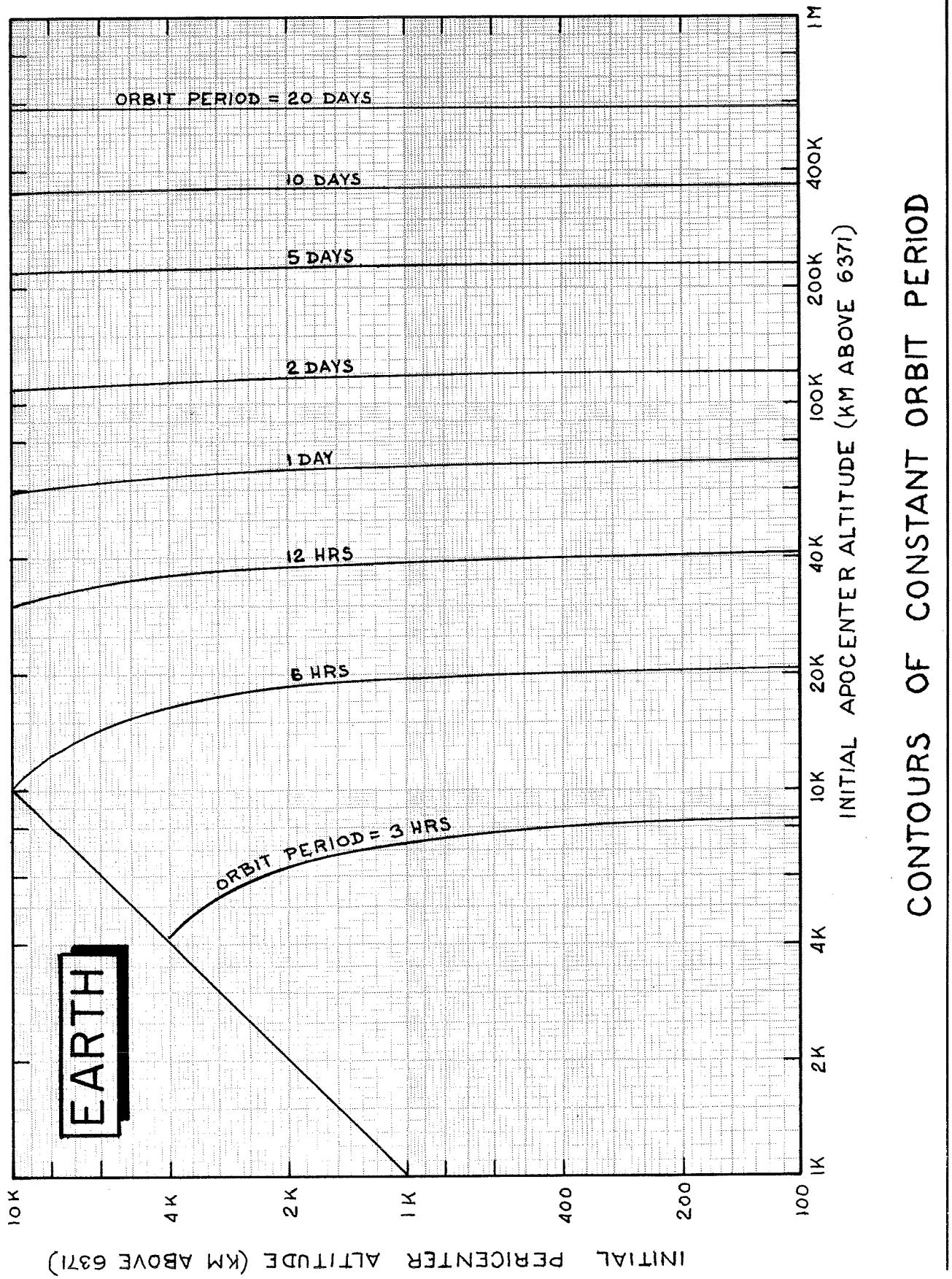

Figure 3.1.3b
Contract No. NAS 5-10782

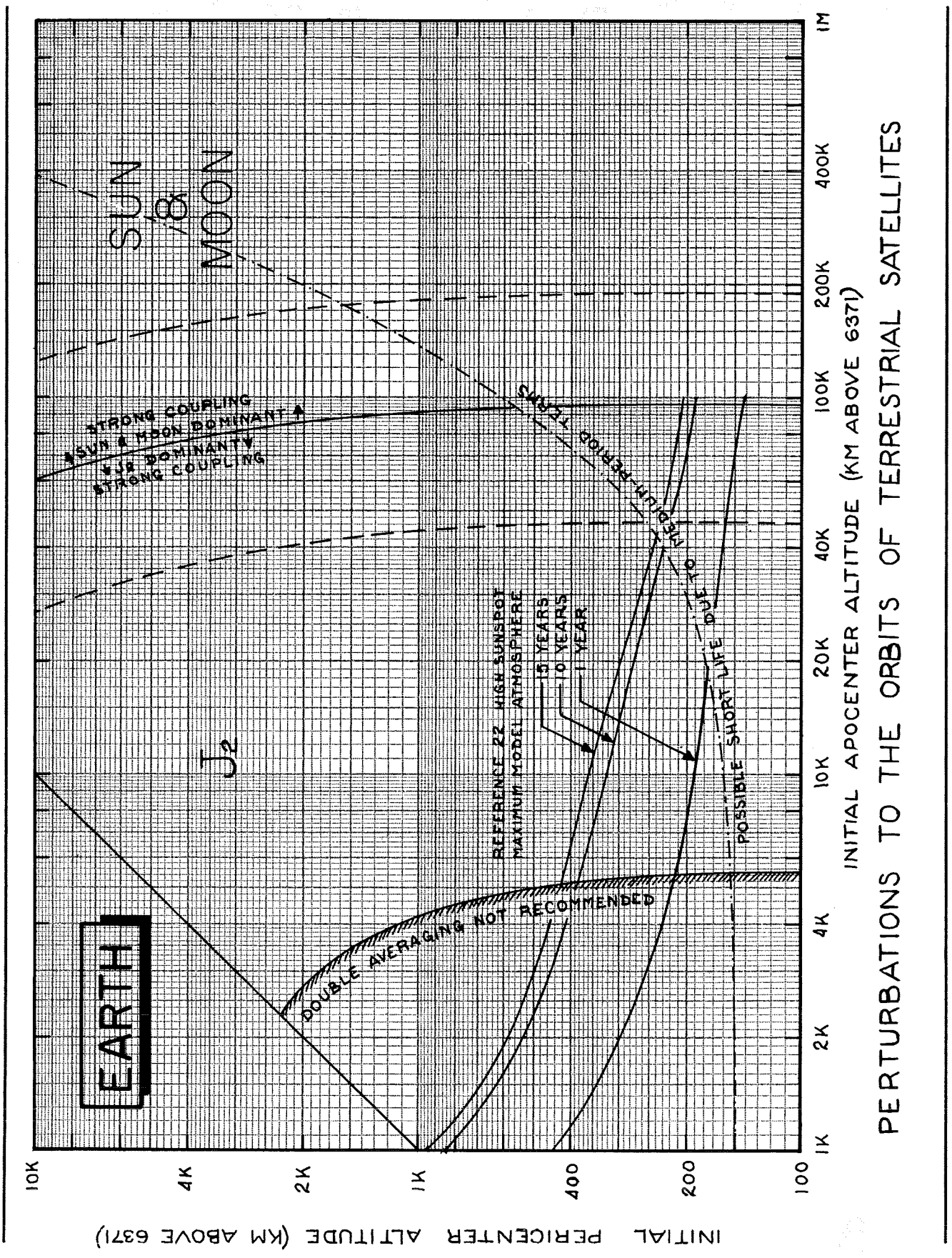

Figure 3. 1. 4a

Contract No. NAS 5-10782

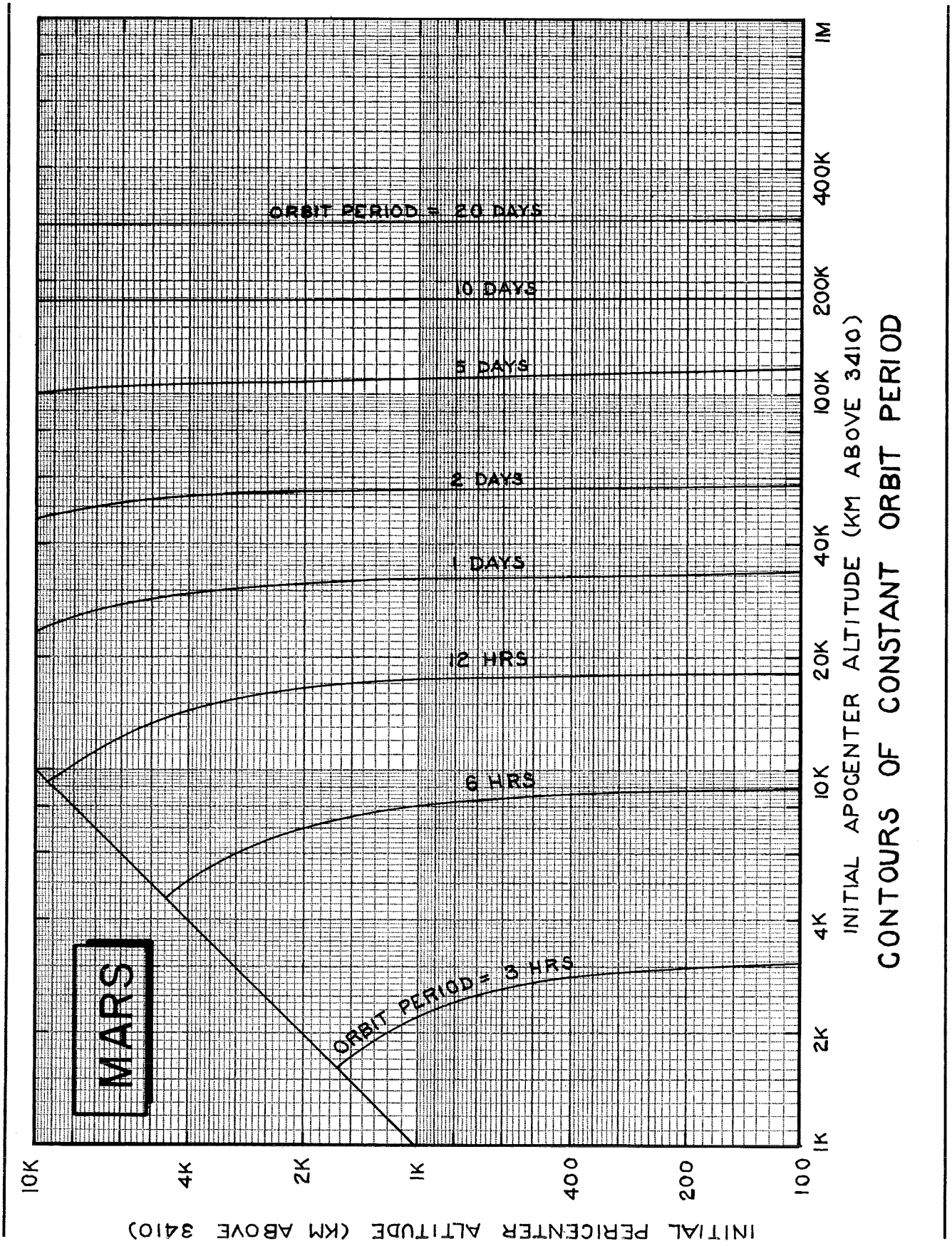

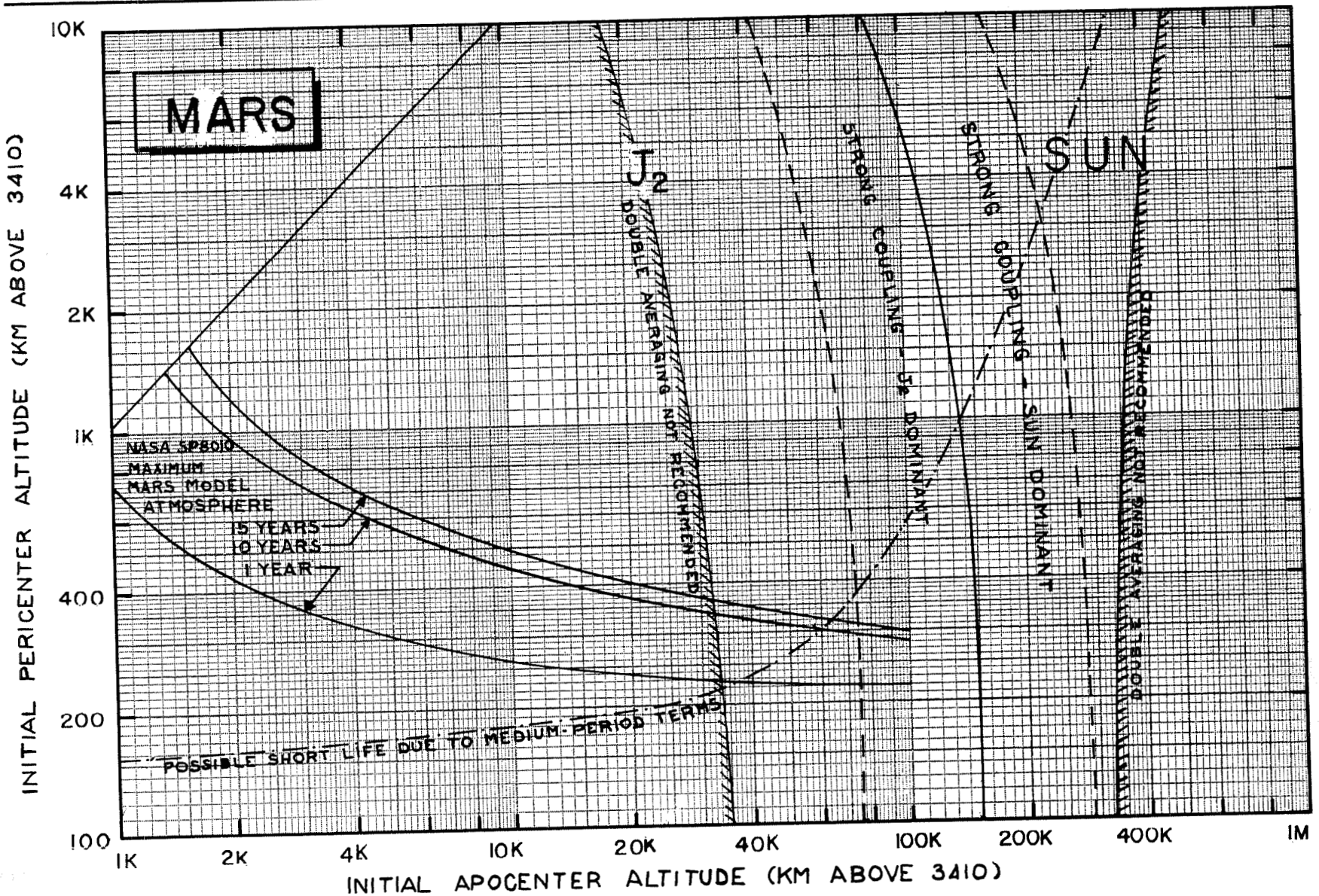

PERTURBATIONS TO THE ORBITS OF MARTIAN SATELLITES

Figure 3.1.4b
Contract No. NAS 5-10782

for an Earth satellite with the same orbital period. The results of Anderson's determinations (Reference [illegible]) of the oblateness of Venus indicate a very small value for J_2. The [illegible]ble lack of signifi[illegible]nt oblateness indicates that, for Venus, the dominant perturbing forces will be the solar gravitational field and (below about 300-km altitude) the Venusian atmosphere.

The largest magnitude of J_2 (-15×10^{-6}) for Venus reported to date was used in Figure 3.1.2 to show a possible (although not likely) strong coupling region between oblateness and third-body perturbations. In the figure, a solid line starting at about 14,000 km on the apocenter altitude scale rises almost vertically and slowly curves to the left. This curve will be called the equal perturbation curve in this and subsequent discussions. On either side of the equal perturbation curve is a region of strong coupling set off by dashed curves having almost the same shape. The left-hand dashed curve will be called the lower strong coupling curve and the right-hand dashed curve will be referred to as the upper strong coupling curve. The equal perturbation curve is defined as the locus of points where the maximum rate of change of argument of pericenter (magnitude only) caused by the third-body perturbations is equal to the [illegible]imum rate resulting from (the assumed) oblateness.

The region inside the dashed curves is the region where we can expect the motion to become very complicated because of third-body-oblateness coupling if we assume that J_2 for Venus is as large in magnitude as assumed in the calculations for Figure 3.1.2. But the magnitude of J_2 is probably about 1/10 of the value assumed here. (J. Anderson has recently stated that his current best estimate of J_2 for Venus is zero ($\pm 10 \times 10^{-6}$).) In that case the equal perturbation curve would become the upper strong coupling curve, since the rate of $\bar{\omega}_L$ varies linearly with J_2. We can, therefore, expect almost no coupling if the apocenter altitude is above about 14,000 km. The energy required to inject a spacecraft into such a small orbit will probably be prohibitive for many early missions and, in those cases, we can expect to

deal with third-body perturbations alone. For these reasons the following quantitative information will be presented for the situation where no oblateness is present. Later we shall check to ascertain the effects of various assumed values of J_2 on some of the examples. This philosophy is recommended for design purposes until more is known about the gravitational field of Venus.

The alternately dotted and dashed curve of Figure 3.1.2 sets off the region where the maximum medium-periodic variations in eccentricity (under the influence of third-body perturbations alone) will cause the pericenter altitude to drop to 150 km. To obtain the maximum variations, we assumed that the inclination of the orbit to Venus' orbit plane was zero and used the formula:

$$\delta e_{max} = \frac{15}{8}\frac{n'\mu'}{n}\left(1+\frac{4}{3}e'\right) e \sqrt{1-e^2}.$$

The pericenter variation due to twice δe_{max} was used to determine the dot-dashed curves of Figures 3.1.1 - 3.1.4. As the inclination increases, the medium-periodic terms decrease in magnitude, but the long-periodic terms increase so that a smaller δe can still cause the pericenter altitude to fall below 150 km. If a long lifetime is desired, the orbit should certainly not be chosen below (or to the right of) the dot-dashed curve. Orbits near the curve should be selected with care to avoid the possibility of a short lifetime as a result of a combination of the long- and medium-periodic variations in eccentricity.

The curves labeled 15 years, 10 years and 1 year are curves of constant lifetime under the influence of the (non-rotating) NASA SP8011 maximum density, maximum solar activity model Venus atmosphere V5 (Reference 17). The curves were generated by the technique described earlier with the assumption of Newtonian flow and constant drag coefficient ($C_D = 2.0$) for an

assumed vehicle whose mass is 150 kilograms and whose effective cross section is 2.25 square meters. The curves of constant lifetime in Figure 3.1.2 were obtained from Figure 3.1.5, which shows lifetime versus initial pericenter-altitude for curves of constant initial apocenter altitude. Some liberties were taken with the fairing of the curves and the lifetimes shown may be in error by several hundred days near the tops of the curves.

The character of the atmosphere is clearly shown in Figure 3.1.5. The atmosphere is very dense below 150 km and almost non-existent above 300 km. The very sharp drop in density between 100 and 300 km is seen in Table II-2 of Appendix II which was taken from page 16 of Reference 17[1]. The density falls off over 8 orders of magnitude in the 200 km span. When we come to the discussion of Mars's atmosphere, we shall find a different story. It turns out that the "thin" model atmospheres of Mars have much larger effects on lifetime than the "thick" Venus models.

The shaded curve near the right margin of Figure 3.1.2 sets off the region beyond which the third-body perturbations are so strong that one of the assumptions of the averaging theory may be violated. The assumption is that the quantities ω_L, Ω_L, $\omega_L - \Omega_L$ and $\omega_L + \Omega_L$ are slowly varying during one revolution of the disturbing body around the central primary. Experience has shown that the rate of change of Ω_L is typically about half of that of ω_L. The shaded curve, then, sets off the region where the maximum value of ω_L is 2/3 of the disturbing body's mean motion, or, for Venus, 1.1 degrees/day. It is recommended that orbits to the right of the shaded line be simulated by numerical integration of the singly averaged or unaveraged (actual) equations of motion.

In Figure 3.1.2 there is a conspicuous absence of information about the long-periodic, third-body effects on lifetime. The reason for this omission is that the perturbations depend so markedly on inclination and argument of pericenter that it is necessary to present the information on several diagrams. Figures 3.1.6, 3.1.7 and 3.1.8 show the effects of semi-major axis, initial inclination and initial argument of pericenter (apse angle) on the time

[1] All the model atmospheres used are presented in Appendix II, and appear in order of ascending distance of the planet from the Sun.

Figure 3.1.5
Contract No. NAS 5-10782

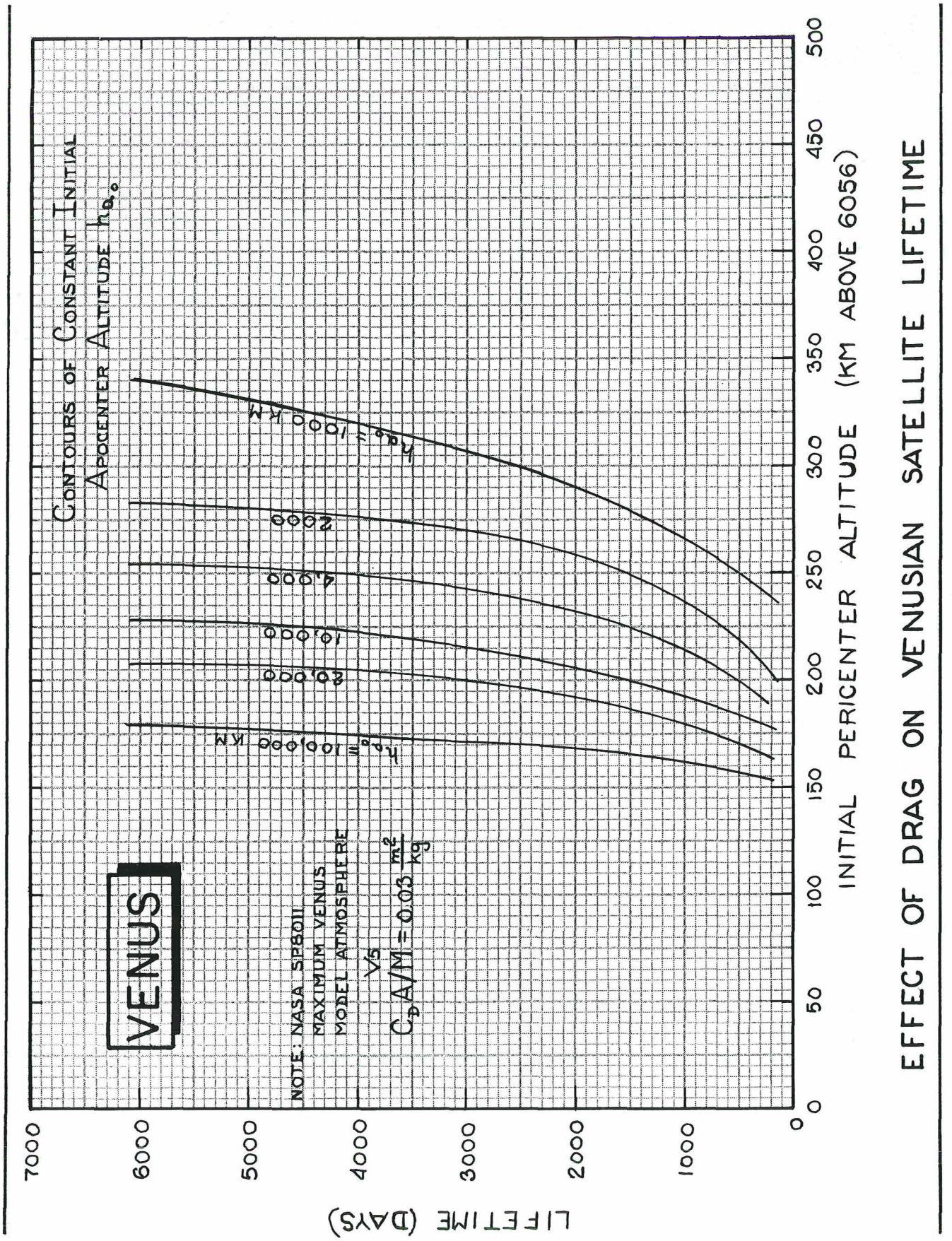

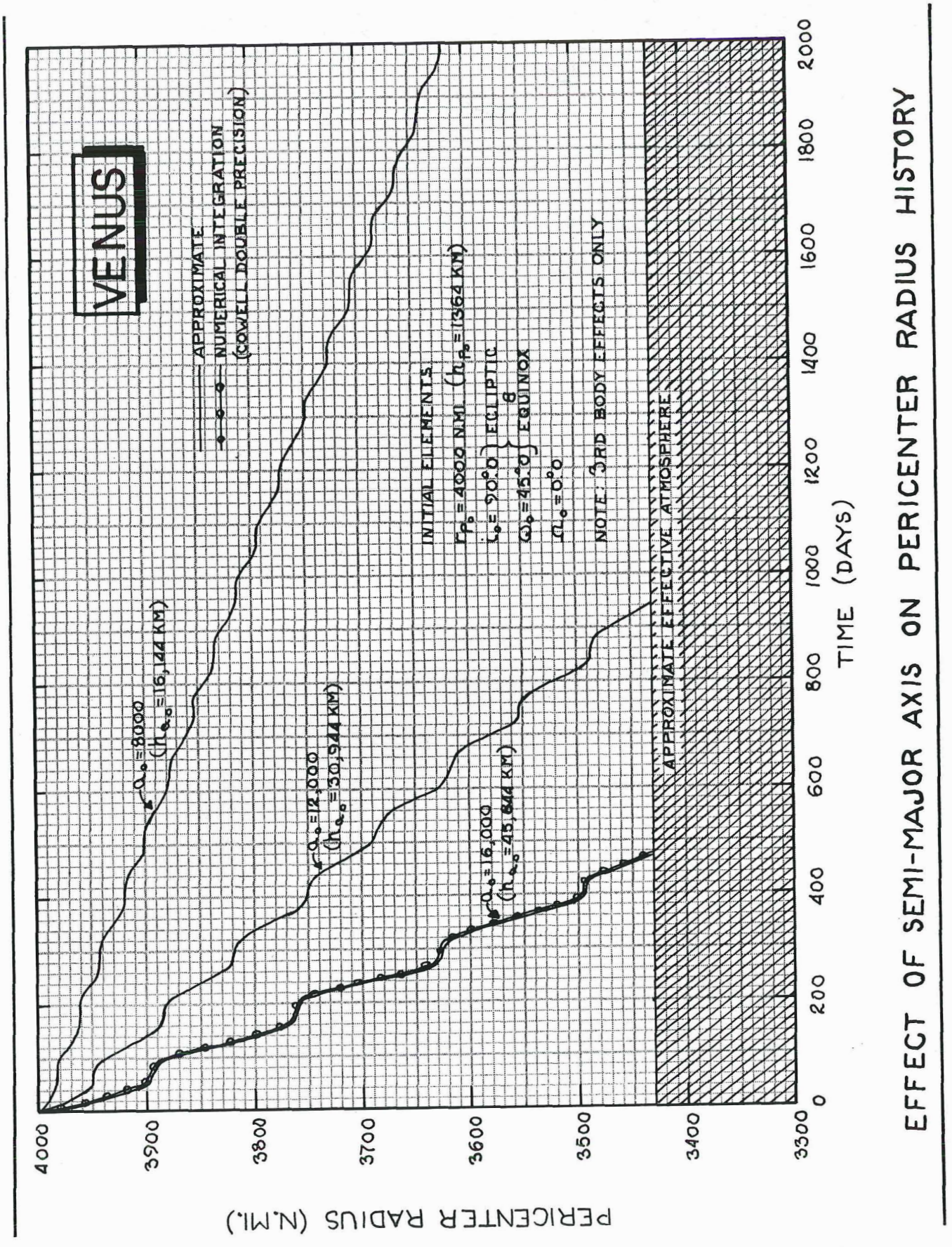

EFFECT OF SEMI-MAJOR AXIS ON PERICENTER RADIUS HISTORY

Figure 3.1.7
Contract No. NAS 5-10782

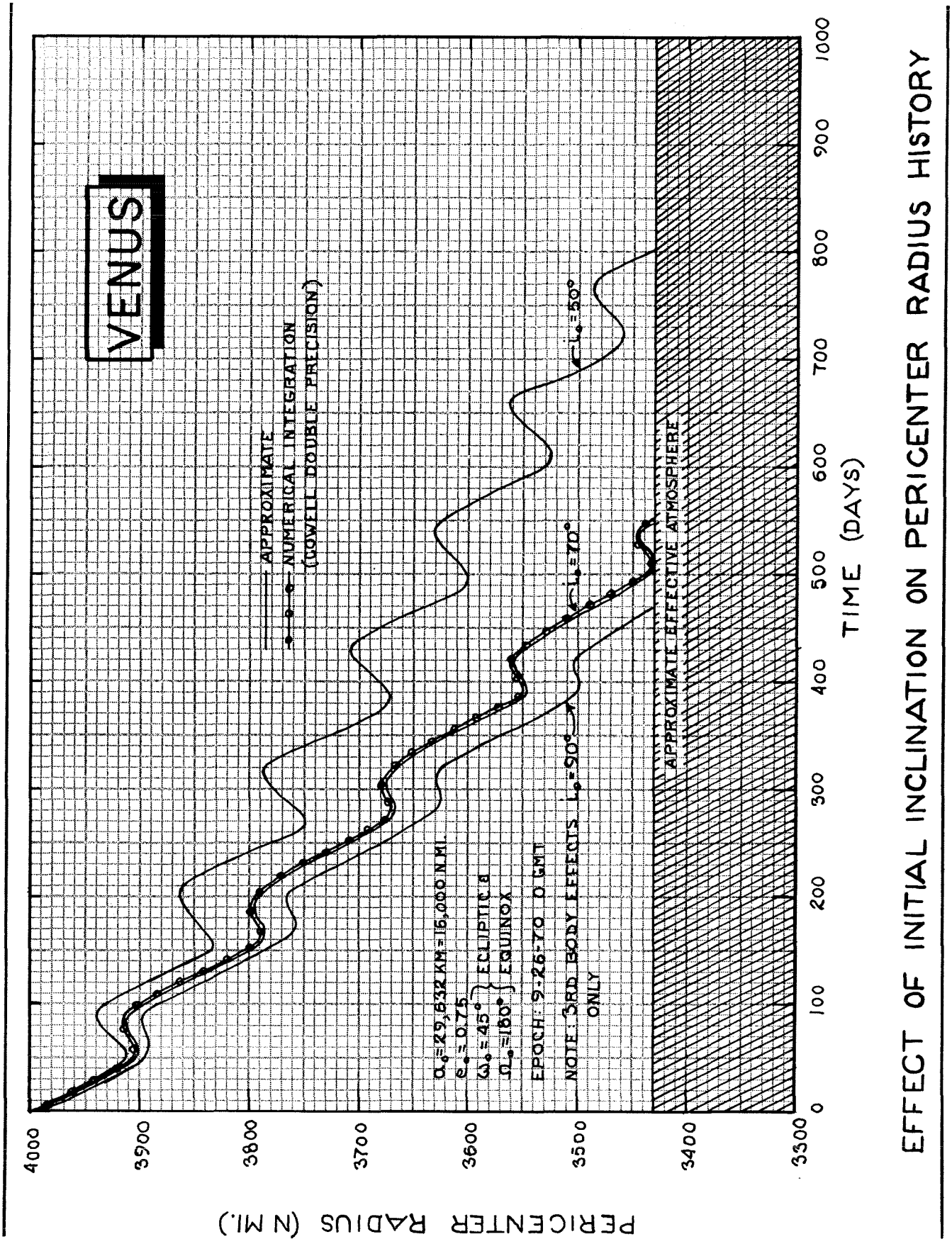

EFFECT OF INITIAL INCLINATION ON PERICENTER RADIUS HISTORY

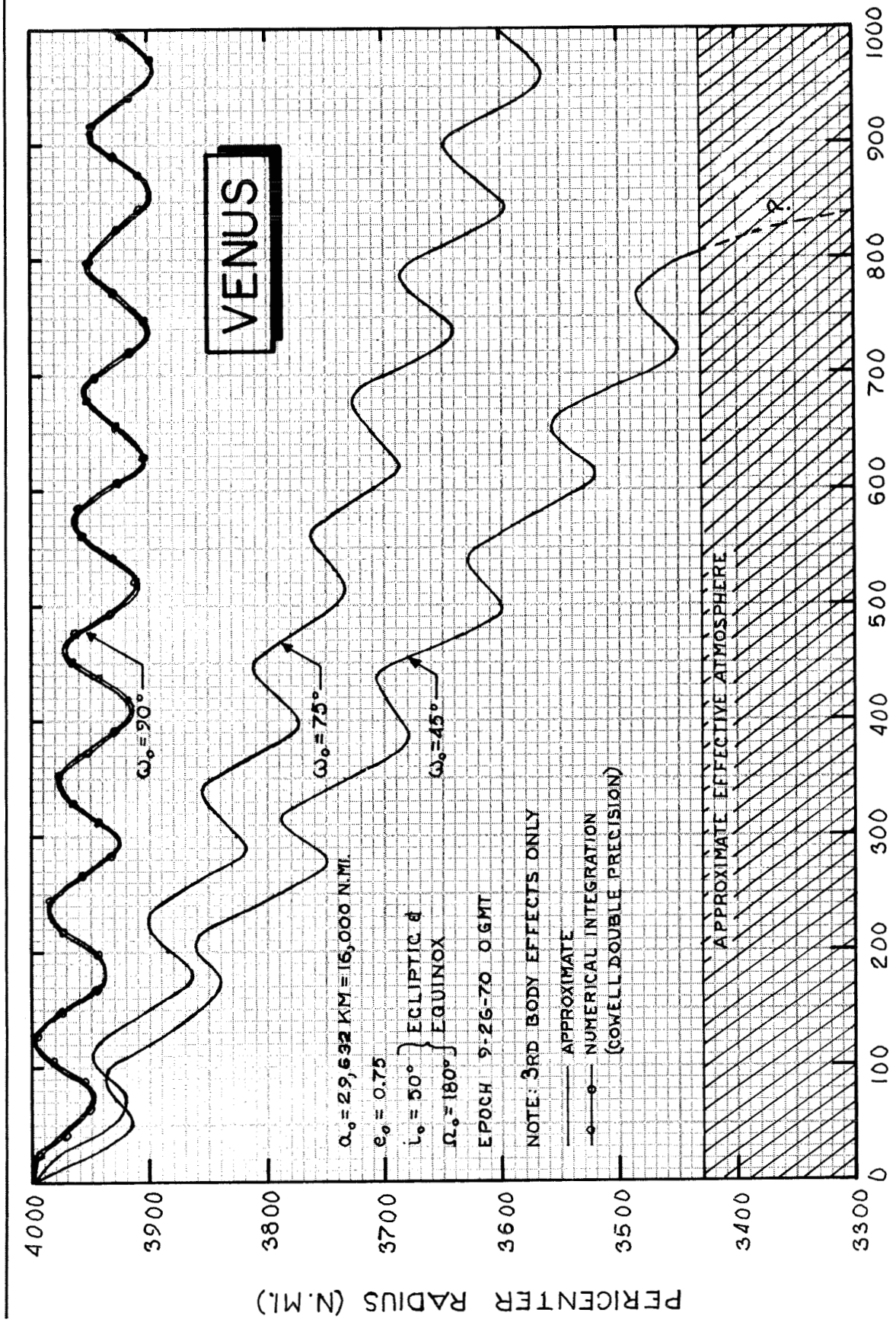

EFFECT OF INITIAL APSE ANGLE ON PERICENTER RADIUS HISTORY

history of the pericenter radius. Notice that all the curves are practically straight lines with the medium periodic variations superimposed on the near-linear long-periodic changes.

One of the curves of each diagram (indicated by a solid line connecting circled points) shows the results of a numerical integration of the actual equations of motion. These comparison cases were run on a double precision N-body computer program that integrates (numerically) the accelerations resolved along the rectangular coordinates of a non-rotating reference frame. The agreement of the solutions indicates that we can simulate the third-body effects over long periods of time by means of the approximate techniques of Section 2.

Even though our best estimate of J_2 for Venus is zero, it is instructive to assume several values and examine the effects of such flattening on the pericenter history. Figure 3.1.9 shows such a comparison and indicates that the effects of oblateness make only very slight differences in lifetime even if the apocenter altitude is as low as 10,000 km. In view, however, of the large uncertainty of the value of J_2 for Venus it is probably safest from a planetary quarantine standpoint to keep the initial apocenter altitude above 10,000 km for the first 5 years of the early flights. If a 15-year lifetime is to be guaranteed under the assumption of the maximum Reference 17 atmosphere model, the pericenter altitude should remain above 300 km for most of the flight. An initial orbit of 500-km pericenter altitude and 20,000-km apocenter altitude would leave a comfortable margin of safety.

Mars

The red planet contains about one tenth of the Earth's mass while its radius is a little more than half that of the Earth. The oblateness coefficient for Mars, however, is nearly twice that of the Earth and the cold Martian atmosphere may extend upward so far that satellites a thousand kilometers above the surface will have lifetimes of no more than a few Earth years.

Figure 3.1.9
Contract No. NAS 5-10782

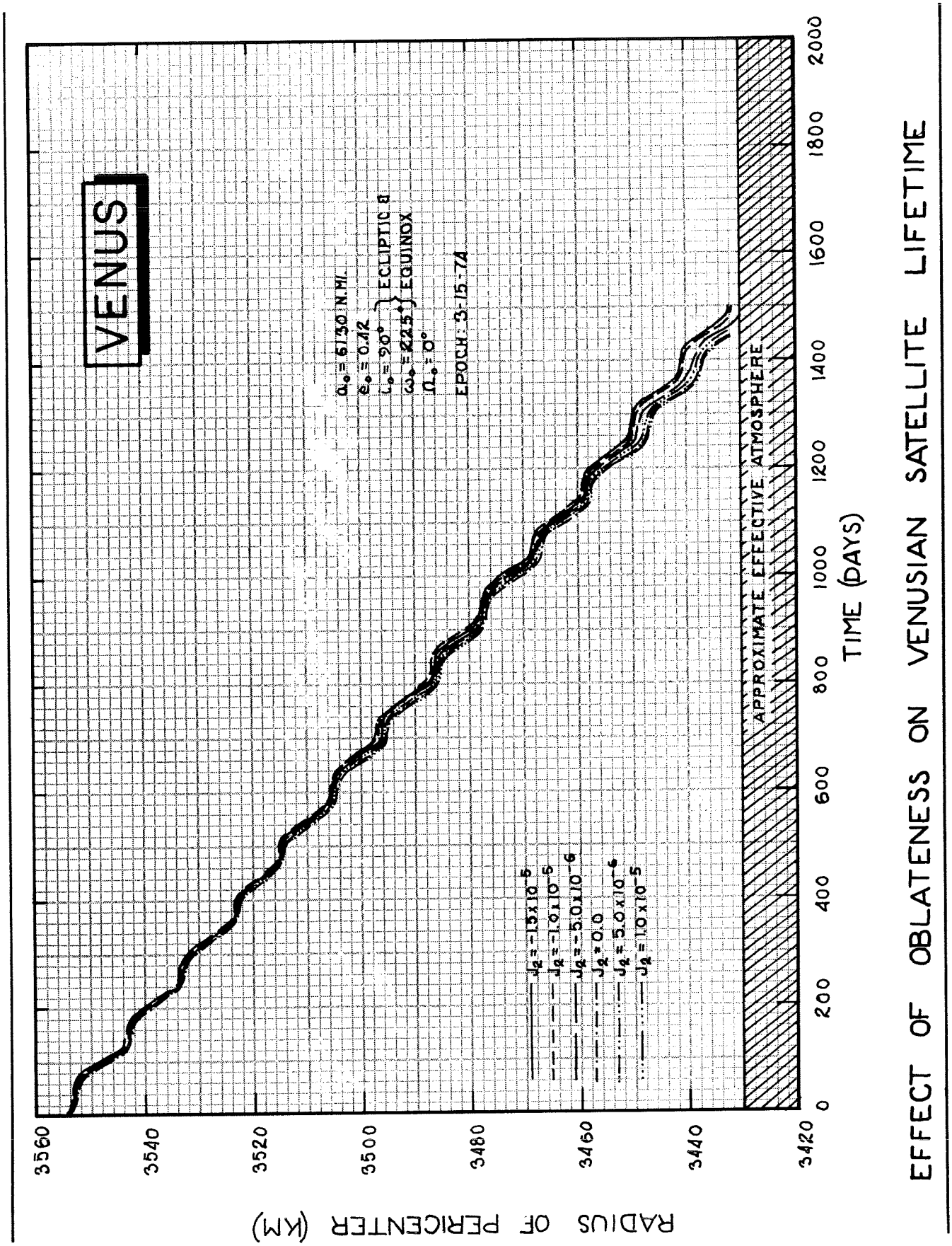

EFFECT OF OBLATENESS ON VENUSIAN SATELLITE LIFETIME

This combination of physical properties promises to provide celestial mechanicians and mission analysts with more than a few headaches over the next several years. In this survey, we give only a brief introduction to the problem, isolate the regions where the approximate techniques of Section 2 are applicable, and give some examples to substantiate the results. Later, recommendations will be made as to the most efficient methods for solving the orbit prediction problem in the very complex region below 30,000 km.

Figure 3.1.4b shows much of the survey information for Mars. The strong coupling region is shown by dashed curves as in Figure 3.1.2b. For Mars, the strong-coupling region is so high that we can expect most orbits to be completely dominated by the oblateness. At the lower strong coupling curve, the oblateness can cause the pericenter to rotate as fast as 0.25° per day.

The effects of the Reference 18 maximum Mars model atmosphere are shown in terms of curves of constant lifetime (in Earth years). The 15-year lifetime curve occurs at a very high altitude and suggests that it will be difficult to get very close to the Martian surface without running a significant risk of early orbit decay. The curves of constant lifetime under a non-rotating maximum model atmosphere were cross-plotted from Figure 3.1.10 which, like Figure 3.1.5 for Venus, shows lifetime versus initial pericenter altitude for curves of constant initial apocenter altitude. Reference to Table II.4 in Appendix II will show the very gradual decrease of density with altitude for the maximum Mars atmosphere model. This model was taken from page 8 of Reference 18. Even though the surface density for Mars is much less than that of Venus or Earth, the density above 300 km is much larger than the maximum Venus model (V5) density. In the Venus model, the density at 340-km altitude is 1.16×10^{-15} g/cc. The density of the maximum Mars model is still greater than that value at an altitude of 2,000 km.

To verify the accuracy of the approximate atmosphere calculations we have compared one of the apocenter histories with the results of a double

Figure 3.1.10
Contract No. NAS 5-10782

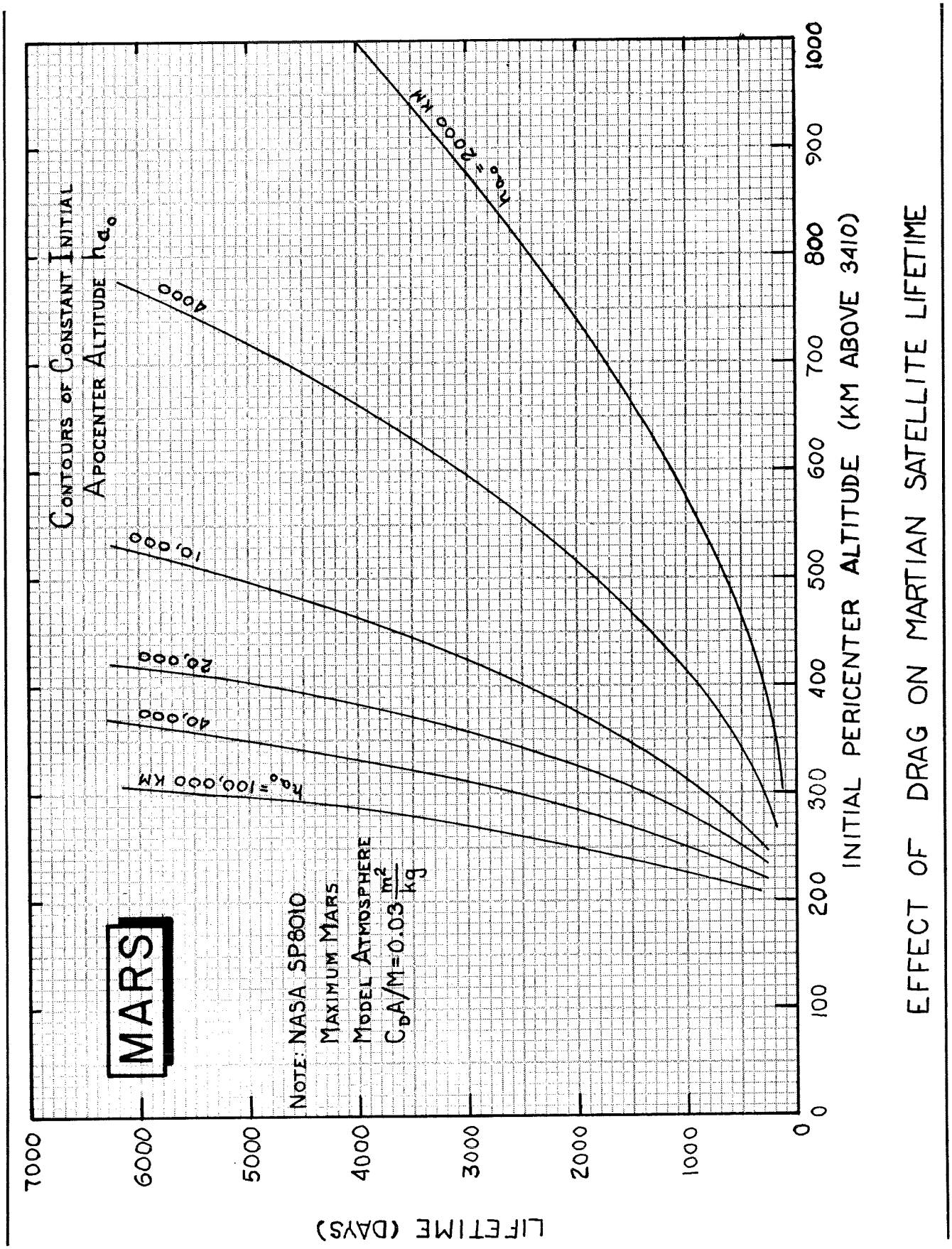

EFFECT OF DRAG ON MARTIAN SATELLITE LIFETIME

precision Cowell simulation (see Figure 3. 1. 11). The same density profiles and drag parameters were used in each simulation and, in the full numerical integration case, the oblateness and spin rate of the planet were set to zero. The agreement of the solutions indicates that the approximate technique is sufficiently accurate for these introductory studies.

There are several Martian atmosphere models in the literature. Unfortunately, they do not all agree on how dense the upper atmosphere might be. We have used the Reference 18 maximum model because it was compiled with information from the flight of Mariner IV. It is recommended that, before the first orbit mission, all the available information be reviewed thoroughly to make certain that the best possible atmosphere models are available to mission planners.

The dot-dashed curve of Figure 3. 1. 4b shows the region where the maximum (third-body perturbations only) medium-periodic variations will cause the pericenter altitude to fall to 150 km. If one wishes to know the order of magnitude of the medium-periodic variations in pericenter altitude he may simply subtract 150 km from the pericenter altitude shown by the dot-dashed curve. Here, as with Venus, it is recommended that orbits near the dot-dashed curve be selected with extreme caution if a long lifetime is desired.

The shaded curve near the right edge of Figure 3. 1. 4b sets off the region above which the doubly averaged equations are not recommended for predicting the effects of third-body perturbations. This recommendation is based on the possibility that the long-periodic effects on the elements (especially ω_L and Ω_L) may cause the orbit to move faster than Mars moves around the Sun. Such rapid motion of the elements would violate the assumptions of the double averaging technique. This is in direct analogy to the recommendation that Venus orbits to the right of the shaded curve of Figure 3. 1. 2 be simulated by integration of the singly averaged equations or the complete unaveraged equations.

Figure 3. 1. 11
Contract No. NAS 5-10782

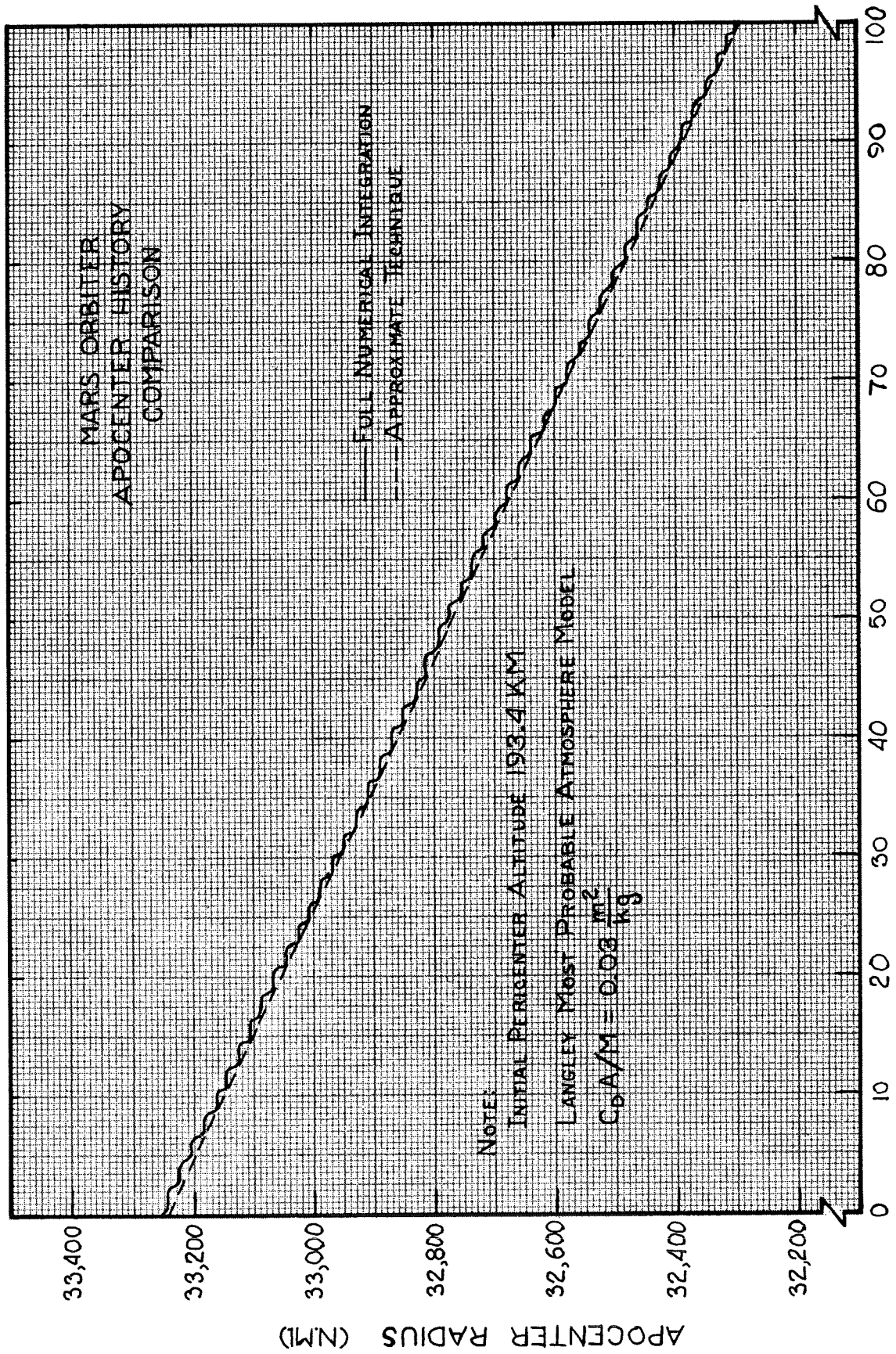

EFFECT OF DRAG ON APOCENTER RADIUS

On the Venus diagram (Figure 3.1.2b), there was no limit below which double averaging was not recommended. This is because even the largest magnitude of J_2 estimated for Venus is too weak to move the orbit faster than Venus' motion around the Sun. The strong oblateness of Mars, however, is sufficient to move the orbit faster than the planet's mean motion for a very considerable range of orbits. The shaded curve to the left of the lower strong coupling curve is the author's estimate of the lower limit of applicability of the double averaging techniques of Section 2. Fortunately, below the shaded curve, the third-body perturbations are small enough that they can probably be ignored for preliminary design purposes. But, below the curve, testing the double averaging theory against numerical integration for the long time periods of interest from a planetary quarantine standpoint would be prohibitively expensive. To simulate an orbit of 300-km pericenter altitude by 20,000-km apocenter altitude for only 100 days required more than 20 minutes of 1108 computer time for a double precision Cowell integration. Also, in the region below the shaded curve, the oblateness effects are so strong that the higher order effects of J_2^2, J_3, and J_4 are probably more important than the effects described by the techniques of Section 2.

At this point, it is tempting to say that, below the left-hand shaded curve, we should use a theory intended to describe motion in an oblate field and consider the third-body effects as small perturbations to be added to the oblateness effects. We might then use the double averaging theory for high orbits and the oblateness theory for close satellites. One reason for not recommending this two-theory approach is that the atmospheric effects tend to lower the apocenter. This effect would require a switch from one theory to the other for any decaying orbit that started out above the shaded curve in Figure 3.1.4. There is, however, a more important reason for recommending more sophisticated techniques than those of Section 2. The reason is that there is the possibility of strong resonance between the effects of oblateness and the medium periodic third-body perturbations. Breakwell and Hensley (Reference 14) have studied the theoretical aspects of resonance between oblateness and the long-periodic third-body effects and

have predicted some remarkable variations in pericenter altitude. These variations, however, would necessarily have an extremely long period and would be of little practical consequence. One of the implications of resonating medium-periodic terms is that very large variations in pericenter could occur in less than half a planetary year. Considering any of the pericenter histories in this report, one may imagine what would happen if, at some point, the medium periodic variations did not turn over and oscillate around the long-periodic motion but, instead, continued downward at the maximum rate. The pericenter would change drastically in a very short time.

Physically, these hypothetical resonances between oblateness and medium-periodic third-body effects correspond to situations where the oblateness of the central planet causes the orbit to move in such a way as to maintain the same orientation with respect to the sun-planet line. The orbit, then, presents the same "side" to the Sun all the time and the disturbing force can remain nearly constant for as long as the orbit maintains its synodic orientation.

These points will be discussed later when recommendations are made as to how the combined effects of third-body, oblateness, and atmospheric perturbations can be efficiently predicted. We now continue with the survey information for Mars in order to present, more specifically, the regions of applicability and the accuracy of the techniques of Section 2.

In the Venus survey, we assumed that the third-body perturbations will dominate the motion and then, after studying the third-body effects, checked some examples to show the effects of possible values of J_2. For Mars, we must begin with the complexities of the coupling between the two disturbing forces since the motions of the orbits of Phobos and Deimos make it unmistakeably clear that Mars's gravitational field is strongly oblate.

Figure 3.1.12 is an example of strong coupling between oblateness and third-body perturbations. In this example, the oblateness is dominant and,

Figure 3.1.12
Contract No. NAS 5-10782

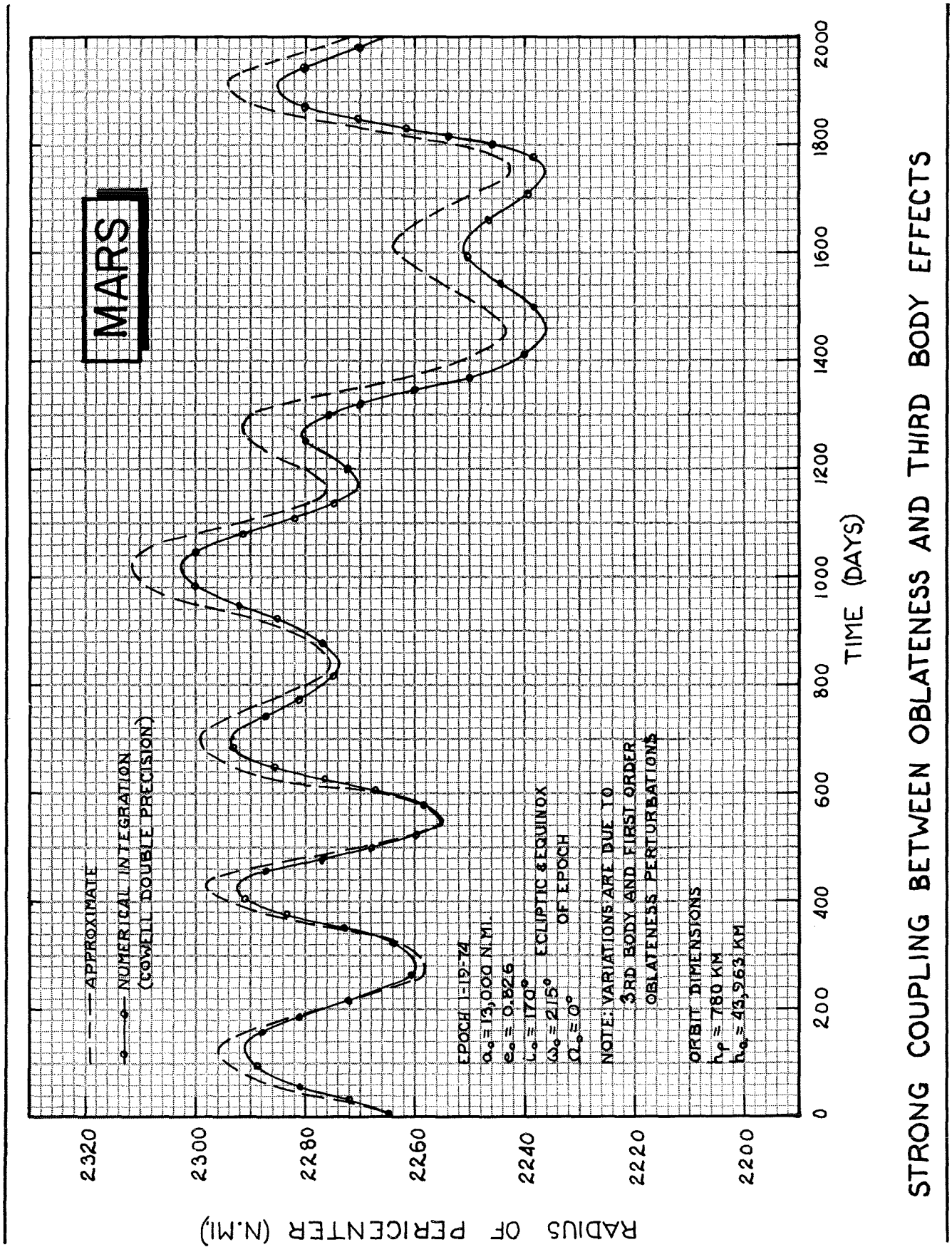

STRONG COUPLING BETWEEN OBLATENESS AND THIRD BODY EFFECTS

we see the marked effect of J_2 on the character of the motion. Figure 3.1.13 shows an example of strong coupling with third-body perturbations dominant. Here, even though the oblateness effects are small, they are still large enough to prevent impact. The oblateness could just as easily have been the cause of impact in some situations where third-body effects alone would have given long lifetimes.

Figures 3.1.12 and 3.1.13 also show the results of numerical integrations of the actual equations of motion (Cowell-double precision) as circled points connected by solid lines. These comparisons show that the approximate techniques of Section 2 are sufficiently accurate for preliminary mission design work but they also show that there are errors which were not encountered when strong oblateness effects were absent. These errors are due to two separate effects. The first is that there are terms of order J_2^2 in the averaged disturbing function that cause long-periodic variations in eccentricity proportional to J_2. The second (and principal) cause of error is that the motion of the argument of pericenter is large enough to violate the assumptions of the double averaging theory to a small degree. These errors could become significant near resonance situations where the frequencies of the medium-periodic terms become small. It is recommended that the frequencies of the medium-periodic terms be monitored during simulations using the techniques of Section 2.

In Figure 3.1.14, a large orbit is simulated to show the accuracy of the approximate techniques for orbits where the oblateness perturbations are negligible. The short-periodic (per orbit period) variations are large enough to be noticable in this example and are shown on the plot. Orbits this large would probably occur only if the injection retro rocket burned out prematurely.

Figure 3.1.13
Contract No. NAS 5-10782

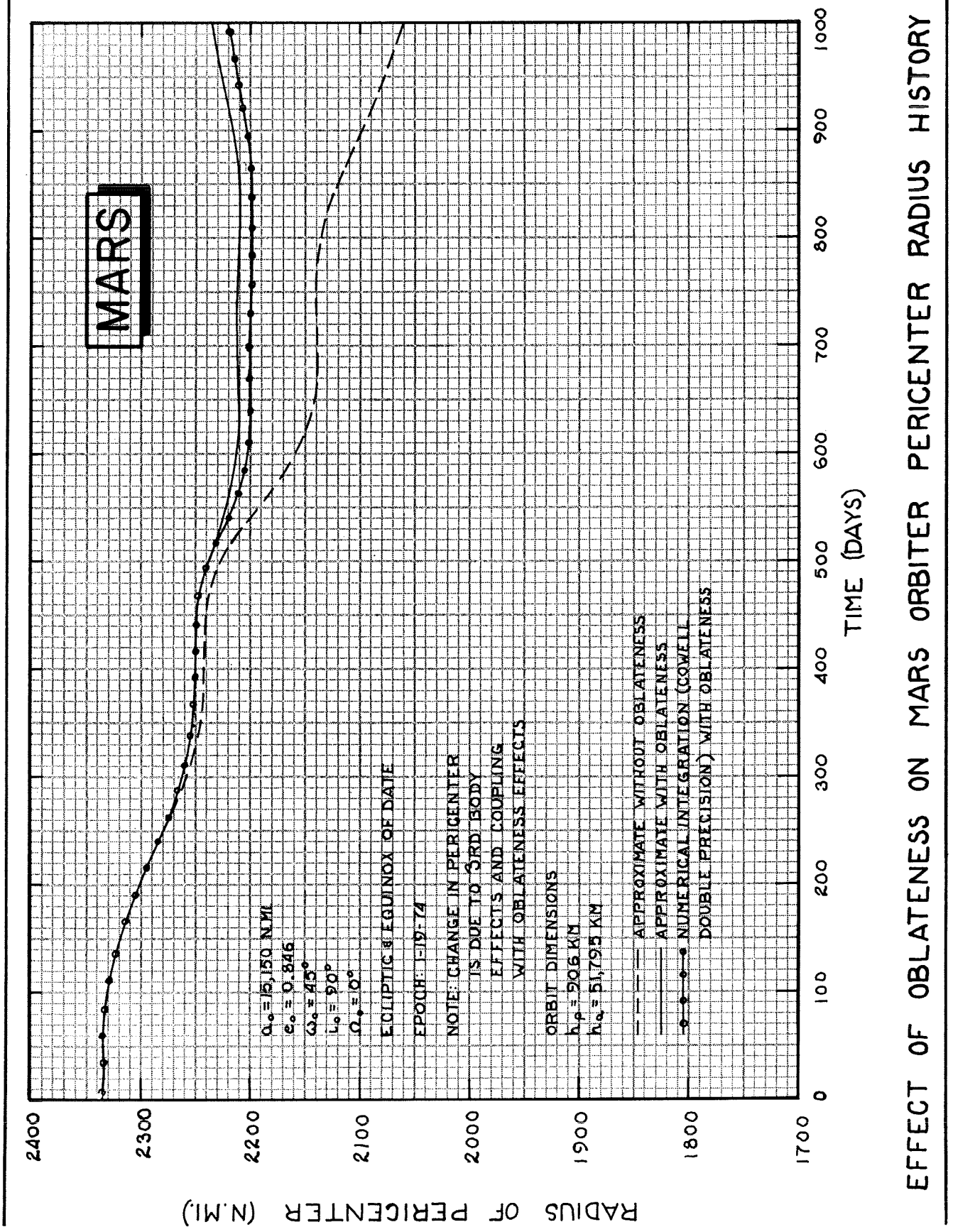

EFFECT OF OBLATENESS ON MARS ORBITER PERICENTER RADIUS HISTORY

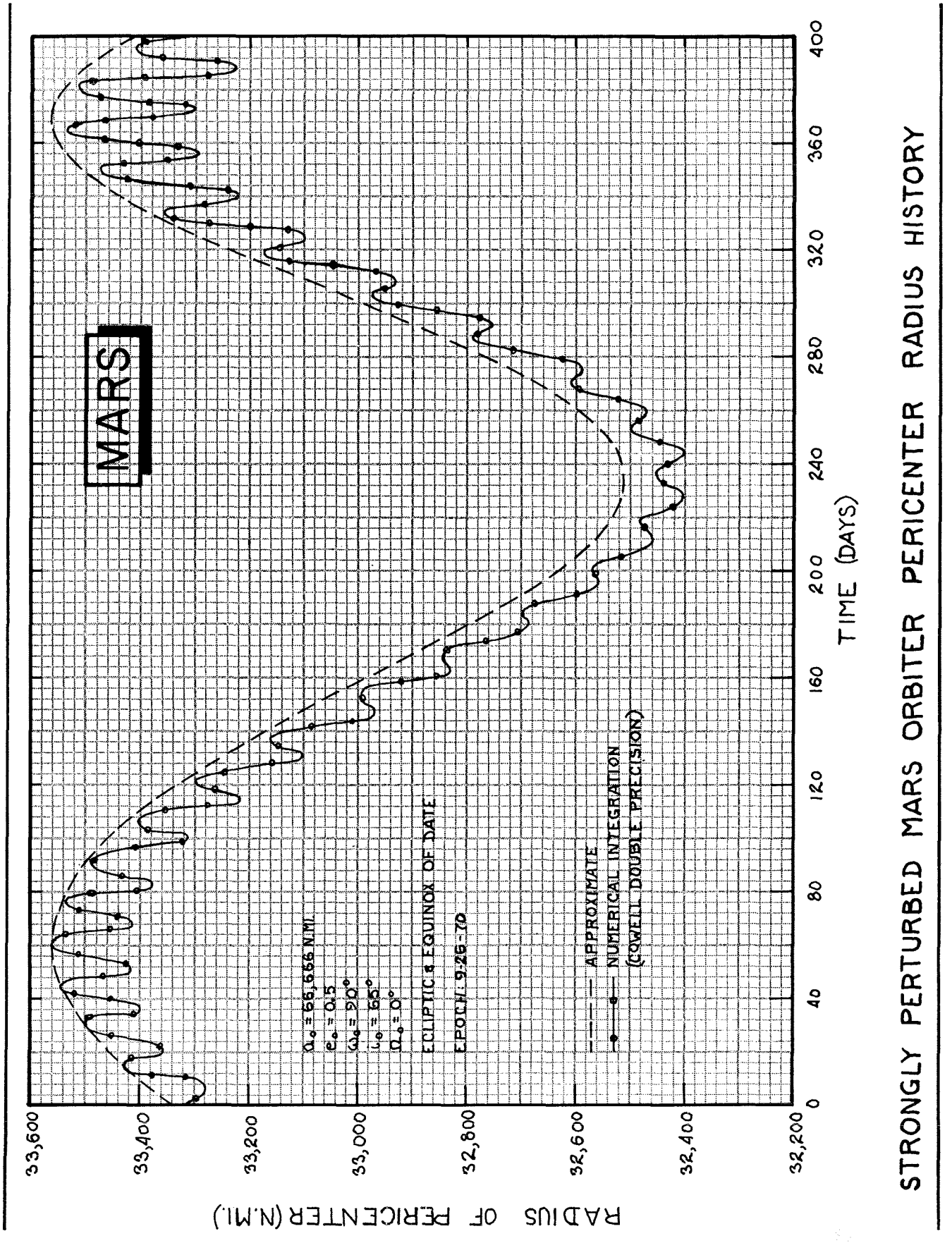

STRONGLY PERTURBED MARS ORBITER PERICENTER RADIUS HISTORY

In this survey, the effects of atmospheric drag were evaluated separately from the combined effects of third-body and oblateness perturbations. Whereas this philosophy is probably realistic for Venus orbiters, the possibility of a significant high-altitude atmosphere for Mars suggests that coupling between the oblateness and atmospheric effects will be a major factor in the long-term orbit prediction for Martian satellites. The very strong oblateness of Mars indicates that, for orbits whose apocenter altitudes are below about 30,000 km, the higher order harmonics of the planet's gravitational field could be more important than the variations we describe with the techniques of Section 2.

In order to adequately study the orbit evolution problem for close Mars orbiters, the author considers it absolutely essential to include the combined effects of (1) atmospheric drag, (2) central planet non-sphericity (including J_3 and J_4) and (3) third-body perturbations. The techniques required must work for high eccentricities and for a wide range of semi-major axes. It is the author's considered opinion that no analytic theory exists that is capable of meeting the above requirements. It is therefore recommended that a system of semi-analytic techniques be used for mission analysis and in-flight determination of orbit injection conditions. A system of techniques will be described later that will range in complexity from the methods of Section 2 to a completely numerical approach involving the numerical solution of the variational equations in Gauss's form.

Mercury

Mercury is so close to the Sun that the solar gravitational field is a very strong perturbing force for satellites of the innermost planet. The eccentricity of Mercury's orbit is over 0.2 and the effects of such a large value of e' on a Mercury orbiter are striking. The medium-periodic variations in pericenter radius for such a satellite are alternately large and small according as Mercury is near perihelion or aphelion.

Even though recent estimates (Reference 19) of the flattening of Mercury indicate a larger value of J_2 than for Venus, the strength of the third-body effects for Mercury orbiters puts the strong coupling curves even lower than

the corresponding curves for Venus. Figure 3. 1. 1b shows the regions where the three major disturbing forces will probably be dominant. The figure indicates that third-body perturbations are by far the most important and, in fact, are so strong that the lower strong coupling curve does not appear on the diagram. The effects of a maximum density model of the Mercurian atmosphere (Reference 20) are shown as lines of constant lifetime in Earth years and are shown more specifically in Figure 3. 1. 15. This diagram shows lifetime versus initial pericenter altitude for curves of constant initial apocenter altitude. The assumptions made were the same as those for the Venus and Mars studies except for the assumed density profile. Table II. 1 in Appendix II gives the density model used for this survey. Notice that this model, like the Mars model, is more dense at high altitudes than the Earth or Venus models. We should therefore expect to encounter problems similar to those encountered for the Mars orbit prediction problem when we simulate the effects of the maximum density Mercury model atmosphere of Reference 20. It should be noted that there is considerable doubt about the density of the Mercurian atmosphere as is clearly pointed out in Reference 20. The maximum density models for Mercury and Mars are probably conservative estimates reflecting our necessarily limited knowledge of the planetary atmospheres. The results of this survey, then, should be considered an unlikely upper limit below which we should proceed cautiously with the first planetary orbiters.

The value of J_2 used for the evaluation of third-body-oblateness coupling in Figure 3. 1. 1b was obtained from the work of Liu in Reference 19 where a theoretical estimate of the dynamical figure of Mercury was presented. Let the three principal moments of inertia of Mercury be represented by I_x, I_y, I_z where

$$I_z > I_y > I_x .$$

Liu obtains the following results:

$$\frac{I_z - I_x}{I_z} \geq 7 \times 10^{-5}$$

Figure 3.1.15
Contract No. NAS 5-10782

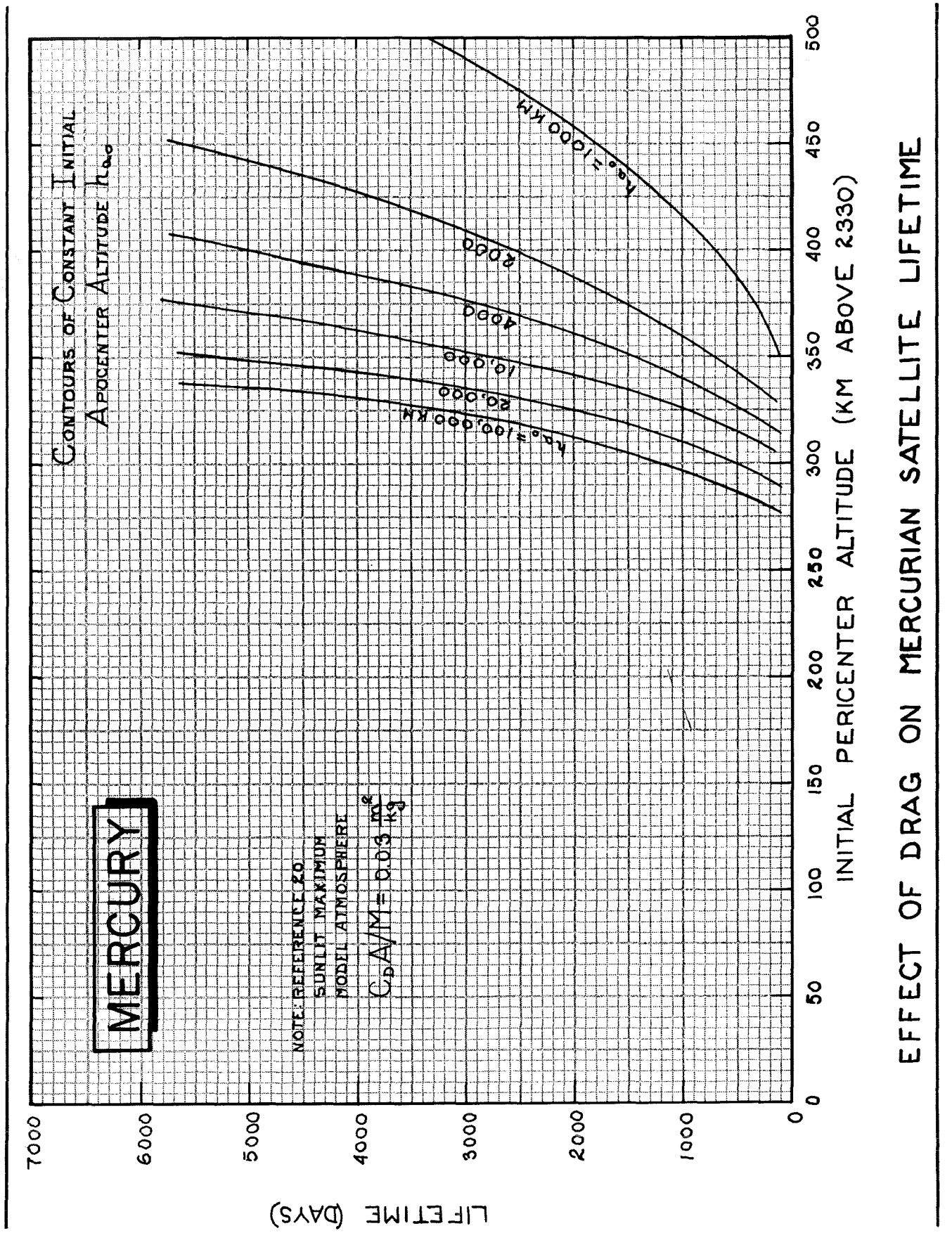

EFFECT OF DRAG ON MERCURIAN SATELLITE LIFETIME

$$\frac{I_z - I_y}{I_z} \geq 5 \times 10^{-5}$$

$$\frac{I_y - I_x}{I_z} \geq 2 \times 10^{-5}$$

Liu's theory is that, in the distant past, Mercury was in a molten state and was in hydrostatic equilibrium. Isostatic adjustment of the crust during a very rapid solidification period caused the ratios of the moments of inertia to increase from very small values to at least the values given above. In another paper (Reference 21) Liu obtained an estimate of the secular decrease of the polar moment of inertia I_z. Liu's calculations indicate that the polar moment decreased slowly during an epoch of cooling that lasted about 48 million years. The rate given by Liu indicates that I_z has decreased by about 0.5% since the planet was in hydrostatic equilibrium as a liquid globe. For practical purposes, then, we can assume that the polar moment has approximately the value it had before departure from hydrostatic equilibrium. We therefore assume that

$$I_z = 2/5\, mr_e^2$$

where m is the total mass of Mercury and r_e is the mean equatorial radius of the planet. Ignoring the ellipticity of the equator, we obtain an estimate of J_2 for Mercury as follows:

$$J_2 \approx \frac{I_z - I_x}{I_z} \cdot \frac{I_z}{mr_e^2} \approx (7 \times 10^{-5}) \quad (2/5)$$

or

$$J_2 \approx 2.8 \times 10^{-5}.$$

To be strictly correct we should have included the equatorial nonsphericity as described in Chapter 3 of Reference 10 but the calculation would lower the value of J_2 and we wish to make our estimate slightly higher since Liu stated

that the ratios $(I_z - I_x)/I_z$ and $(I_y - I_x)/I_z$ were greater than or approximately equal to the values given above. Unfortunately, Liu gives no estimate of the errors in his calculations. Dr. Kaula of UCLA, using arguments based on comparisons of Mercury with the Earth and the Moon, has recently (Private communication, November 1969) given an estimate of an upper limit on J_2 for Mercury. He stated that it is very unlikely that J_2 for Mercury is greater than 7×10^{-5}. The author concludes that the value of J_2 is probably between 2×10^{-5} and 4×10^{-5} and, for this survey, has adopted the value

$$J_2 = 2.8 \times 10^{-5}$$

for use in calculations of the strong coupling curves of Figure 3.1.1b.

This very small estimate of J_2 and the great strength of the solar gravitational perturbations indicate that third-body effects will probably dominate the motion of all but very close Mercurian satellites. The high eccentricity of Mercury's orbit about the Sun will cause the strong third-body perturbations to be much more complex than they were for Venus orbiters and we can expect the terms of Equation 13 with e' as a factor to be very important in the orbit prediction problem. Figure 3.1.16 shows the effects of e' on the time history of the pericenter radius for a Mercury orbiter. The solid curve was obtained with the approximate techniques of Section 2 and the dashed curve was generated in the same way except that the terms involving e' were set to zero in the generation of the dashed curve. The circled points represent the results of a Cowell double precision numerical integration of the actual equations of motion. The comparisons not only demonstrate the striking effects of e', but they also show that the approximate techniques give an accurate representation of the actual motion. Figure 3.1.17 is a comparison of the approximate technique with numerical integration for a very large orbit. This orbit is just below the shaded curve of Figure 3.1.1b and the comparison indicates how the approximate technique begins to fail as the perturbations become so strong that the assumptions of the double averaging theory are violated.

This completes the survey for orbiters of the three inner planets; Mercury, Venus, and Mars. Emphasis has been placed upon the effects of the three major disturbing forces, third-body, oblateness, and atmospheric

Figure 3.1.16
Contract No. NAS 5-10782

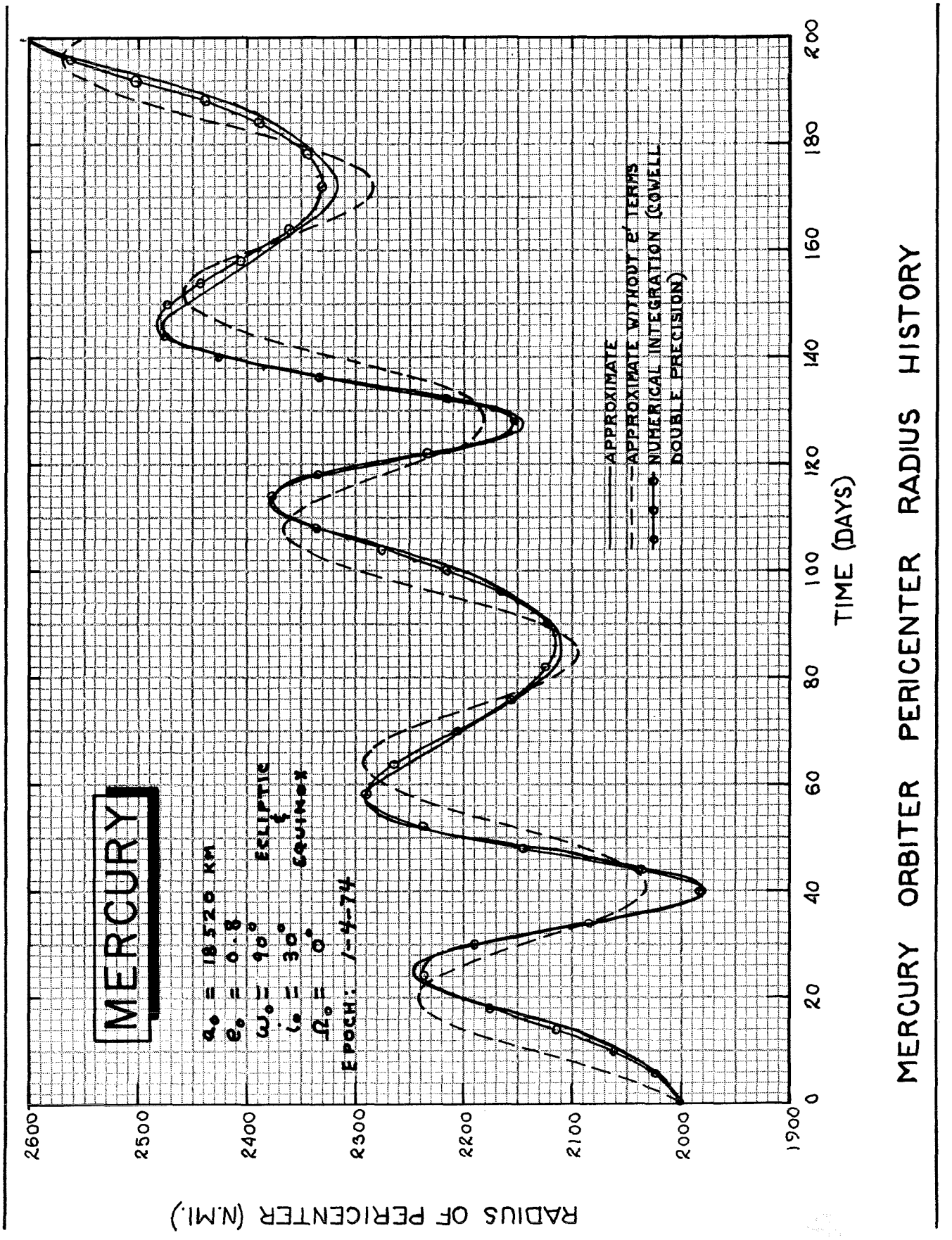

MERCURY ORBITER PERICENTER RADIUS HISTORY

Figure 3.1.17
Contract No. NAS 5-10782

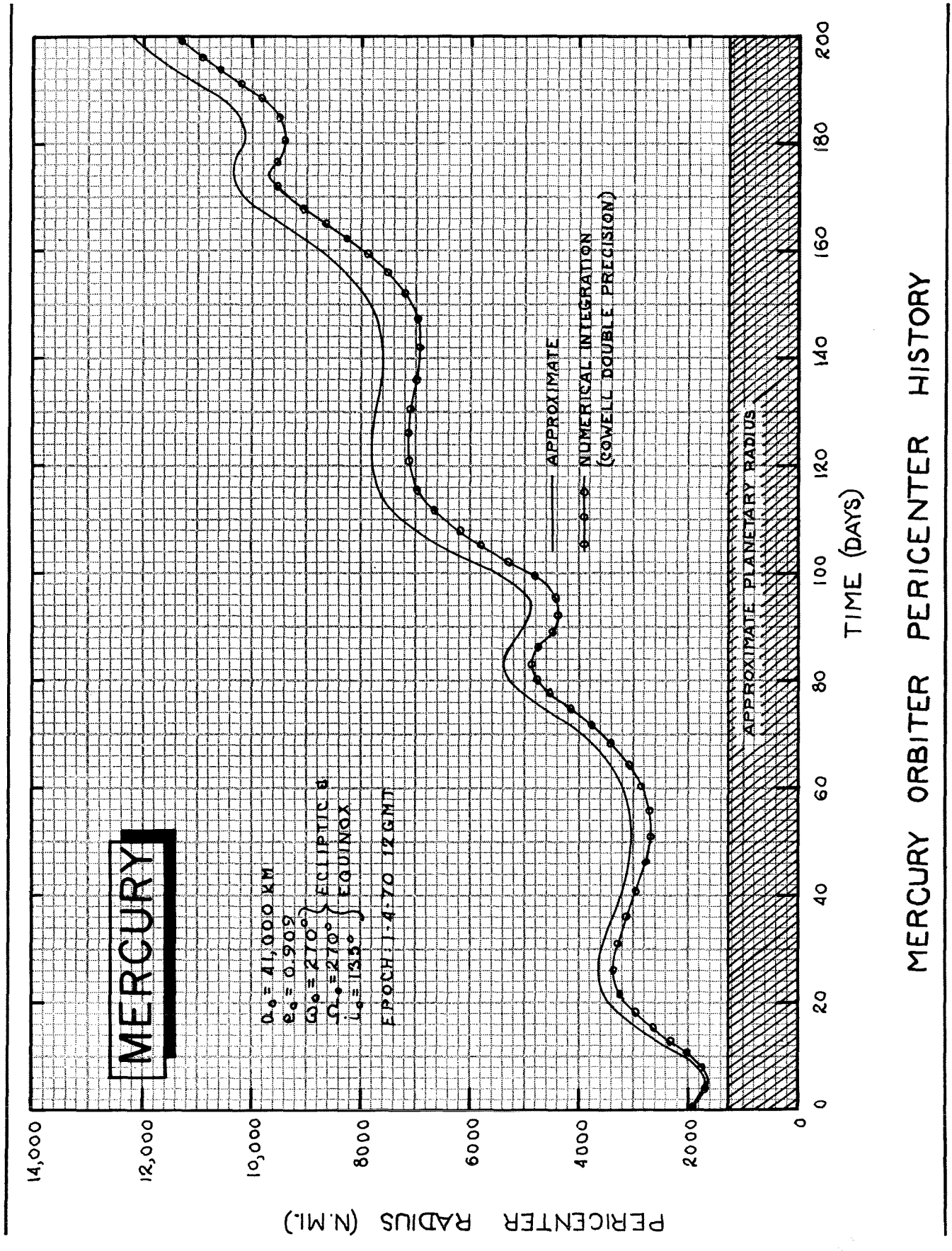

MERCURY ORBITER PERICENTER HISTORY

perturbations and upon the interactions of those forces and their effects on the long term motion of satellites of each planet.

Earth

The orbit prediction problem for artificial Earth satellites is necessarily more complex than the corresponding problem for planetary satellites since the Moon's gravitational field introduces a fourth major contribution to the perturbations. Indeed, the long periodic effects of the Moon are stronger than those due to the Sun's influence. The double-averaging theory, furthermore, is applicable to Earth satellites only over a limited range of orbits and is probably not worth the effort required to test the more complicated formulae that would be required to include the effects of a fourth body. Even though the techniques of Section 2 are recommended only for preliminary analysis of Earth satellite orbit evolution, it is instructive to perform the same kind of survey that was done for the other planets. Such a survey will make it possible for one to compare the magnitudes of the various disturbing forces with the magnitudes of the perturbations for satellites of the other planets. This will allow persons familiar with the orbit prediction problem for Earth satellites to compare satellites of the other planets with those of the Earth in the long-term orbit prediction problem.

Figure 3.1.4b shows the same kind of information about Earth satellites as was presented for planetary orbiters. The primary assumption is that the orbits of the Earth and the Moon are coplanar. (The Moon's orbit is actually inclined about 5 degrees to the ecliptic.) This assumption permitted a realistic definition of strong coupling between oblateness and the combined effects of Lunar and Solar gravitational perturbations. The regions where medium-periodic Luni-solar perturbations could cause a short lifetime are set off by a dot-dashed curve as was done for the other planets. For the Earth, however, there are two different medium-periodic frequencies - a semi-monthly variation and a semi-annual variation. It is interesting to note that, whereas the long-periodic lunar perturbations are about 50 percent larger than the long-periodic solar perturbations, the medium-periodic effects of the Sun are larger than the semi-monthly lunar perturbations. We can therefore, expect the Moon to dominate the long-term motion and the Sun to dominate the medium-periodic motion if oblateness perturbations are negligible. The shaded curve of Figure 3.1.4b sets off the

region below which double averaging is not recommended even for preliminary analysis. This estimate of the lower limit of applicability of the double-averaging theory is based on the possibility that oblateness perturbations might cause the orbit to turn faster than the Earth moves around the Sun. In such a situation, resonance between the oblateness and the medium-periodic Solar perturbations could give rise to very rapid changes in pericenter altitude. The singly-averaged third-body equations do not suffer from this shortcoming of the double-averaging theory and could be used to great advantage in Earth satellite orbit prediction even for very close satellites. No upper limit was placed on Figure 3. 1. 4b since the author is uncertain of the range above which the short-periodic (per satellite orbit period) lunar perturbations will become important from a practical point of view. Even the singly averaged equations should probably not be used for Earth satellites whose apocenter altitude is above about 200, 000 kilometers.

In the atmospheric studies for the other planets, we always used a maximum model density profile. In order to provide a valid comparison for Earth satellites a model atmosphere was chosen that corresponds to a high (but not unrealistically high) sunspot maximum. This model will not only provide a reference point for comparison of the maximum atmospheric effects of the planetary atmospheres but will also point out the conservatism inherent in the use of such maximum models for orbit prediction. In this survey, we have tried to place an upper limit on the planetary atmospheric effects. For detailed mission planning, however, the effects of the atmospheric models should be carefully considered with regard to the probability that the density will actually be as large as was assumed.

Figure 3. 1. 4b shows curves of constant lifetime for satellites under the influence of a non-rotating, high sunspot maximum, Spring-Fall atmosphere model of Reference 22. Table II. 3 in Appendix II gives the density profile and Figure 3. 1. 18 shows lifetime versus initial pericenter altitude for curves of constant apocenter altitude. It should be recalled that for Earth and Mars the atmospheric rotation can cause the rates of the semi-major axis and eccentricity to vary by 5 to 10 percent with the sense of the variation depending upon the equatorial inclination.

Figure 3.1.18
Contract No. NAS 5-10782

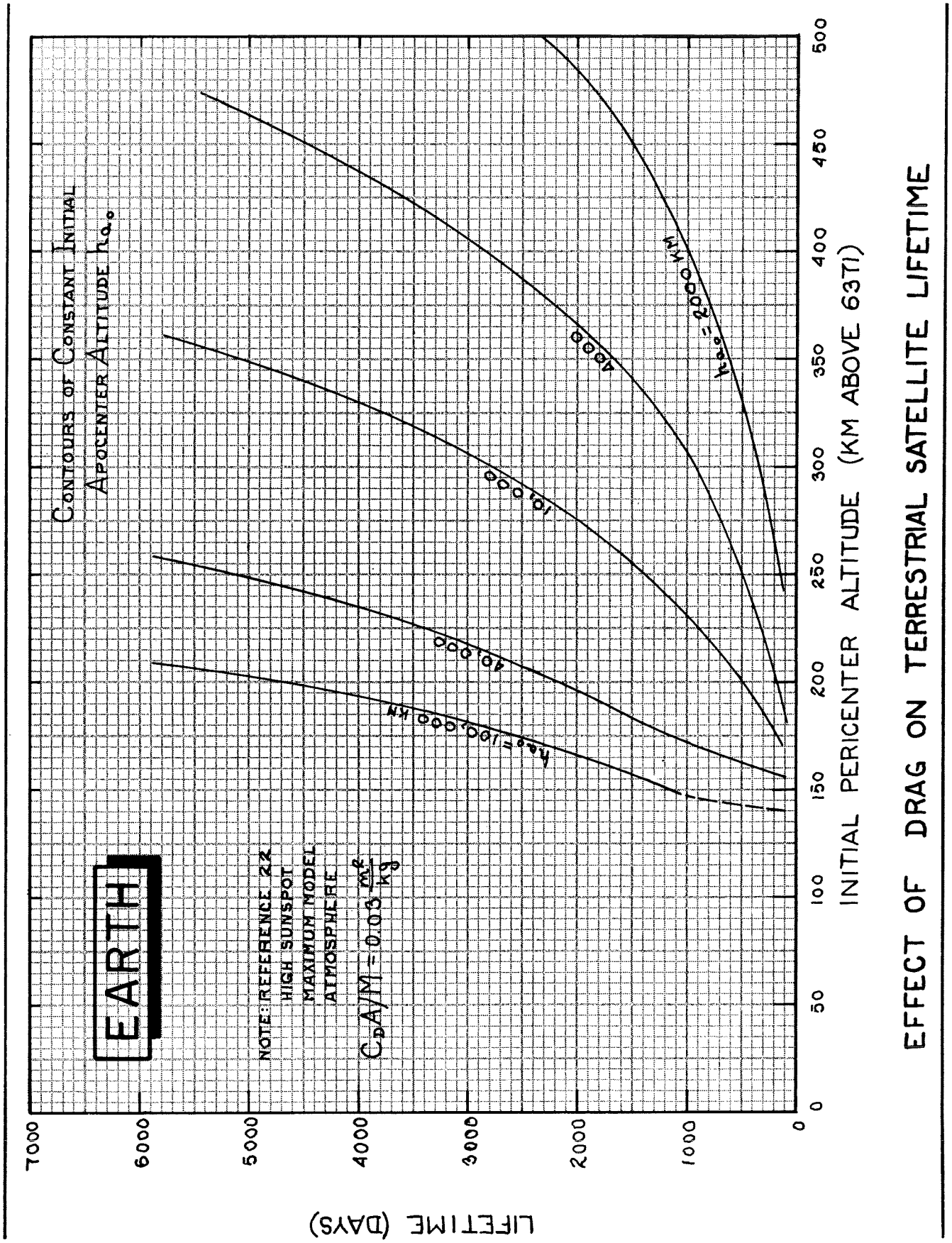

The information of Figure 3. 1. 4b has been presented primarily for reference purposes so that the perturbations acting on planetary satellites can be evaluated in terms of their relative strength or weakness as compared with the perturbations to Earth satellites. With the four-planet survey complete, we now return to Venus and Mars for some applications of the approximate techniques to real-world mission analysis problems.

APPLICATION TO SOME REAL MISSIONS

In the previous survey the orientation and shape of the orbit was discussed as if any orbit could be selected provided that it had a long lifetime. In the real world, the orbit is constrained by the approach geometry, the size of the injection motor, and a variety of communication and shadowing requirements. In this section, the advantages of very fast orbit prediction techniques are demonstrated for some feasible Venus and Mars approach trajectories in the 1970's. Maps of the impact parameter plane that require thousands of lifetime predictions are constructed and regions of high-and low-lifetime are shown for a realistic range of retro (Δv) capability.

Of more fundamental importance is the reason for orbiting the planets in the first place--the gathering of scientific information about our celestial neighbors. To provide information that will help show the kinds of scientific information that will be available for measurement, we include the time history of the position of the orbit for some orbits that might actually be obtained. In one case, the position of the pericenter with respect to the Sun-Venus line is shown. In another example, the ground trace of the pericenter point is shown on a map of the Martian surface. Before these detailed studies are presented, it is necessary to give a brief introduction to the language of interplanetary flight dynamics.

The impact parameter plane is one which passes through the center of the planet and is normal to the incoming asymptote of the approach hyperbola. The TRS ($\vec{T}$, $\vec{R}$, and $\vec{S}$ mutually orthogonal unit vectors) coordinate system (used for aiming point selection in trajectory analysis) is defined with the $\vec{T}$ axis the intersection of the impact parameter plane and the ecliptic (or equator or orbit plane) with $\vec{T}$ positive to the right. The $\vec{R}$ axis is in the impact parameter plane and directly downward. The $\vec{S}$ axis, then, forms a

right-hand system and points into the paper in the following figures. The reader may imagine himself skewered by the incoming excess velocity vector with his feet along the positive $\vec{R}$ axis and his extended right arm pointing along the $\vec{T}$ axis. The $\vec{S}$ axis, then, points directly from him to the center of the target planet. If we pass a plane parallel to the ecliptic and through the observer, his head is always above that plane (on the same side as the North ecliptic pole).

The impact parameter B is just the semi-minor axis of the approach hyperbola. A vector $\vec{B}$ is usually defined to specify the aiming point of the approach trajectory. This vector lies in the TR plane and has the length of the semi-minor axis of the hyperbola. The semi-major axis of the apprach hyperbola and the orientation of the incoming asymptote are fixed by selection of launch and arrival dates. Hence, the specification of $\vec{B}\cdot\vec{T}$ and $\vec{B}\cdot\vec{R}$ is sufficient to uniquely define the two-body orbit which describes the motion during a close approach to the target planet. Notice, that a given closest approach distance depends not only upon the magnitude of B but also upon the semi-major axis of the hyperbola. This means that the planet will appear larger in impact parameter space than it is in reality but will appear to be the same size for all incoming trajectories having the same energy (semi-major axis).

By stepping through different values of the direction and magnitude of the B vector, we can sequentially define a family of approach trajectories. If we assume that a retro velocity is added in the direction opposite the velocity vector at closest approach, we obtain a good approximation to the family of captured orbits which would be obtained if maximum use were made of an actual retro rocket. In this way, we can associate with each aiming point ($\vec{B}$ vector) a unique set of orbit elements and, therefore, a unique time history and lifetime. Using the approximate techniques we can afford to study a great many aiming points and, by cross-plotting, generate a detailed map of the impact parameter plane showing lines of constant lifetime for a given incoming asymptote and incremental velocity capability. We begin with a mission to Venus in 1972.

Venus 1972

A spacecraft could be launched in May of 1972 and arrive at Venus on September 26 of that year. The approach trajectory would have an excess speed (V_∞) of about 5.1 km/sec and the hyperbolic excess velocity vector would have right ascension and declination[1] of 91.1° and -28.9° with respect to the (Earth) ecliptic and equinox.

The size, shape and orientation of the orbit that can be obtained by firing a retro-rocket of given capability depends markedly upon the position of the aiming point in the impact parameter plane. It is, therefore, valuable to be able to study the evolution of orbits obtained by changing the aiming point of the approach trajectory since, by examining a large number of possible approaches, we can design the trajectory not only to satisfy the mission constraints but also to give the largest amount of scientific information.

With the above goals in mind, let us consider the details of constructing a lifetime map of the impact parameter plane. We first assume that the retro-rocket will be fired near the closest approach point on the approach hyperbola and that the effective change in velocity will be applied along the vehicle's pre-retro velocity. These assumptions are not unrealistic since it is to be presumed that the most efficient use will be made of the on-board propulsion system. We further suppose that the scientific payload will have been optimized and that some given amount (say 2.0 km/sec) of incremental velocity will be available. We now choose various values of the impact parameter, B, in a region that will yield pericenter altitudes near some desired value (say 1,000 km). For each of these values of B, we can sweep the aiming point around in a circle in the impact parameter plane. Automating this procedure on the computer and using the methods of Section 2, we can can easily construct plots of lifetime versus position on circles of constant B

1. These terms, normally reserved for describing longitude and latitude on the Earth's celestial sphere, will be meant here to specify the orientation of the excess vector in various coordinate systems.

for each of the values we select. Figure 3.2.1 is such a plot for the Venus 1972 approach. The approach energy is rather high for this trajectory and the incremental velocity (ΔV) required to obtain even a large orbit (1,000 by 50,000 km) is accordingly high. The data for this case, however, was available from a previous analysis and provides a good example of how the lifetime maps are constructed. Later, we shall study a Venus approach in 1973 that is much more attractive from an energy standpoint.

Notice, in Figure 3.2.1, that there are three distinct regions of (relatively) low lifetime. The regions near 0° and 180° are vanishing and the region near $\phi_{TR} = 90°$ is becoming more pronounced as B increases. This effect is caused by complex phase relationships between the initial argument of pericenter and initial inclination of the orbit. These relationships depend upon the energy of the approach hyperbola, the position of the closest approach point and, most importantly, upon the declination of the incoming asymptote. The maps of the impact parameter plane, then, will change as the approach geometry changes and we must construct a new map for each significantly different approach.

From Figure 3.2.1, we can cross-plot onto a diagram of the impact parameter plane and construct contours of constant lifetime for a given value of ΔV. Figure 3.2.2 is an example of such contour maps which, if we still have senses of humor in the midst of these complexities, might be called Disney plots because of the resemblance of the contours to the ears of a famous cartoon character. In Figure 3.2.2, the regions of low lifetime near $\phi_{TR} = 0°$ and $\phi_{TR} = 180°$ are vanishing with increasing B. That is, the lifetime is becoming greater as the impact parameter becomes greater. In the region near the R axis ($\phi_{TR} = 90°$) the opposite is true - the lifetime is decreasing as B increases. It would seem, from the plot, that the approach trajectory should pass over the north ecliptic pole of Venus if a long lifetime is desired. For this particular trajectory, the region near $\phi_{TR} = 270°$ does provide the biggest target but, as we shall see in the data

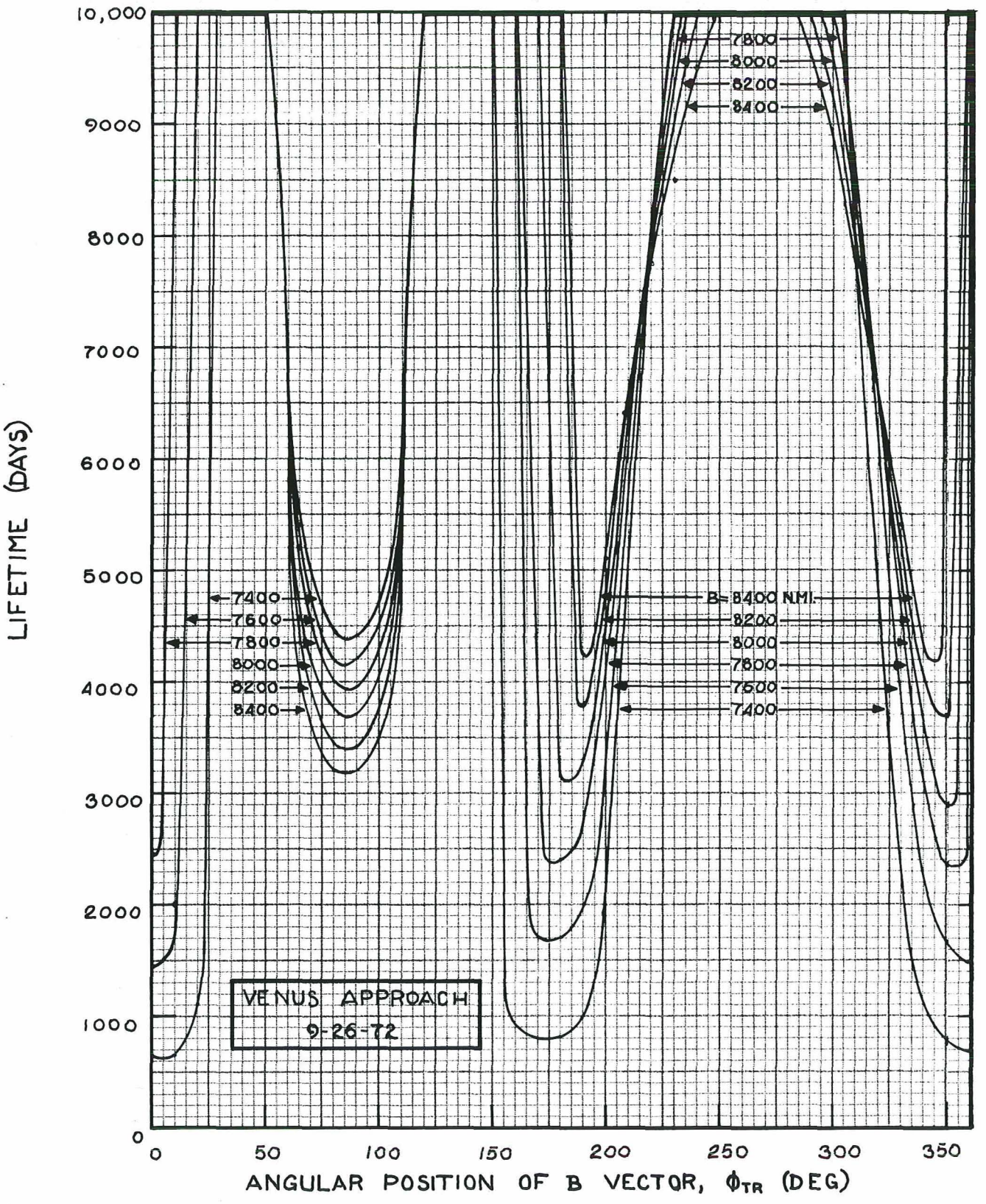

CONTOURS OF CONSTANT IMPACT PARAMETER

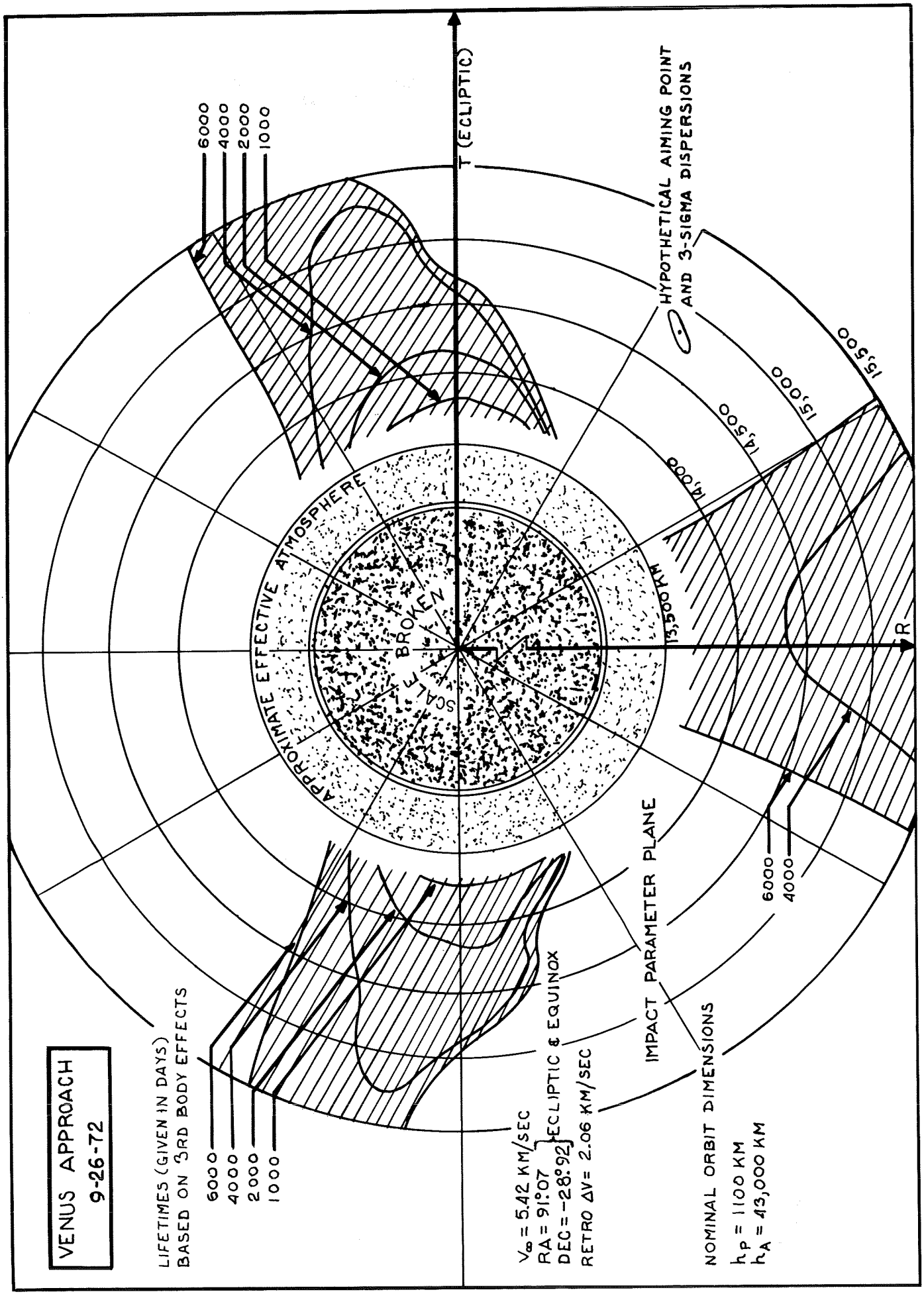

CONTOURS OF CONSTANT DYNAMIC LIFETIME

for the Venus '73 mission, the regions below the T axis ($\phi_{TR} \approx 30°$ or $\phi_{TR} \approx 150°$) are more satisfactory from a lifetime standpoint since those regions would yield long lifetimes even if only a very low incremental velocity capability were available. Approximately 360 10,000 day lifetime predictions were required for the curves of Figure 3.2.2 and the author estimates that if the predictions had been made by numerical integration of the actual equations of motion, the generation of the data would have required about 60 hours of CDC 6600 computer time. The small program used for the generation of the data for Figure 3.2.2 required about 50 seconds of 6600 time to apply the techniques of Section 2 to the 360 initial orbits. We thus see the very great advantage to be had from rapid approximate techniques in that we can study enough aiming points to permit the efficient selection of a nominal approach to the planet.

Venus 1973

For the Venus '72 mission, a value of retro velocity (ΔV) was picked that gave a reasonable orbit about Venus and then contours of constant lifetime were plotted on the impact parameter plane. A mission with much lower energy requirement could be flown that leaves Earth in late November 1973 and arrives at Venus on March 15, 1974 with the following incoming hyperbolic excess velocity:

V_∞ = 3.0775 km/sec
Right Ascension = 315.52° } ecliptic and
Declination = -24.11° } equinox

For this mission, we shall construct three plots as shown in Figure 3.2.1 and cross-plot contours of constant 15 Earth-year lifetime for each of three different retro velocity (ΔV) values. This procedure will show how, with the approximate techniques, we can trade retro ΔV for acceptable target area in the impact-parameter plane.

The three sets of curves of lifetime versus ϕ_{TR} will not be presented as they are identical in form to Figure 3.2.1. Suffice it to say that their generation required over a thousand lifetime predictions. Cross-plotting the results of the lifetime predictions onto a diagram of the TR plane, we obtain Figure 3.2.3. The contours are labeled according to the value of ΔV assumed for each set of lifetime calculations. For this approach, the three values of ΔV correspond approximately to the following nominal initial orbit altitudes:

ΔV	h_{p_o}	h_{a_o}
1.23 km/sec	1,000 km	35,000 km
1.15	1,000 km	43,000 km
1.00	1,000 km	54,200 km

To obtain these initial orbit parameters, the magnitude of the impact parameter, B, must be about 23,150 km. Changing the value of B causes a considerable change in the size of the orbit and as we move the aiming point outward, the semi-major axis of the post-retro orbit increases (for this approach) by about twice the amount of change in B.

The contours of Figure 3.2.3 clearly show the regions of high and low lifetime for the March '74 approach. The figure points out that, if a long lifetime is desired, the approach should not be over the north ecliptic pole unless plenty of reserve ΔV is available. Even in the cases of the higher values of ΔV, subnominal performance of the retro could result in a short lifetime whereas, if the aiming point is below the T axis (as recommended on the figure), even a very low amount of retro velocity would still yield an orbit with a long lifetime. It should be noted, however, that the aiming point recommendation is made from lifetime considerations only. The main point is that, with the approximate technique and a small amount of time on a good computer, a great deal of valuable information can be easily obtained for the mission planner.

Figure 3.2.3

Contract No. NAS 5-10782

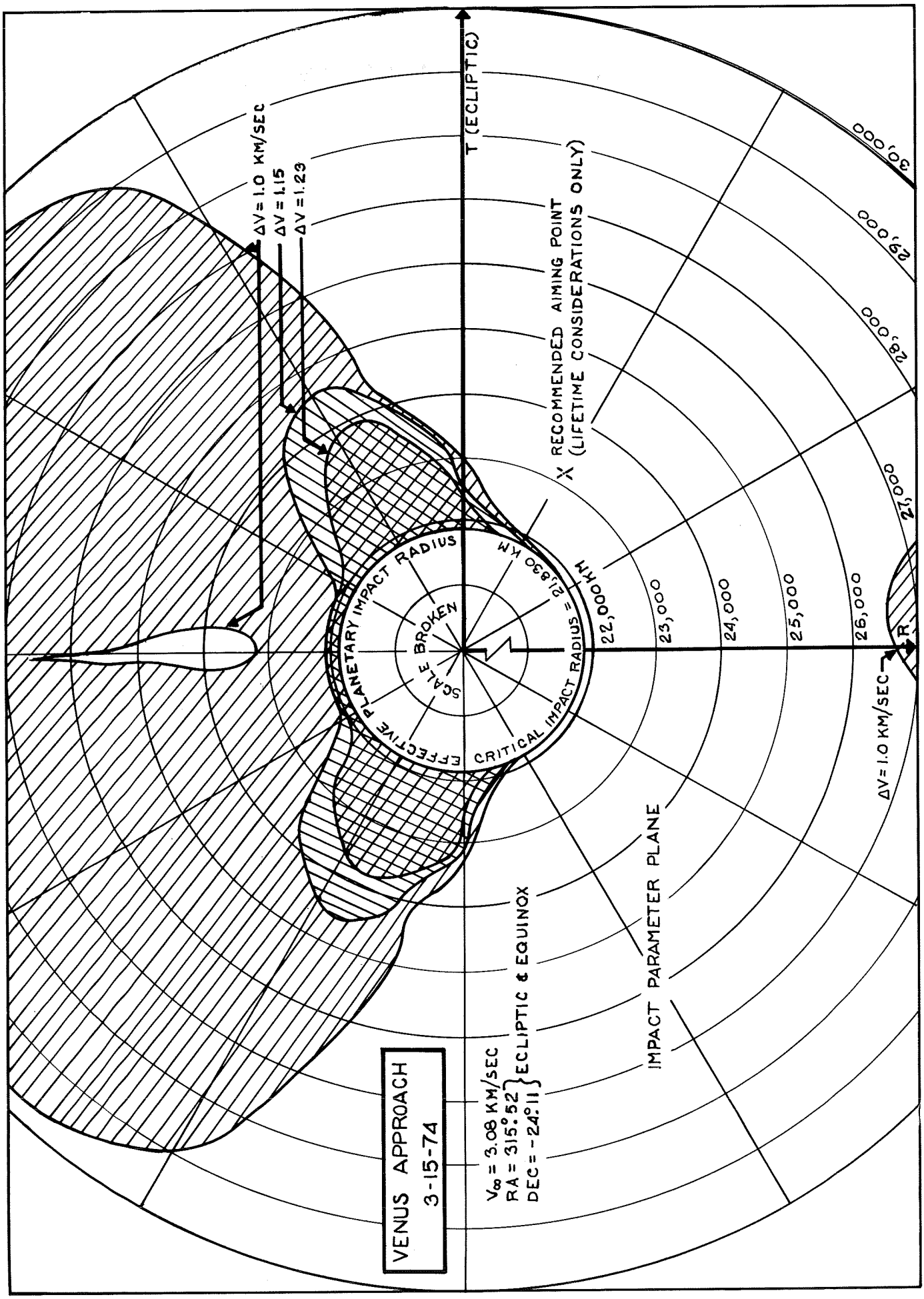

A Possible Orbit

Having selected an aiming point region that looks good from a lifetime standpoint, let us examine the time history of an orbit that might be obtained by firing a rocket in line with the velocity vector at closest approach on the incoming hyperbola. Assuming that ΔV is 1.23 km/sec, the resultant orbit would have the following elements:

$a = 23,457$ km	$\omega = 284.^{\circ}15$	ecliptic
$e = 0.699$	$i = 37.^{\circ}77$	and
$f = 0^{\circ}$	$\Omega = 350.^{\circ}80$	equinox

Epoch: March 15, 1974

Figure 3.2.4 shows the time history of the pericenter position during the first 700 days after injection. The latitude is given with respect to the Venus orbit plane, and the longitude is measured from the instantaneous Sun-Venus line. Examination of information like that given in Figure 3.2.4 can be of much value to mission planners by allowing them to select an aiming point that will yield the most desirable orbit from a scientific standpoint.

Mars 1973

The complex interactions between the three disturbing forces for Martian satellites make it very difficult to construct accurate lifetime contours in the impact parameter plane. Because of these difficulties, no aiming point regions will be recommended. The author feels that considerable further study is necessary before such recommendations can be made. The short-periodic coupling between oblateness and atmospheric effects, the possibility of resonance between the oblateness and medium-periodic third-body effects, and the possibility of strong higher order non-sphericity effects should be carefully considered before an actual mission is designed.

Two maps of the impact parameter plane have been prepared - one shows the effects of third-body and oblateness effects only, the other includes the possible effects of a dense high-altitude atmosphere. The presentation of such a map implies that we have included all three effects in the lifetime predictions - a capability that was not tested in the previous survey work. For this reason we present a pericenter history comparison of a Cowell

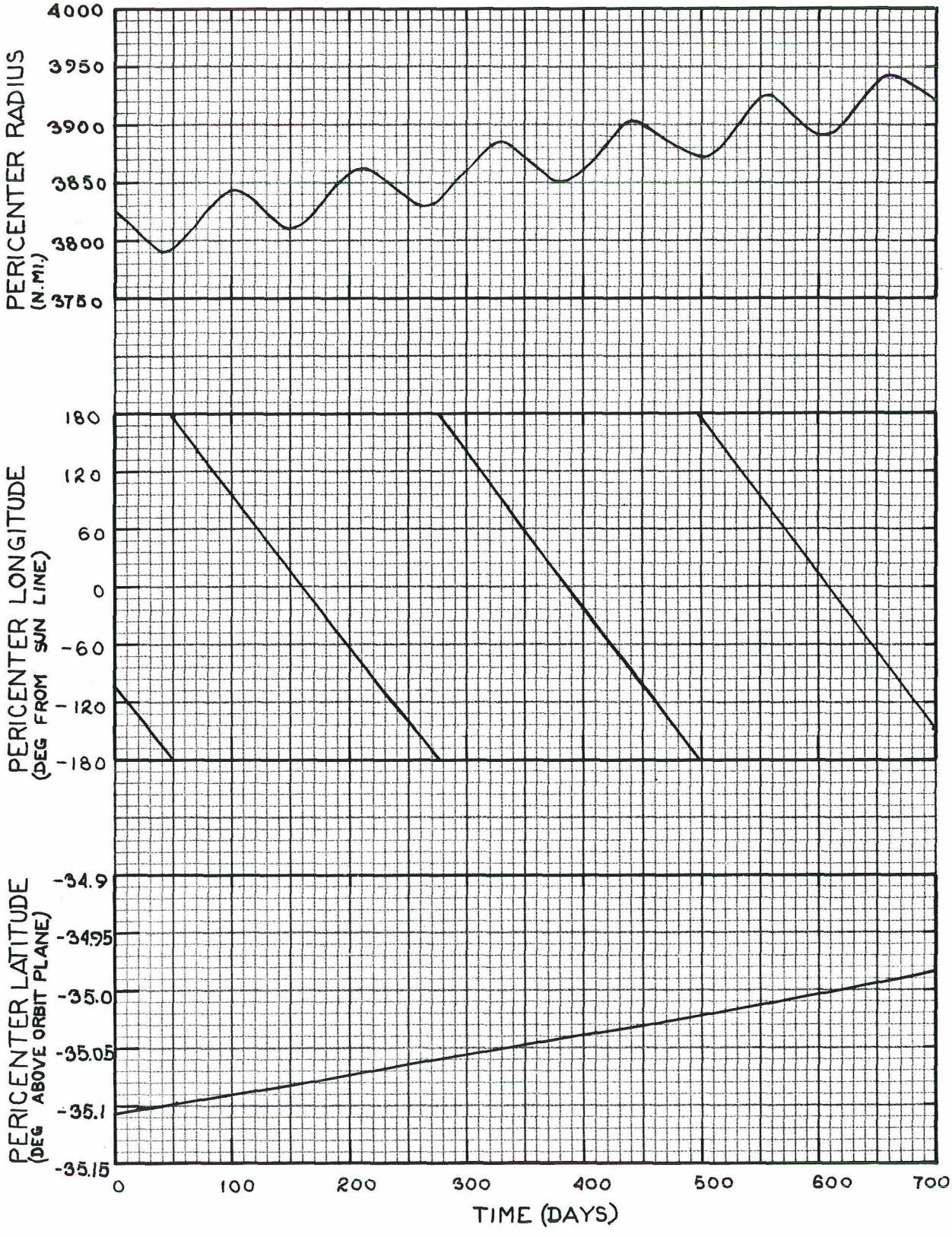

VENUS ORBITER PERICENTER HISTORY

double precision numerical integration and the approximate techniques of Section 2 where the approximate curves were obtained by numerical integration of the long-periodic effects of third-body, oblateness and drag perturbations. The medium periodic variations in eccentricity were then superimposed onto the long-periodic solution as in Equation (12) of this report. Figure 3.2.5 shows the comparison and indicates that a fairly realistic simulation can be obtained by the approximate methods. Figure 3.2.6 shows the history of the semi-major axis and displays the principal effects of drag on the orbit.

In an earlier study, the author erroneously assumed that the principal effects of drag could be accounted for by using an effective planetary radius 150-km larger than the actual Martian radius. The results of this assumption are shown in Figure 3.2.7 which, like the Disney plots for Venus, show contours of constant lifetime in the impact parameter plane. The effects of oblateness are immediately apparent - the character of the contours is completely different from the Venus curves because of the very strong oblateness of Mars. For this reason, the small program used to generate the data was modified to include the atmospheric effects along with the other disturbing forces. The same Mars approach was re-run on the modified program and the results appear in Figure 3.2.8.

The difference between Figures 3.2.7 and 3.2.8 is remarkable when we consider that the change is due only to the atmosphere above 150 km. The elimination of large areas as possible aiming points shows that we should include atmospheric effects in any realistic attempt to select an aiming point. Further, the possibility of such a dense upper atmosphere for Mars and the (known) very strong oblateness of Mars suggest that we should have included the short-periodic (per orbit period) coupling between the two effects. This study has not considered the practical effects of such coupling or the possible significance of higher order harmonics but there is little doubt that these effects should be carefully studied before a multimillion-dollar spacecraft is sent to Mars and expected to stay in orbit for 15 years.

In order to present information that may be valuable from a scientific point of view, we include the time history of the pericenter position on a map of Mars. This orbit is not a realistic one since the inclination is low with

Figure 3.2.5
Contract No. NAS 5-10782

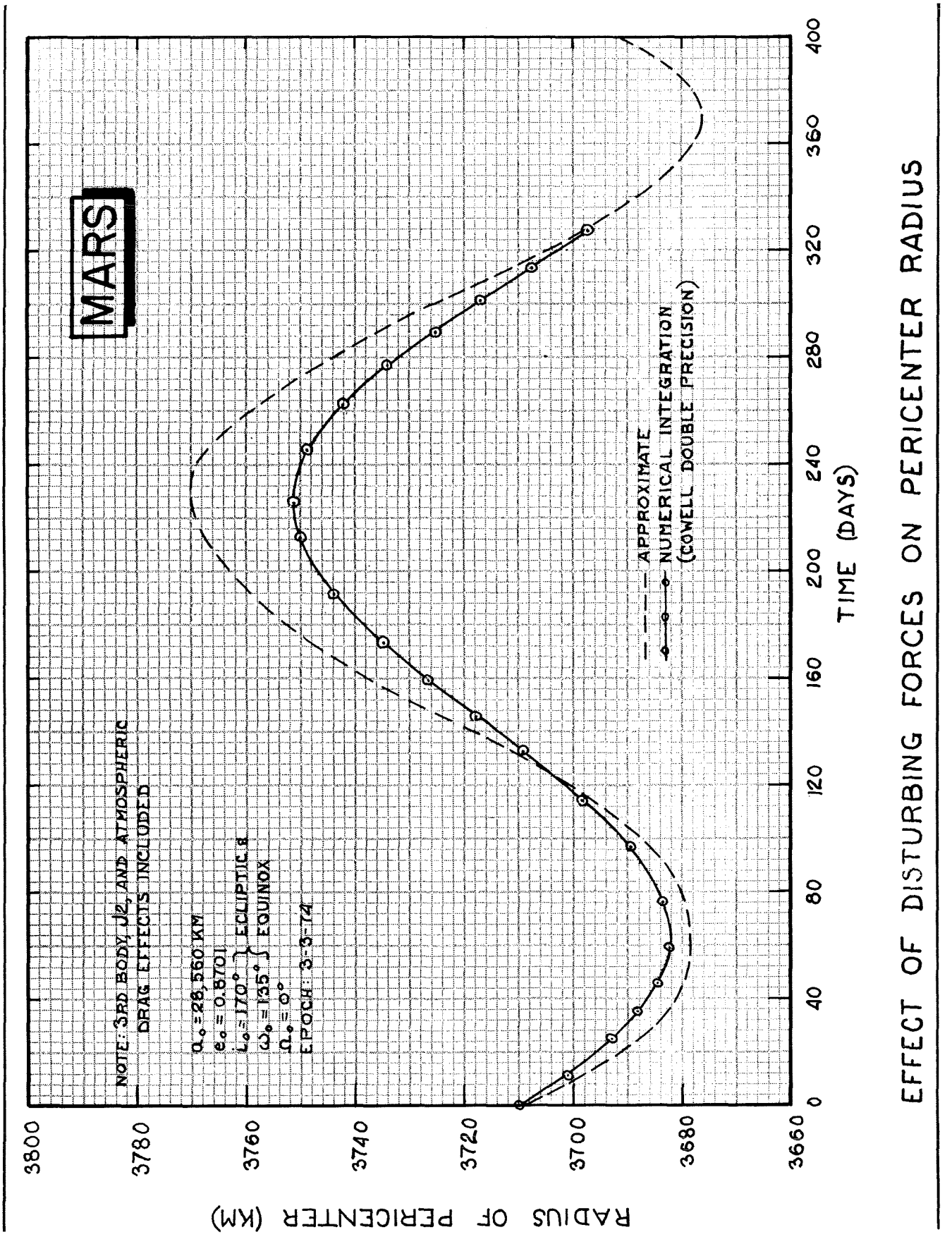

EFFECT OF DISTURBING FORCES ON PERICENTER RADIUS

Figure 3.2.6
Contract No. NAS 5-10782

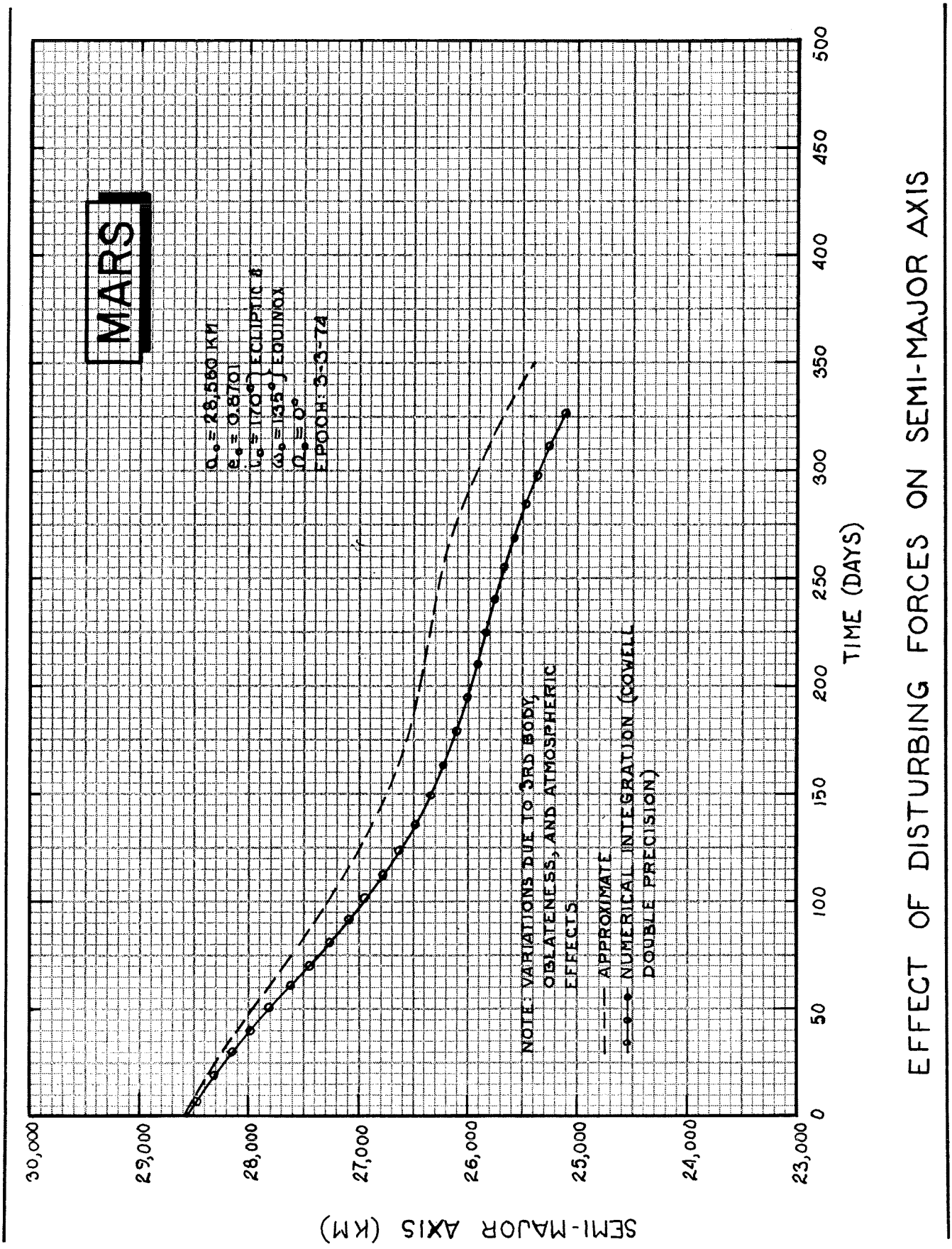

EFFECT OF DISTURBING FORCES ON SEMI-MAJOR AXIS

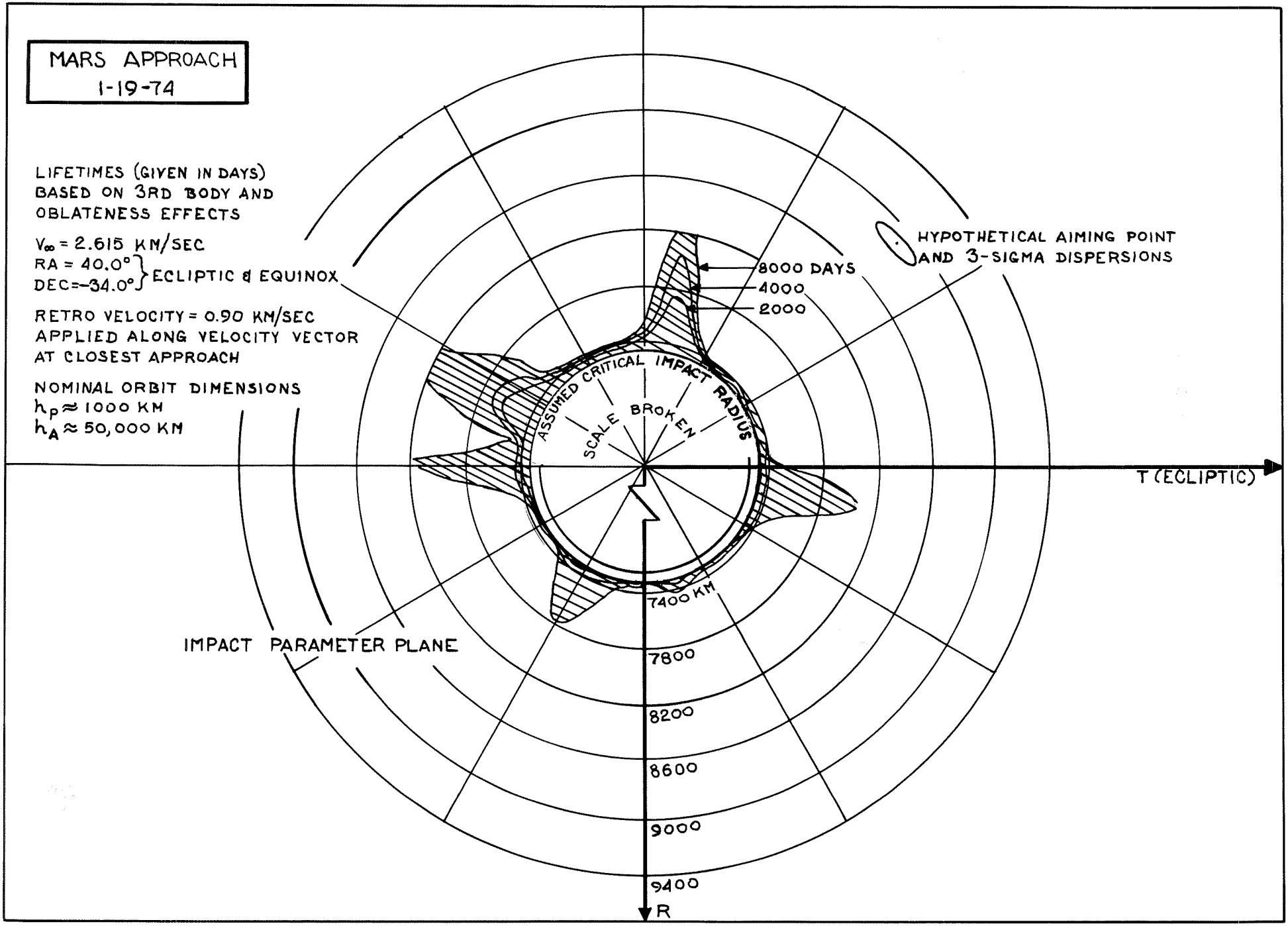

CONTOURS OF CONSTANT DYNAMIC LIFETIME

Figure 3.2.7
Contract No. NAS 5-10782

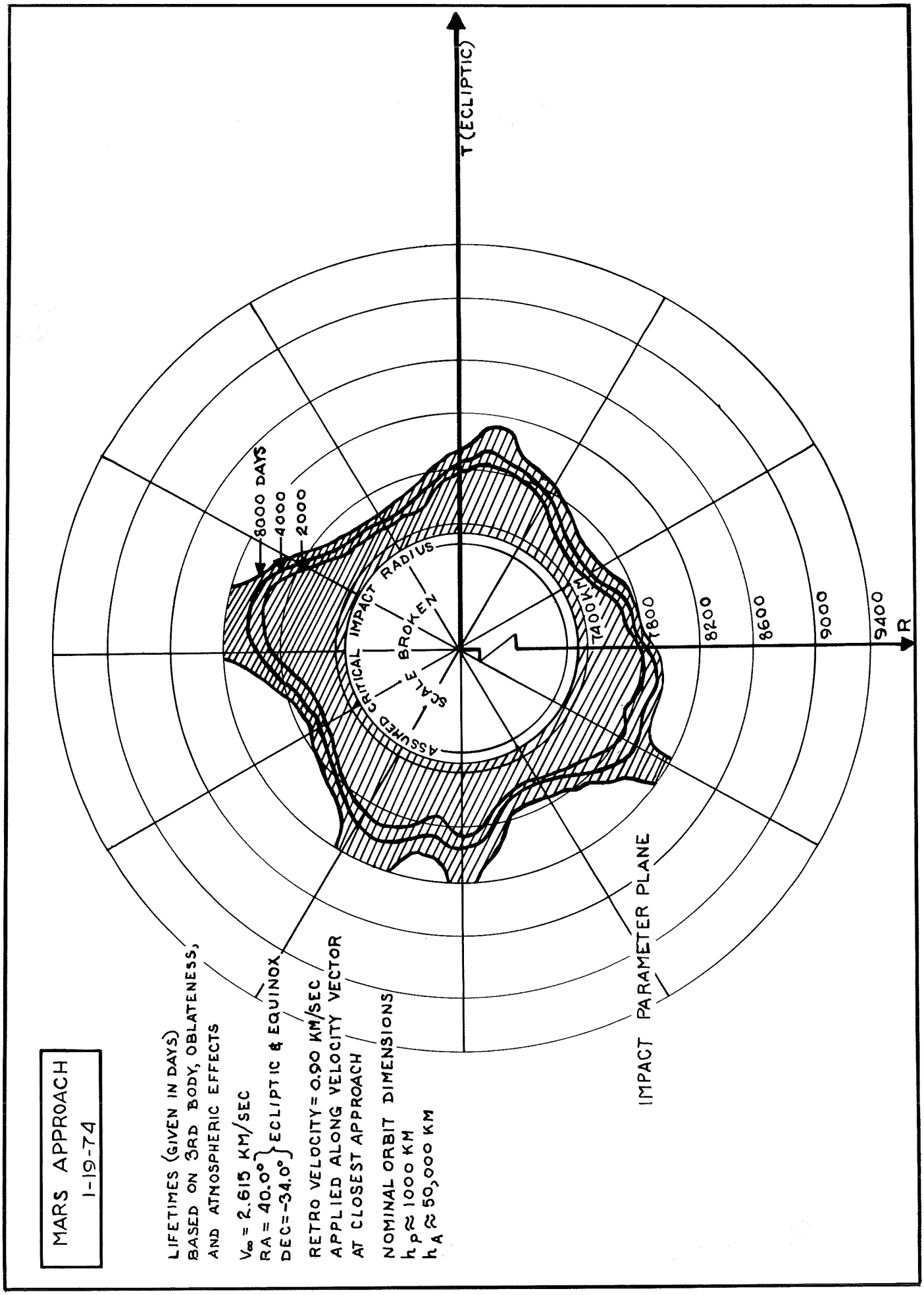
MARS APPROACH
1-19-74
LIFETIMES (GIVEN IN DAYS)
BASED ON 3RD BODY, OBLATENESS,
AND ATMOSPHERIC EFFECTS
V_∞ = 2.615 KM/SEC
RA = 40.0°
DEC = -34.0°
ECLIPTIC & EQUINOX
RETRO VELOCITY = 0.90 KM/SEC
APPLIED ALONG VELOCITY VECTOR
AT CLOSEST APPROACH
NOMINAL ORBIT DIMENSIONS
$h_p \approx$ 1000 KM
$h_A \approx$ 50,000 KM
T (ECLIPTIC)
R
IMPACT PARAMETER PLANE
8000 DAYS
4000
2000
ASSUMED CRITICAL IMPACT RADIUS
BROKEN
SCALE
7400 KM
7800
8200
8600
9000
9400
CONTOURS OF CONSTANT DYNAMIC LIFETIME

respect to the Martian orbit plane but the numerical integration from which the data were taken was meant to serve a dual purpose. The caluculations were also made to give an idea of the shadow-time per orbit period that can be expected for a Martian orbiter. For a given semi-major axis and eccentricity, the total amount of time spent in shadow will be maximized for orbits with low inclinations with respect to the planet's orbit around the Sun.

Figure 3.2.9 shows the history of the position of the sub-pericenter point on the Martian surface for an orbit whose initial pericenter altitude is 300 km and whose initial apocenter altitude is 50,000 km. The circled points show the position of the vehicle a selected pericenter passages. The revolution number is given beside each circled point. The period of this orbit is about 40 hours and is decreasing under the influence of atmospheric drag. Since the Martian day is about 24.5 hours, the sub-pericenter point seems to "hop around" on the Martian map. The important point is that, for the first year, the latitude of the sub-pericenter point remains between -10° and -30°. This orbit, then, would be less than satisfactory were low altitude data desired for the entire Martian surface. On the other hand, if it were desired to concentrate on the latitude range from -10° to -30°, this orbit would be ideal.

Figure 3.2.10 shows the time spent in shadow for the same orbit and shows how the shadow-time per orbit period changes with time during the mission. This kind of information is valuable to spacecraft designers and, although the data of the figure were obtained from the full numerical integration, they could have been generated quite accurately with the approximate techniques. It is recommended that computer programs using the approximate techniques include the capability to calculate the average shadow-time per orbit period from the average orbit elements and the position of the Sun.

We have presented some possible applications of the approximate techniques of Section 2 and have shown how they can be used to great advantage by mission analysts. Also presented were some curves showing the time histories of some quantities of interest from a scientific point of view in order to give an idea of how the techniques can be used to select an orbit that will provide the most desirable scientific information.

Figure 3.2.9
Contract No. NAS 5-10782

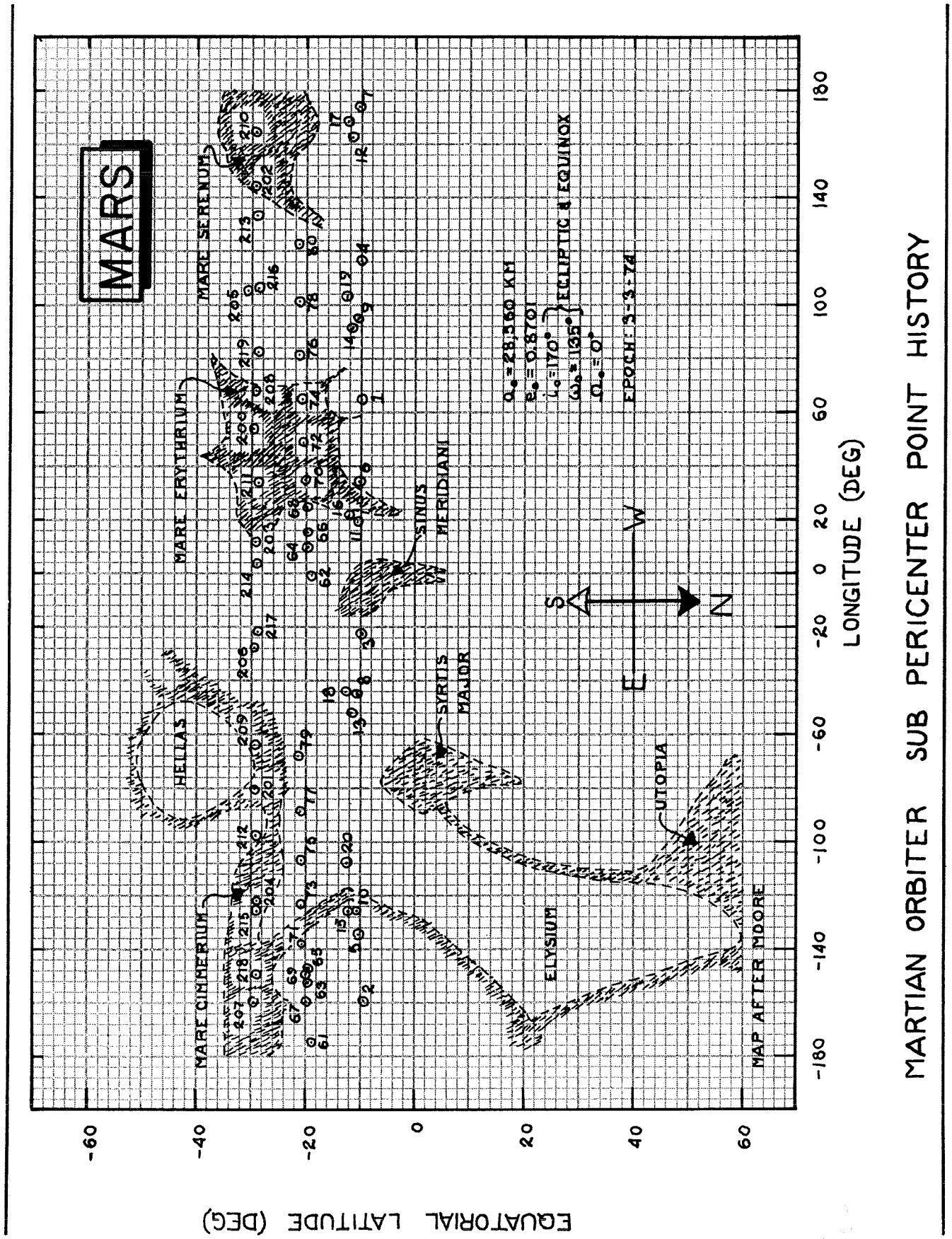

MARTIAN ORBITER SUB PERICENTER POINT HISTORY

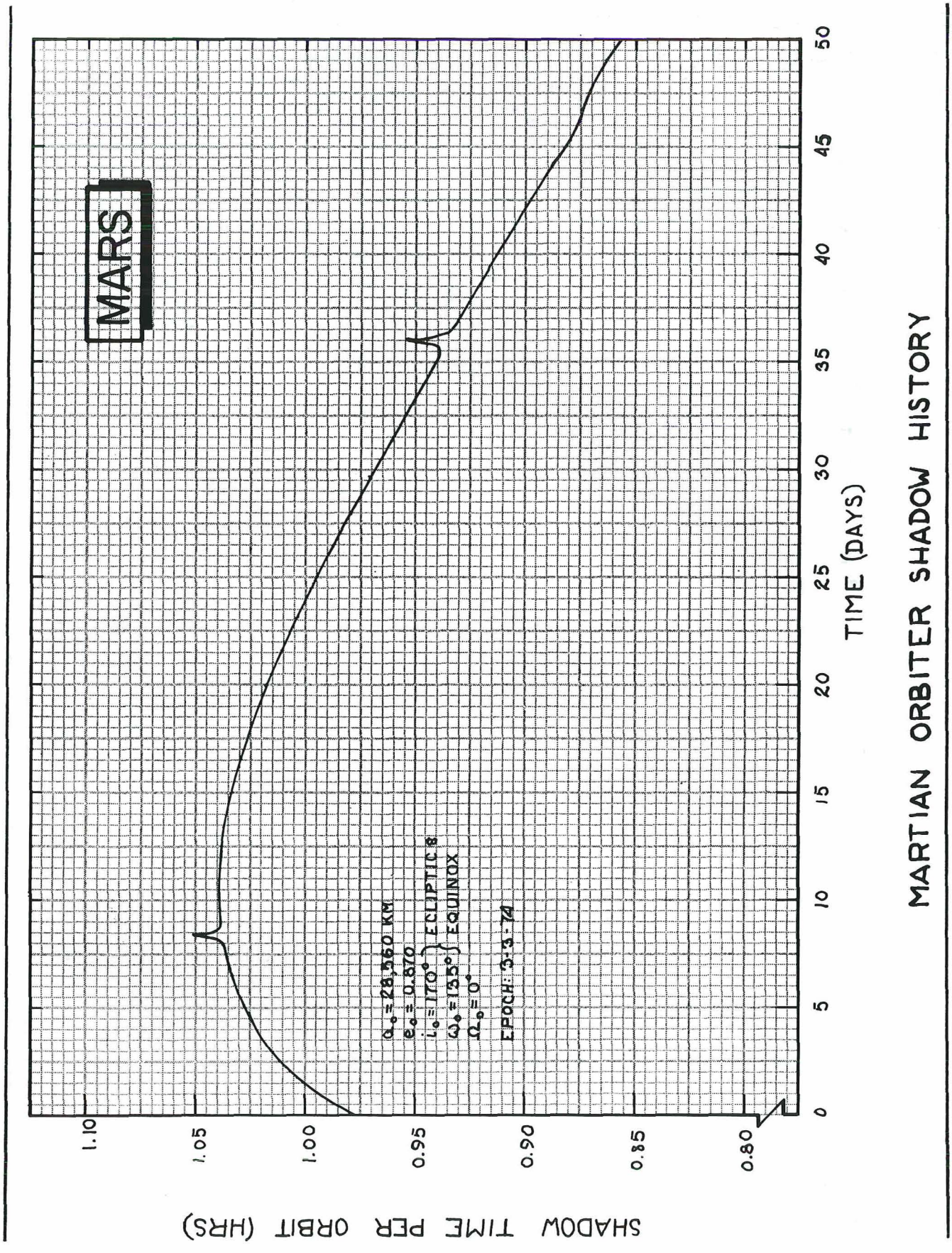

MARTIAN ORBITER SHADOW HISTORY

In the previous analyses several factors have been mentioned as possible trouble areas in the long-term orbit prediction problem and there are several factors that were not mentioned at all. In the next section, we take up these neglected factors and their possible significance to the design of actual planetary orbit missions.

NEGLECTED FACTORS

There are a great many disturbing effects that have not been considered here. Shapiro (Reference 19) presents an excellent discussion of many perturbations that should be included in an accurate orbit determination philosophy. Some of these effects can even become dominant for abnormal satellites. For example, solar radiation pressure is the dominant disturbing force for balloon satellites like the Echo series and electrostatic drag can have a large effect on small metallic objects like the controversial needles of a few years ago. For normal spacecraft, however, most of these "minor" perturbation are truly insignificant for all but the most stringent analyses.

On the other hand, there are several points that need clarification and some errors that need explaining. The author feels that it is the responsibility of a proponent of an approximate method not only to show that the technique works but also to show where the method fails. The most important argument for this attitude is that it helps fix the direction of future research. Less important perhaps, but no less cogent is the fact that it helps the reader in his evaluation of the method as it may apply to his needs. We therefore present the following discussions which, in the author's opinion, encompass the most significant omissions of the preceding studies.

The first point is that of the short-periodic coupling between oblateness and atmospheric effects. This phenomenon is most pronounced for satellites whose pericenter points are near the poles or the equator. The coupling takes on a less formidable appearance if we think in terms of the physics of the problem. We know that, in the drag-free problem, the energy of the satellite must not change. That is

$$E = \frac{V^2}{2} + (-U) = \text{constant}$$

where

$$U = \frac{k^2 m}{r}\left\{1 + \frac{Jr_e^2}{r^2}\left(\frac{1}{3} - \sin^2\beta\right) + \ldots\right\}$$

with β the equatorial latitude of the satellite. Clearly, the instantaneous semi-major axis must change during one revolution of the satellite in its orbit since

$$\frac{1}{a} = \frac{2}{r} - \frac{V^2}{k^2 m}$$

This means that, if we are using the mean semi-major axis (the average value over one revolution), the spacecraft must be going faster or slower, for a given value of r, than the speed we calculate from the average semi-major axis. The difference, of course, is greater at low altitudes. But this is where the atmospheric drag and the velocity are maximized and the drag is a velocity-dependent force. Thus, by using the Keplerian elements to obtain the speed for the drag calculations, we commit an error at the worst possible point - the closest approach point. Such an omission is bound to cause errors in the average rates of change of the elements for highly eccentric orbits disturbed by atmospheric drag. It is therefore recommended that this problem be studied further and that adequate modifications be incorporated in future long-term orbit prediction schemes.

Referring now to Equation (9) of Section 2, we find a second source of error that may be significant for large orbits. The infamous expression +... implies that there are higher order terms in the disturbing function that have not been considered in the averaging theory. Recall that the expansion was in terms of the ratio of satellite distance to disturbing body distance r/r'. Brouwer and Clemence (Reference 10) outline the procedure for expanding the disturbing function beyond the second power of r/r' and indicate how quickly the expressions become almost unmanagable even in the low-inclination approximation for Earth's moon. The very great difficulty of developing an accurate lunar theory for high-inclination, high-eccentricity orbits leads us to recommend numerical solutions if the orbit is so large that the terms not included in Equation (9) become important. An efficient way to deal with this point will be outlined in the next section.

Even though solar radiation pressure is usually negligible for normal spacecraft, this third shortcoming of the techniques of Section 2 should be remedied. An approximate solution to the problem could be easily included in the double averaging theory if the assumption that the vehicle spends a negligible time in shadow is valid. Such an extension to the theory would be very valuable to mission designers who might want to use the solar pressure to stabilize an otherwise short-lived orbit.

Of perhaps the most practical importance, is the inability of the techniques of Section 2 to describe the high-order oblateness effects. The author has attempted to transform the second order effects of J_2 to the orbit plane frame used in the double averaging technique. The expressions for the rates become very involved and abound in complicated numerical singularities. These difficulties lead to a recommendation of a more accurate (and more numerical) technique that will be described in the next section. For Venus orbiters, the very low estimates of J_2 permit us to use the double averaging theory for a wide range of orbits. For Mars, however, the very strong oblateness indicates that, for close satellites, the effects of J_2^2, J_3, and J_4 may be much more important than the effects considered here. The author has found that Mars could have a very large value of J_3 without our being able to detect such non-sphericity in the motion of Phobos.

Although the masses of the natural Martian satellites are very small, collision with or very close approaches to Phobos or Deimos are unlikely possibilities that should, nevertheless, be considered in detailed Mars orbit mission analyses. Mission planners should have access to the most accurate ephemerides for the two natural satellites of Mars.

In the next section, recommendations for further study will be directed primarily toward rectifying the above omissions.

Page intentionally left blank

Section 4
RECOMMENDATIONS FOR FURTHER STUDY

In the preceding studies, it has been shown that the approximate techniques of Section 2 work very well for Venus orbiters and tolerably well for Martian satellites but it is clearly of value to rectify the shortcomings mentioned in the previous paragraphs. It is relatively easy to perform the kind of survey study of this report. It is quite different to actually solve the orbit dynamics problems for a real mission. The primary purpose of this section is to recommend a set of techniques through which it will be possible to resolve the orbit prediction problem in an actual mission design and flight control situation.

It is recommended that a set of compatible computer subprograms be developed to incorporate the following four levels of orbit prediction capability.

LEVEL I

This level should consist of the following:

1. Numerical integration of:
   - Doubly averaged third-body equations
   - First order effects of oblateness
   - Long-term effects of atmospheric drag obtained by mechanical quadrature.
2. Superposition of:
   - Medium periodic third-body effects on eccentricity as in Equation (12).

This lowest level technique is just the method described in Section 2 and is recommended because the technique works so well for Venus orbiters

that a significant advantage in speed can be had over the next level. For example, any of the Venus orbiter pericenter histories of Section 3 could have been generated accurately with one or two numerical integration steps. The medium-periodic effects could then have been determined very rapidly from Equation (12) of this report and the power series from the numerical integration routine. In many cases, a 1,000 day computing interval could be used for the long-periodic integration with no significant loss of accuracy. The speed advantage to be had by such a scheme could be of great value where a large number of orbits are to be simulated. Construction of detailed impact parameter maps or Monte Carlo analyses to determine the probability of achieving a long lifetime would derive considerable benefit from the techniques recommended for Level I. This level is recommended primarily for very rapid simulation of Mercury, Venus, and high apogee ($h_{a_o} \geq 30,000$ km) Mars orbiters. For more accurate predictions and for close Mars satellites, the next level should be employed.

LEVEL II

The main difference between this level and the previous one is that, for Level II, the singly-averaged third-body equations are to be integrated numerically to obtain the medium-periodic third-body variations of the orbital elements. Integration of the singly averaged equations yields much more accurate results in the situations where oblateness so dominates the motion that the orbit moves faster than the central planet around the Sun. The price of this increased accuracy is computing time. The numerical integration routine must now take steps significantly smaller than half a planetary year in order to follow the periodicities in the (singly averaged) equations of motion.

The recommended second level of capability is a numerical integration of:

1. The singly averaged third-body equations, and/or
2. The analytically averaged rates of the elements caused by first- and second-order effects of J_2, (the first non-zero oblateness coefficient), and the first-order effects of J_3 and J_4 (several other

high-order effects could easily be included if necessary. ($J_{2,2}$ will probably be important for very close satellites of Mercury), and/or

3. The rates caused by atmospheric drag, numerically averaged by mechanical quadrature as described in Section 2. (This capability should include atmospheric rotation effects for actual mission design.)

One of the important advantages of the singly averaged equations for third-body effects is that the same number of terms are required in any non-rotating coordinate system. Thus, it is possible to choose the equatorial plane of the central planet as the principal plane without having to evaluate several extra quantities at each computing interval to account for coordinate transformations. In an equatorial coordinate system, it is possible to account for the average high-order oblateness effects in a relatively easy way. Therefore, it is possible to extend the analysis to a high order with ease since the literature is filled with the equations for the average rates of the equatorial orbital elements.

The singly averaged equations may be obtained by averaging Equation (9) of this report with respect to true anomaly, f, and retaining all terms dependent upon the position of the disturbing body. B. Kaufman of Goddard Space Flight Center has recently derived expressions for the singly averaged rates caused by third-body perturbations. The expressions are particularly amenable to efficient computation and, in recent experiments, have been checked against Cowell and Encke integrations with extremely encouraging results. Where the doubly averaged equations break down, the singly averaged equations continue to describe the average motion of the orbit very accurately. This is as it should be since fewer assumptions are made in the derivation of the singly averaged rates than are made in the double averaging theory. Kaufman's equations are not available in the literature but the the interested reader could probably obtain the equations from the author.

At this level certain nuances should begin to appear in the orbit prediction techniques. In Section 2, no mention was made of the variation of the attitude of the spacecraft with respect to its velocity vector and the resultant

change in the effective cross-sectional area that the vehicle presents to the atmospheric disturbances. The difference between the satellite's actual altitude and the altitude above the mean radius of the planet was similarly neglected. These are relatively minor points but it is the sum of a great many minor points that makes the difference between a working, useful computer program and a box of Fortran cards. It is recommended that the calculations for simulating the above effects be included, as options, in future study tools so as to provide the capability for evaluating the importance of the effects.

Before the descriptions of Levels III and IV are begun, it should be mentioned that neither of the first two levels has the capability of including the neglected terms of the third-body disturbing function nor is either capable of simulating short-periodic coupling between atmospheric drag and oblateness effects. In Level III, the first of these points will be taken care of but the short-periodic coupling of oblateness and drag will have to be handled separately.

LEVELS III AND IV

The derivation of the equations for the third level requires, as a starting point, the equations for the fourth. These equations for the instantaneous rates of the Keplerian orbital elements are taken from page 147 of Reference 11. Reference 10 also presents the variational equations in Gauss's form on page 301. They are:

$$\dot{a} = \frac{2e \sin f}{n\sqrt{1-e^2}} R' + \frac{2a\sqrt{1-e^2}}{rn} S'$$

$$\dot{e} = \frac{\sin f \sqrt{1-e^2}}{na} R' + \frac{\sqrt{1-e^2}}{a^2 ne}\left[\frac{a^2(1-e^2)-r^2}{r}\right] S'$$

$$\dot{\sigma} = \dot{\phi}_o = \left[\frac{(-e^2)\cos f}{ane} - \frac{2r}{na^2}\right] R' - \frac{(1-e^2)\sin f}{ane}\left[1 + \frac{r}{a(1-e^2)}\right] S'$$

$$\dot{\Omega} = \frac{r \sin u \quad W'}{a^2 n \sin i \sqrt{1-e^2}}$$

$$\dot{\omega} = -\frac{\cos f \sqrt{1-e^2}}{ane} R' + \frac{\sin f \sqrt{1-e^2}}{ane} \left[1 + \frac{r}{a(1-e^2)}\right] S'$$

$$- \frac{r \sin u \cot i}{a^2 n \sqrt{1-e^2}} W'$$

$$\frac{di}{dt} = \frac{r \cos u \, W'}{a^2 n \sqrt{1-e^2}}$$

where

$u = \omega + f$ and $\sigma = \phi_o$ ▫ the mean anomaly at epoch. R', S' and W' are the components of the disturbing accelerations resolved along the radius vector, the in-plane normal to the radius vector (in the direction of satellite motion) and the normal to the orbit plane.

With this formulation, one can include any disturbing forces whatever simply by writing the accelerations resulting from those forces in a non-rotating planetocentric frame and then rotating the accelerations to the R', S', W' frame described above. The equations should be integrated numerically with an efficient predict-correct scheme. (A self starting routine such as the Runge-Kutta technique may be useful for some applications). Care should be taken to eliminate any unnecessary calculations in the evaluation of the derivatives. An efficient automatic computing interval selector should also be employed.

The above is a description of Level IV of the recommended study tool and provides an excellent basis for evaluation of the three lower levels. Level IV is, of course, exact and must be paid for in computing time. The reason for leaving the description of Level III to the last will be obvious to those who have read Section 2.3. There remains only to place integral signs

in front of the expressions and transform the independent variable from time to true anomaly. The rates, then, are to be averaged by mechanical quadrature before they are integrated. It is recommended that the averaging be done with respect to true anomaly as was done for the atmospheric drag effects in Section 2.

Of the four levels of orbit prediction capability recommended above, only Level IV is capable of describing short-periodic coupling between oblateness and drag perturbations. The three lower levels have been derived with the assumption that the motion is Keplerian during one revolution of the satellite around the central body. The speed of a satellite of an oblate planet is not Keplerian, as discussed in Section 3.3 and, if velocity dependent forces are present, the short-periodic variations in speed should be accounted for. It is, therefore, suggested that the major effects of short-periodic coupling between oblateness and drag can be accounted for by making use of the integral of energy in the problem of motion around an oblate planet. That is, whenever the speed is required for calculation of the accelerations caused by atmospheric drag, the magnitude of the velocity should be calculated in such a way as to maintain the sum of kinetic and potential energy (including all harmonics being used in the simulation) at a constant value during that revolution of the satellite. In this way the magnitude of the atmospheric drag forces will be much more accurately calculated and the decay rate simulation will improve accordingly.

The above techniques, if efficiently programmed and studied carefully to eliminate unnecessary calculations, will provide an extremely useful tool for pre-mission analysis, and for practically any orbit prediction problem for many years to come.

Section 5
CONCLUSIONS

This report has given an introduction to the orbit prediction problem for artificial planetary satellites. Emphasis has been placed on the major perturbations acting on satellites of each inner planet, on the complex interactions of those perturbations, and on the influence of the disturbing forces on the orbit evolution and lifetime of satellites of the inner planets.

In Section 2 an approximate method for simulating the time history of the orbit elements, including the second order effects of the disturbing body's orbital eccentricity was presented. An efficient numerical technique was also presented that permits the simulation of the effects of atmospheric drag on orbit evolution. This method involves the numerical averaging of the differential equations for the orbital elements in a way that eliminates the need for the assumptions of small eccentricity and an exponential density profile.

A four-planet survey in Section 3 presented the major influences of perturbations to the orbits of planetary satellites. Coupling between third-body and oblateness perturbations was defined in terms of the maximum rate of the argument of pericenter caused by either disturbing force acting alone. The uncoupled effects of atmospheric drag were evaluated with respect to their influence on satellite lifetime. Perhaps the most surprising result of the survey is that the maximum Mars model atmosphere (Reference 18) has a much greater effect on lifetime than the maximum Venus model (Reference 17). It was also found that, whereas the approximate methods of Section 2 work extremely well for Venusian orbiters, the very strong oblateness of Mars causes such rapid motion of the orbit that the double averaging theory breaks down for Martian orbiters whose apocenter altitudes are below about 30, 000 km. Mars and Venus were emphasized in the survey since they are of most immediate interest. An estimate of the oblateness of

Mercury was obtained from the work of Liu and some pericenter histories were given for Mercury orbiters. The survey work for Earth satellites was done with the assumption that the orbits of the Moon and the Earth lie in the same plane. The Earth survey was presented primarily for reference.

The methods used for the survey work were combined and used to show the advantages of very rapid orbit prediction techniques in pre-mission analysis and aiming point selection for some possible missions to Venus and Mars in the 1970's. Contours of constant lifetime were constructed on a map of the impact parameter plane and the time histories of some scientifically important parameters were presented.

The major result of the survey and detailed work on Mars and Venus is that the simulation of Martian orbiters is very difficult. Whereas the estimated weak oblateness of Venus and the sharp density gradient of the model Venus atmospheres makes it relatively easy to predict the long-term motion of satellites of that planet, the combination of third-body perturbations, oblateness effects twice as strong as for Earth satellites, and an atmosphere that may extend up to 2,500 km suggests that considerable further study should be directed toward the orbit prediction problem for Martian satellites.

A discussion of neglected factors was included that pointed out the major omissions of the preceding studies. The possible significant factors were: (1) short-periodic coupling between oblateness and drag effects, (2) high-order oblateness perturbations, (3) high-order third-body perturbations, and (4) solar radiation pressure. Also mentioned as possible trouble areas were hypothetical very close approaches to the natural Martian satellites and the possibility of resonance between medium-periodic third-body effects and oblateness perturbations.

The recommendations for further study in Section 4 included the development of a four-level computer program that will permit efficient future study.

It was suggested that high-order oblateness effects, the coupling of atmospheric and oblateness perturbations and the coupled effects of third-body perturbations will be absolutely essential to Martian orbit mission analysis.

It was further recommended that simulation of solar radiation pressure be included in future study tools along with accurate ephemerides of the natural satellites of Mars. Other suggestions included the establishment of an upper bound on the third harmonic of the Martian gravity field and a thorough review of the available atmospheric models for Mars.

It is hoped that the techniques and the numerical experience presented in this report will be of some introductory value in the efforts directed toward the efficient unmanned exploration of the planets.

Page intentionally left blank

REFERENCES

1. Lidov, M. L., Evolution of the Orbits of Artificial Satellites as Affected by Gravitational Perturbation From External Bodies. AIAA Journal Vol. 1, No. 8, Russian Supplement August, 1963. (Original in Russian, 1961.)

2. Kevorkian, J., von Zeipel Method and the Two-Variable Expansion Procedure. Astronomical Journal, Vol. 71, No. 9., pp. 878-885, November, 1966.

3. Eckstein, M., Y. Y. Shi, and J. Kevorkian. Satellite Motion for Arbitrary Eccentricity and Inclination Around the Smaller Body in the Restricted Three-Body Problem. Douglas Paper No. 3489, April 1965. Also published as "Satellite Motion for Arbitrary Eccentricity and Inclination Around the Smaller Primary in the Restricted Three-Body Problem," The Astronomical Journal, Vol. 71, No. 4, pp. 248-263, May, 1966.

4. Williams, R. R., and J. Lorell, The Theory of Long-Term Behavior of Artificial Satellite Orbits Due to Third-Body Perturbations, Jet Propulsion Laboratory, Technical Report 32-916, February 1966.

5. Lidov, M. L., On the Approximated Analysis of the Orbit Evolution of Artificial Satellites, published in Dynamics of Satellites, Academic Press, p. 168, Proceedings of IUTAM Symposium Paris, 1962.

6. Lorell, J., Long Term Behavior of Artificial Satellite Orbits Due to Third-Body Perturbations. Journal of the Astronautical Sciences, pp. 142-149, winter 1965.

7. Uphoff, C., An Approximate Method for Predicting Lunar Satellite Lifetimes and Its Application to a Lunar Orbit Mission Analysis. Presented to the American Astronautical Society Space Flight Mechanics Specialist Conference, University of Denver, Denver, Colorado, July, 1966, AAS Preprint 66-130.

8. Kozai, Y., On the Effects of the Sun and the Moon Upon the Motion of a Close Earth Satellite, Smithsonian Institution Astrophysical Observatory Special Report No. 22, 1959.

9. Brown, E. W., and C. A. Shook, Planetary Theory, Dover Publications, New York, 1964.

10. Brouwer, D., and G. M. Clemence, Methods of Celestial Mechanics, Academic Press, New York, 1961.

11. McCuskey, S. W., Introduction to Celestial Mechanics, Addison Wesley, Reading, Mass.

12. Jacchia, L. G., Static Diffusion Models of the Upper Atmosphere with Empirical Temperature Profiles, Smithsonian Contributions to Astrophysics, Vol. 8, No. 9, pp. 215-257, 1965.

13. Westerman R., Secular Effects of Atmospheric Drag on Satellite Orbits, Astronomical Journal, Vol. 68, No. 6, pp. 382-384, 1963.

14. Breakwell, J. V., and R. D. Hensley, An Investigation of High-Eccentricity Orbits About Mars. NASA SP141, 1967.

15. Brouwer, D., and G. I. Hori, Theoretical Evaluation of Atmospheric Drag Effects in the Motion of an Artificial Satellite, Astronomical Journal, Vol. 66, 1961, pp. 193-225.

16. Anderson, J., Private Communication, September 1969.

17. NASA Special Publication SP8011, Models of Venus Atmosphere (1968), December 1968.

18. NASA Special Publication SP8010, Models of Mars Atmosphere (1967), May 1968.

19. Liu, H. S., On the Figure of Mercury NASA Publication X-643-68-306, May 1968.

20. Vaughan, O. H., Jr., Model Atmospheres of Mercury, NASA Publication TM-X-53693 January 1968.

21. Liu, H. S., Thermal Contraction of Mercury NASA Publication X-643-69-410, September 1969.

22. ESSA, U. S. Standard Atmosphere Supplement, U. S. Govt. Printing Office 1966.

23. Shapiro, I. I., The Prediction of Satellite Orbits, Dynamics of Satellites, Academic Press, pp. 257-312. Proceedings of IUTAM Symposium, Paris, 1962.

24. NASA Document M73-106-0, Viking Project Mars Engineering Model, Langley Research Center, February 1969.

GLOSSARY

Orbital Elements

a	Semimajor axis of osculating eclipse.
e	Eccentricity.
f	True anomaly.
ω	Argument of pericenter measured from the ascending node in the orbit plane positive in the direction of satellite motion.
i	Inclination of the orbit plane to the xy plane of the reference frame.
Ω	Longitude (right ascension) of the ascending node of the satellite orbit measured in the xy plane of the reference frame and positive in the counter-clockwise sense from the x axis.
ϕ	Mean longitude of the satellite; measured from the x axis to the line of nodes, then along the orbit to pericenter, then along the orbit to the mean position of the satellite, $\phi = \omega + \Omega + M$ where M is the mean anomaly of the satellite.
	NOTE: Primed quantities refer to the perturbing body. Doubly primed quantities refer to the central planet's equator. Subscripts L and M refer to the long and medium-periodic variations in all quantities.
n	Mean motion of the satellite.
n'	Mean motion of the perturbing body.
R_C	Mean radius of the central planet.
e_{crit}	Critical eccentricity--the value of e at which the pericenter distance becomes less than the radius of the central planet plus an assumed effective atmosphere.
	NOTE: The subscript 0 refers to epoch time.
C	$\frac{15}{4}\frac{n'^2\mu'}{n}(1+\frac{3}{2}e'^2)$
δ_e	Medium periodic eccentricity variation $\delta_e = e - e_L$

μ' Ratio of the mass of the disturbing body (the Sun) to the combined mass of the Sun and the central planet.

i'' Inclination of the central planet's equator to the central planet's orbit about the Sun.

Ω'' Right ascension of the equator's ascending node on the central planet's orbit plane, measured from the x axis of the OPP frame.

$\bar{i}$ Inclination of satellite's orbit plane to central planet's equatorial plane

$$\cos\bar{i} = \cos i \cos i'' + \sin i \sin i'' \cos(\Omega - \Omega'')$$

$\vec{B}$ Vector having the length of the semi-minor axis of the approach hyperbola and lying in the impact parameter plane. (See Section 3.)

ΔV Impulsive planetary orbit insertion speed increment.

μ_{cp} Gravitational constant of the central planet.

RA Right ascension of the incoming hyperbolic excess velocity vector.

DEC Declination of the incoming hyperbolic excess velocity vector.

ϕ_{TR} Angle specifying the angular position of the $\vec{B}$ vector in the impact parameter plane.

J Coefficient of the second term in the expansion of the disturbing function describing the potential due to an oblate planet; viz

$$U = \frac{k^2 m}{r}\left[1 + \frac{J r_e^2}{r^2}\left(\frac{1}{3} - \sin^2\beta\right) + \ldots\right]$$

where

r is the distance of the satellite from the center of mass of the central planet.
β is the equatorial latitude of the satellite.
r_e is the equatorial radius of the central planet.

k^2	Universal gravitational constant
m'	Mass of disturbing body
m	Mass of central planet
m_s	Mass of the satellite
F	Medium-periodic eccentricity function of Reference 7
F^*	Medium-periodic eccentricity function of this report
p	Semi-latus rectum $p = a(1 - e^2)$

Page intentionally left blank

Appendix I
KOZAI'S DISTURBING FUNCTION [Reference 8]

$$R = n'^2 \mu' a'^2 \left\{ \left[1 + 3\, e' \cos(\phi' - \omega' - \Omega') \right] \left[\left(1 + \frac{3}{2} e^2 \right) A + \frac{15}{8} e^2 B \right] \right.$$

$$\left. - 4\, e' \sin(\phi' - \omega' - \Omega') \left[\left(1 + \frac{3}{2} e^2 \right) A' + \frac{15}{8} e^2 B' \right] \right\}$$

where

$$A = \frac{1}{4} \left(1 - \frac{3}{2} \sin^2 i \right) \left(1 - \frac{3}{2} \sin^2 i' \right)$$

$$+ \frac{3}{16} \sin 2i \sin 2i' \cos(\Omega - \Omega')$$

$$+ \frac{3}{16} \sin^2 i \sin^2 i' \cos 2(\Omega - \Omega')$$

$$+ \frac{3}{8} \sin^2 i' \left(1 - \frac{3}{2} \sin^2 i \right) \cos 2(\phi' - \Omega')$$

$$+ \frac{3}{8} \sin^2 i \cos^4 \frac{i'}{2} \cos 2(\phi' - \Omega)$$

$$- \frac{3}{8} \sin 2i \sin i' \cos^2 \frac{i'}{2} \cos(2\phi' - \Omega - \Omega')$$

$$+ \frac{3}{8} \sin^2 i \sin^4 \frac{i'}{2} \cos 2(\phi' - 2\Omega' + \Omega)$$

$$+ \frac{3}{8} \sin 2i \sin i' \sin^2 \frac{i'}{2} \cos(2\phi' + \Omega - 3\Omega');$$

$$B = \cos^4\frac{i}{2}\cos^4\frac{i'}{2}\cos 2(\phi' - \omega - \Omega)$$

$$+\frac{1}{2}\sin^2 i\left(1 - \frac{3}{2}\sin^2 i'\right)\cos 2\omega$$

$$+\frac{1}{2}\cos^4\frac{i}{2}\sin^2 i'\cos 2(\omega + \Omega - \Omega')$$

$$+\sin^4\frac{i}{2}\cos^4\frac{i'}{2}\cos 2(\phi' + \omega - \Omega)$$

$$+\cos^4\frac{i}{2}\sin^4\frac{i'}{2}\cos 2(\phi' + \omega + \Omega - 2\Omega')$$

$$+\sin^4\frac{i}{2}\sin^4\frac{i'}{2}\cos 2(\phi' - 2\Omega' - \omega' + \Omega)$$

$$+\frac{3}{8}\sin^2 i\sin^2 i'\cos 2(\phi' - \Omega' - \omega)$$

$$+\frac{3}{8}\sin^2 i\sin^2 i'\cos 2(\phi' + \omega - \Omega')$$

$$+\sin i\cos^2\frac{i}{2}\sin i'\cos^2\frac{i'}{2}\cos(2\phi' - \Omega' - 2\omega - \Omega)$$

$$-\frac{1}{2}\sin i\cos^2\frac{i}{2}\sin 2i'\cos(2\omega + \Omega - \Omega')$$

$$+\frac{1}{2}\sin^4\frac{i}{2}\sin^2 i'\cos 2(\omega - \Omega + \Omega')$$

$$+\frac{1}{2}\sin i\sin^2\frac{i}{2}\sin 2i'\cos(2\omega - \Omega + \Omega')$$

$$+\sin i\sin^2\frac{i}{2}\sin i'\cos^2\frac{i'}{2}\cos(2\phi' + 2\omega - \Omega - \Omega')$$

$$- \sin i \cos^2 \frac{i}{2} \sin i' \sin^2 \frac{i'}{2} \cos(2\phi' + 2\omega + \Omega - 3\Omega')$$

$$+ \sin i \sin^2 \frac{i}{2} \sin i' \sin^2 \frac{i'}{2} \cos(2\phi' - 3\Omega' - 2\omega + \Omega).$$

Page intentionally left blank

Appendix II

MODEL PLANETARY ATMOSPHERES

Table II. 1

Mercury Model Atmosphere (Reference 20)

Altitude (km)	Density (g/cc)
0	4.1×10^{-6}
50	9.3×10^{-7}
100	1.5×10^{-7}
150	1.8×10^{-8}
200	1.5×10^{-9}
300	7.0×10^{-12}
400	5.1×10^{-14}
500	5.7×10^{-15}
600	1.5×10^{-15}
700	8.2×10^{-16}
800	6.2×10^{-16}
900	4.7×10^{-16}
1000	3.7×10^{-16}

Table II. 2

Venus Model Atmosphere (SP8011 V5)

Altitude (km)	Density (g/cc)
0	1.12×10^{-1}
50	4.01×10^{-3}
100	8.19×10^{-7}
150	1.59×10^{-11}
200	2.95×10^{-13}
250	2.99×10^{-14}
300	4.34×10^{-15}
350	8.66×10^{-16}
400	2.36×10^{-16}
450	8.23×10^{-17}

Table II. 3

High Sunspot Maximum Earth Model Atmosphere

Altitude (km)		Density (g/cc)
0	ARDC 1959	1.22×10^{-3}
50	CIRA 1965	1.04×10^{-6}
100		5.06×10^{-10}
150		2.1×10^{-12}
200		3.9×10^{-13}
300		6.7×10^{-14}
400	Reference 22	1.9×10^{-14}
500		7.0×10^{-15}
600		2.8×10^{-15}
700		1.3×10^{-15}
800		5.9×10^{-16}
900		2.9×10^{-16}
1000		1.5×10^{-16}

Table II. 4

Mars Model Atmospheres (SP8010 Maximum)

Altitude (km)	Density (g/cc)
0	2.06×10^{-5}
50	1.07×10^{-6}
100	1.16×10^{-8}
150	1.53×10^{-10}
200	9.12×10^{-12}
300	6.79×10^{-13}
400	1.56×10^{-13}
600	3.01×10^{-14}
800	1.17×10^{-14}
1000	6.00×10^{-15}
1500	2.05×10^{-15}
2000	1.37×10^{-15}
2500	9.87×10^{-16}

Langley Most Probable Mars Model Atmosphere
(Reference 24)

Altitude (km)	Density (g/cc)
0	1.47×10^{-5}
100	3.72×10^{-10}
200	6.00×10^{-13}
300	9.57×10^{-14}
400	3.19×10^{-14}
600	9.06×10^{-15}
800	2.87×10^{-15}
1000	1.04×10^{-15}
2000	2.18×10^{-17}